CHARACTERIZATION OF MCR-1

CHARACTERIZATION AND HIGH-THROUGHPUT SCREENING OF THE POLYMYXIN RESISTANCE ENZYME MCR-1

By ARTHUR SIERON, B. Sc

A Thesis Submitted to the School of Graduate Studies in Partial Fulfilment of the Requirements for the Degree Master of Science

McMaster University

Department of Biochemistry and Biomedical Sciences

Hamilton, Ontario, Canada

MASTER OF SCIENCE (2017)

TITLE: Characterization and high-throughput screening of the polymyxin resistance enzyme MCR-1.

AUTHOR: Arthur Sieron, B. Sc. (McMaster University)

SUPERVISOR: Dr. Gerard D. Wright

NUMBER OF PAGES: xv, 118

Lay Abstract

Polymyxins are potent antibiotics that are threatened by the spread of multi-drug resistant bacteria. Resistance to these antibiotics is relatively rare, although the recent discovery of a mobile polymyxin resistance enzyme, MCR-1, threatens the future use of this antibiotic for treating infections, as it can readily transfer to other bacteria. The goal of this work was to search for a natural product inhibitor of MCR-1 in order to reverse its ability to confer resistance to polymyxins. A color-changing assay was conducted with MCR-1 in hopes of establishing a method to study the inhibition of MCR-1 *in vitro*. Additionally, amino acid substitutions were generated in MCR-1 to better understand how key amino acids affect enzyme function, as well as transmembrane domain truncations to determine if it was possible to create a shorter functioning variant of MCR-1.

Abstract

Polymyxins are potent antibiotics that bind to the outer membrane of Gram-negative bacteria, entering the cell and disrupting the inner membrane, resulting in cell death. They were traditionally used as antibiotics of last resort, but the recent surge of multidrug resistant pathogens has renewed interest in these antibiotics. The emergence of polymyxin resistance determinants such as the recently discovered plasmid-mediated phosphoethanolamine transferase MCR-1 may put a strain on the future effectiveness of this antibiotic.

One method to combat the rise in antibiotic resistant bacteria is through the identification and development of antibiotic adjuvants. These are small molecules that are able to inhibit the resistance mechanism, allowing previously ineffective antibiotics to once again become effective at treating bacterial infections. In this work, a high throughput cell-based screen was conducted using an in-house library of Actinomycete-derived crude cell extracts in order to search for a natural product inhibitor of an *E. coli* strain expressing *mcr-1*. In addition, the development of a new enzyme assay was attempted using purified MCR-1 C-terminal catalytic domain and a chromogenic substrate to test enzymatic activity *in vitro*, in hopes of establishing a simple means of studying inhibition of MCR-1. The structure-function relationship of MCR-1 was also explored by generating amino acid substitutions and studying their effect on the ability of the enzyme to confer resistance to colistin, as well as the generation of MCR-1 transmembrane truncation mutants to determine if it was possible to generate a shorter variant of MCR-1 that retained its enzymatic activity. This work furthers our understanding of the biochemistry and enzymology of MCR-1, and outlines attempts to identify inhibitors of MCR-1 in order to re-sensitize resistant bacteria to polymyxins.

Acknowledgements

As my time as a graduate student comes to an end, I look back and reflect on the last two years of this amazing experience and wonder how it flew by so quickly. It seems like just yesterday I was an undergraduate student working in the Wright lab, and now I'm finishing up the last bit of my graduate studies. Sometimes I look back in awe at the series of events that have led to me where I am today; it seems like it all worked out remarkably well.

This project would not have been possible without my supervisor, Dr. Gerry Wright, who has been a great source of guidance throughout my graduate studies. I dearly admire your work ethic and breadth of knowledge – it's as if you know something about everything, and I have very much cherished the opportunity to learn from you. I want to thank you for giving me the opportunity to be a part of such an amazing environment where I could work alongside yourself and other members of the Wright lab. For all your hard work, support, and discussions about my research, I am in debt to you. In addition, I would like to thank the members of my committee, Dr. Eric Brown and Dr. Fred Capretta, for their continued support throughout this period of time. I have enjoyed the chance to learn from you during my undergraduate and graduate studies.

I am grateful for all of the members of the lab that have contributed to my learning and skill development, and made my stay a warm and pleasant one. You have all made me feel very welcome over the last few years. To Dr. Georgina Cox, who has taken the time to introduce me to various experimental techniques throughout my undergraduate studies, which I have continued to build on to this day. Thank you for your support and encouragement to pursue graduate studies during a time where I was unsure of which path to take next. To Daniel Pallant, who has taken the time to teach me Actinomycete culturing methods and further processing of crude cell extracts, and who patiently answered many of my "Does this culture look okay to you?" questions. To Dr. Jarrod Johnson, who has supervised me as I dabbled in chemical synthesis and supported me throughout my project, providing insight from a chemist's perspective. To Matthew Surette, who has always been available to discuss my experimental results and brainstorm ideas, as well as keeping late nights in the lab interesting. To Haley Zubyk, who was my first undergraduate mentee, a source of comedic relief, and an extra pair of hands to help me when things were piling up – you've made me a proud mentor. To Beth Culp and Allison Guitor, who have provided encouragement and a positive attitude when science became frustrating. I thank you all for the amazing experiences you have provided me with. I would also like to thank Carson Weber, a life-long friend who I could always count on, and one who was always ready to lend a helping hand to both myself and my family; Fraser McCready, a friend and fellow scientist who I always looked forward to catching up with and sharing my progress in the lab; Taylor Barras, an old housemate who made my stay in Hamilton one of the best experiences possible; and Taylor Gray, whose love and support has helped me get through anything that came my way.

Finally, I would like to thank my family for their love and support, not only throughout these last few years, but throughout my whole life. The lessons you have taught me and the work ethic you have instilled in me have made me into the person I am today. To my father, Marek, for motivating me to work and study hard, but to also take time for myself, and my mother, Lidia, for her encouragement, love, and support. I dedicate this work to all of you.

Table of Contents

List of Figures

List of Tables

List of Abbreviations

AMA	aspergillomarasmine A
ARP	Antibiotic Resistance Platform
BCA	bicinchoninic acid
bp	base pair
CAMHB	cation adjusted Mueller-Hinton II broth
CAMPs	cationic antimicrobial peptides
CLSI	Clinical and Laboratory Standards Institute
CMS	colistin methanesulfonate
DMSO	dimethyl sulfoxide
DTT	dithiothreitol
EDTA	ethylenediaminetetraacetic acid
EtOAc	ethyl acetate
EUCAST	European Committee on Antimicrobial Susceptibility Testing
HEPES	hydroxyethyl piperazineethanesulfonic acid
kb	kilobase
kDa	kilodalton
Kdo	3-deoxy-D-*manno*-oct-2-ulosonic acid
KPC	*K. pneumoniae* carbapenemase
L-Ara4N	4-amino-4-deoxy-L-arabinose
L-α-γ-Dab	L-α-γ-diamino-butyric acid
LB	lysogeny broth
LPS	lipopolysaccharide
MALDI-TOF-MS	matrix-assisted laser/desorption time-of-flight mass spectrometry
MCR-1	mobile colistin resistance 1
MDR	multi-drug resistant
MIC	minimum inhibitory concentration
NDM	New Delhi metallo-beta-lactamase
Ni-NTA	nickel nitrilotriacetic acid
NMR	nuclear magnetic resonance
NPL	Natural Product Library
OD_{600}	optical density measured at a wavelength of 600 nanometers
OD_{625}	optical density measured at a wavelength of 625 nanometers
OM	outer membrane
PCR	polymerase chain reaction
PDB	protein data bank
PEtN	phosphoethanolamine

PMBN	polymyxin B nonapeptide
*p*NP	*p*-nitrophenol
*p*NP-Ac	*p*-pitrophenyl acetate
*p*NP-PEtN	*p*-nitrophenyl phosphoethanolamine
psi	pounds per square inch
rpm	revolutions per minute
SAM	*Streptomyces* Antibiotic Activity Media
SDS	sodium dodecyl sulfate
TFA	trifluoroacetic acid
THF	tetrahydrofuran
UDP-diacyl-GlcN	uridine diphosphate diacyl glucosamine
UDP-GlcNAc	uridine diphosphate *N*-acetylglucosamine
WAC	Wright Actinomycete Collection
WT	wild-type
Z’	Z prime

Declaration of Academic Achievement

Arthur Sieron performed the majority of the experiments, data collection, and analyses presented in this thesis. The report was also prepared by Arthur.

Supervisor Dr. Gerry Wright and committee members Dr. Eric Brown and Dr. Fred Capretta, and collaborators Dr. Jarrod Johnson and Dr. Georgina Cox provided guidance and direction throughout the project.

Synthesis of *O*-(*p*-nitrophenylphosphoryl)ethanolamine TFA salt was performed with the assistance of Dr. Jarrod Johnson. Submission of the samples for NMR experiments and assigning of chemical shifts was performed by Dr. Jarrod Johnson.

Cloning, overexpression, and purification of the MCR-1 C-terminal catalytic domain were performed by Haley Zubyk.

Chapter 1.
Introduction

1.1 Antibiotics and antibiotic resistance

In recent years, the emergence of multi-drug resistant (MDR) bacteria that do not respond to conventional methods of treatment has increased[1]. In addition, horizontal acquisition of new antibiotic resistance determinants such as KPC and NDM carbapenemases by previously susceptible bacteria, or spontaneous chromosomal mutations that are vertically transmitted, are responsible for the increasing emergence of multi-drug resistance. These acquisitions render many of our most dependable antibiotics ineffective, and their prevalence has been declared the greatest public health threat of the 21st century that must be urgently addressed[2].

The main issue of continued emergence of antibiotic resistant bacteria, specifically Gram-negative human pathogens, stems from the overuse and misuse of antibiotics in clinical and agricultural settings[3]. The number of novel antibiotics that are entering the clinic each year is declining, contributing to this problem[4,5]. With no new drugs in the pipeline, there is an overwhelming need to preserve the effectiveness of current antibiotics and delay the spread of resistance. One method of preserving current antibiotics is the use of antibiotic adjuvants[6], small molecule inhibitors that disrupt the activity of the resistance element and allow the antibiotic to interact with its target.

1.2 Using antibiotic adjuvants to overcome antibiotic resistance

With limited development of new antimicrobial compounds, there has been an emerging trend to preserve our existing antibiotics through the use of antibiotic adjuvants. These are small molecules that restore the bioactivity of antibiotics in resistant bacteria through the inhibition of resistance mechanisms, allowing the antibiotic to interact with its target[6–8].

The earliest example of this approach is clavulanic acid, which was discovered in the 1970s[9]. It is a β-lactam inhibitor of serine β-lactamases that covalently binds to the active site of the enzymes and inactivates them, protecting the co-administered β-lactam antibiotic from hydrolysis[6,8]. Another more recently discovered antibiotic adjuvant, aspergillomarasmine A (AMA), is a fungal natural product that overcomes the resistance mechanism of metallo-β-lactamases by chelating Zn^{2+} atoms necessary for enzyme function and hydrolysis of β-lactams[7].

This approach of combining antibiotics with antibiotic adjuvants has great potential for clinical use because the antibiotic's mechanism of action will be unobstructed. In cases where the adjuvant mimics the natural substrate of the enzyme, there is little incentive to develop a resistance mechanism to the adjuvant, or in the case of AMA, there is little pressure to abandon the use of essential cofactors to achieve the same resistance mechanism. The use of antibiotic adjuvants provides another means of attack against the evolving issue of antibiotic resistance and allows us to prolong the use of our most effective and endangered drugs. Unfortunately, identifying antibiotic adjuvants is challenging and the continued emergence of resistance is straining current

treatment options. Therefore, there has been increased use of previously discovered antibiotics such as polymyxins which have had limited use due to their nephrotoxic and neurotoxic properties[10].

1.3 Biosynthesis of lipopolysaccharide in *E. coli*

The dominant constituent of the outer leaflet of the outer membrane (OM) is lipopolysaccharide (LPS)[11]. The LPS can be divided into three parts consisting of lipid A, core oligosaccharide, and a long polysaccharide called the O-antigen (Figure 1-1). Lipid A is the highly conserved hydrophobic component of LPS, and is responsible for many of the host toxic effects related to Gram-negative infections[11]. It is composed of a glucosamine disaccharide, which is bis-monophosphorylated at positions 1 and 4', and acyl fatty acid chains[12]. Lipid A acts as a hydrophobic anchor to stabilize the OM, with tight packing of the acyl tails, and additional divalent cations such as Mg^{2+} and Ca^{2+} serve as cross-bridges between adjacent LPS molecules, providing further stability[13,14]. The core oligosaccharides are divided into the inner core (proximal to lipid A), and the outer core which provides a point of attachment for the O-antigen[13]. The inner core is well conserved within a genus or family and typically contains 3-deoxy-D-*manno*-oct-2-ulosonic acid (Kdo) and L-*glycero*-D-*manno*heptose residues, whereas the outer core is more diverse. The O-antigen is the most diverse part of the LPS, consisting of more than 60 monosaccharides and 30 different noncarbohydrate components[13,15].

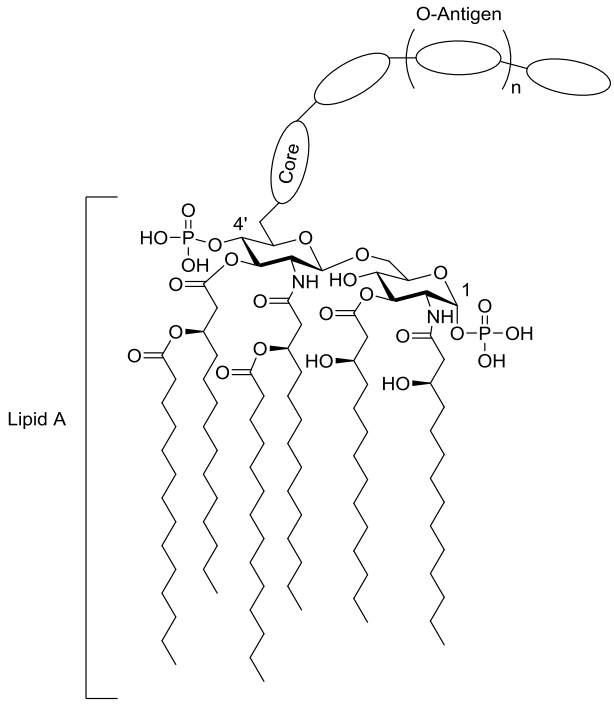

Figure 1-1: Structure of *E. coli* lipopolysaccharide.
The structure of lipid A, shown with simplified core polysaccharides and O-antigens due to their variable compositions. The core region is usually composed of 10-15 monosaccharides and the O-antigen contains a few monosaccharides that can be repeated multiple times. Adapted from Wang *et al.*[11].

Synthesis of LPS is initiated within the cytoplasm, beginning with uridine diphosphate *N*-acetylglucosamine (UDP-GlcNAc)[13,15] (Figure 1-2). Enzymes LpxA, LpxC, and LpxD catalyze the addition of two 3-OH fatty acid chains to the 2- and 3-positions of UDP-GlcNAc to form uridine diphosphate diacyl glucosamine (UDP-diacyl-GlcN). Following this step, UDP-diacyl-GlcN is hydrolyzed by LpxH to form lipid X[16,17], and lipid X and its precursor UDP-giacyl-GlcN are then condensed by LpxB to form disaccharide-1-P[18,19]. The 4' position of disaccharide-1-P is phosphorylated by LpxK, forming lipid IV_A[20,21], following which, the addition of two Kdo residues to the 6' position of lipid IV_A is mediated by KdtA[22]. The distal glucosamine unit is further

modified by the addition of a secondary lauroyl residue and a myristoyl residue by LpxL and LpxM, respectively, forming Kdo_2-lipid A[23]. The core oligosaccharides are then assembled onto lipid A, residing on the cytoplasmic surface of the inner membrane, with the help of several membrane-associated glycosyltransferases, forming core-lipid A. This product sits in the inner membrane facing the cytoplasm, where it is flipped to the periplasmic face of the inner membrane by MsbA, an essential inner-membrane ABC transporter[24,25].

The early stage O-antigen, residing on the cytoplasmic face on the inner membrane, is flipped to the periplasmic face of the inner membrane by Wzx[11]. The O-antigen is polymerized by Wzy and Wzz, forming O-antigen repeats. These are then transferred onto lipid A by WaaL, resulting in the formation of LPS. LPS is shuttled from the periplasmic face of the inner membrane to the periplasmic face of the outer membrane by cytosolic protein LptB, inner membrane proteins LptC, LptF, and LptG, and periplasmic protein LptA[26–28]. The final step involves the flipping of LPS into the outer leaftlet of the outer membrane, a step carried out by the outer membrane proteins LptD and LptE[11,29].

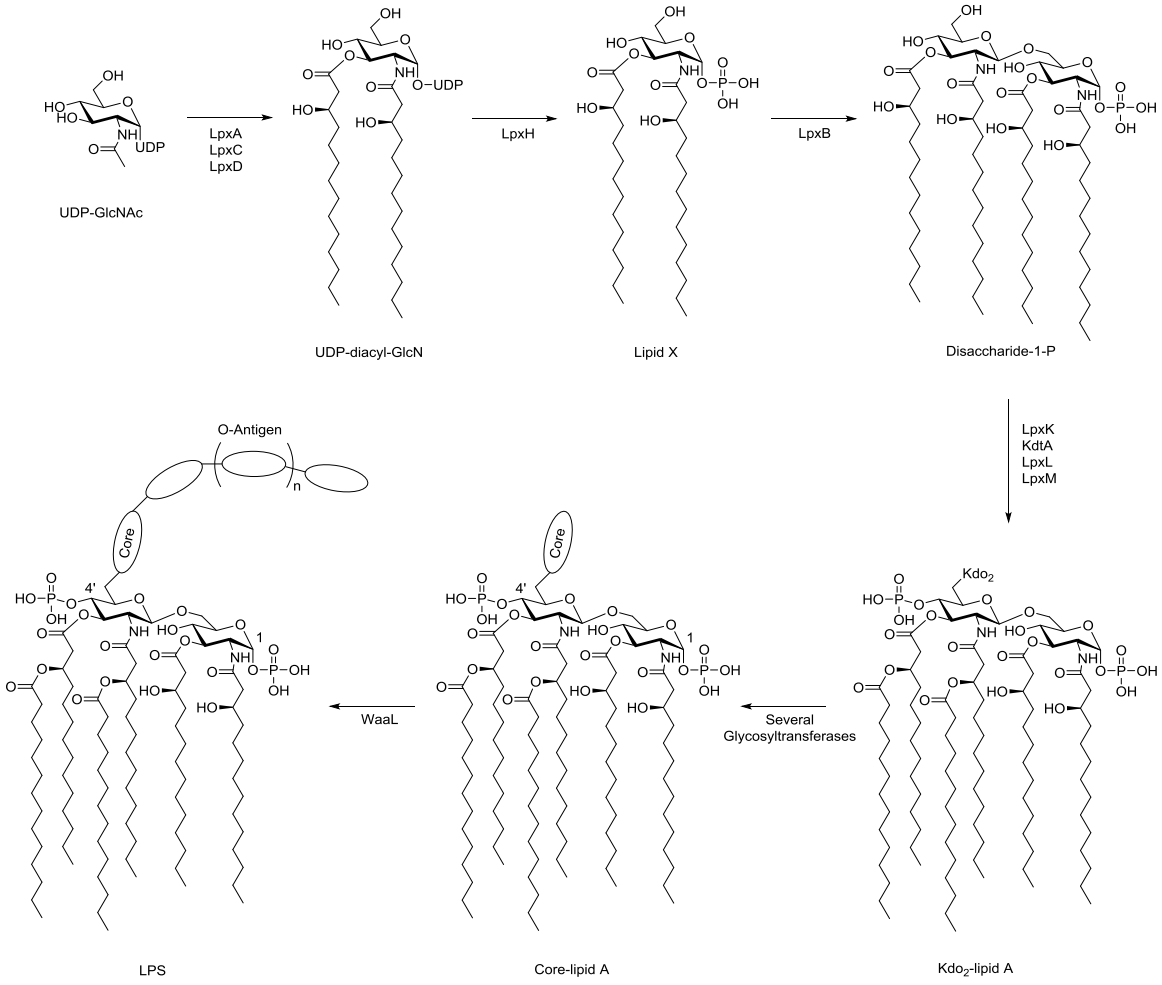

Figure 1-2: Synthesis of lipopolysaccharide in *E. coli*.
A simplified biosynthetic pathway of lipopolysaccharide in *E. coli*. The enzymes involved in reactions are displayed beside each arrow, indicating the flow of the reaction pathway. The structure of lipid A is shown with simplified core polysaccharides and O-antigens due to their variable compositions. Adapted from Wang *et al.*[11].

1.4 The polymyxins

1.4.1 Structure and properties of polymyxins

Polymyxins, discovered in 1947[30,31], are a class of cationic antimicrobial peptides (CAMPs) consisting of five different compounds, polymyxin A-E[32,33]. They are non-

ribosomal peptides produced by *Paenibacillus polymyxa* and play an essential role in the innate immunity of Gram-positive bacteria. These cationic polypeptides exhibit broad-spectrum antimicrobial activity against Gram-negative bacteria including most species of Enterobacteriaceae[34]. Of the polymyxins, only two are used in the clinic: polymyxin B and polymyxin E (colistin) (Figure 1-3). They share a similar decapeptide structure composed of a cyclic heptapeptide ring with a tripeptide side chain acylated by a fatty acid at the amino terminus[10]. They differ by one amino acid at position 6, where D-phenylalanine in polymyxin B is replaced by D-leucine in colistin. Polymyxins also contain cationic L-α-γ-diamino-butyric acid (L-α-γ-Dab) residues, resulting in a polycationic structure at pH 7.4 with a total charge of +5[10,32]. In addition, they contain two hydrophobic domains, the N-terminal fatty acyl chain and the D-Phe^{6}-L-Leu^{7} segment on polymyxin B or D-Leu^{6}-L-Leu^{7} on colistin, that contribute to the amphipathicity critical for antibacterial activity[35].

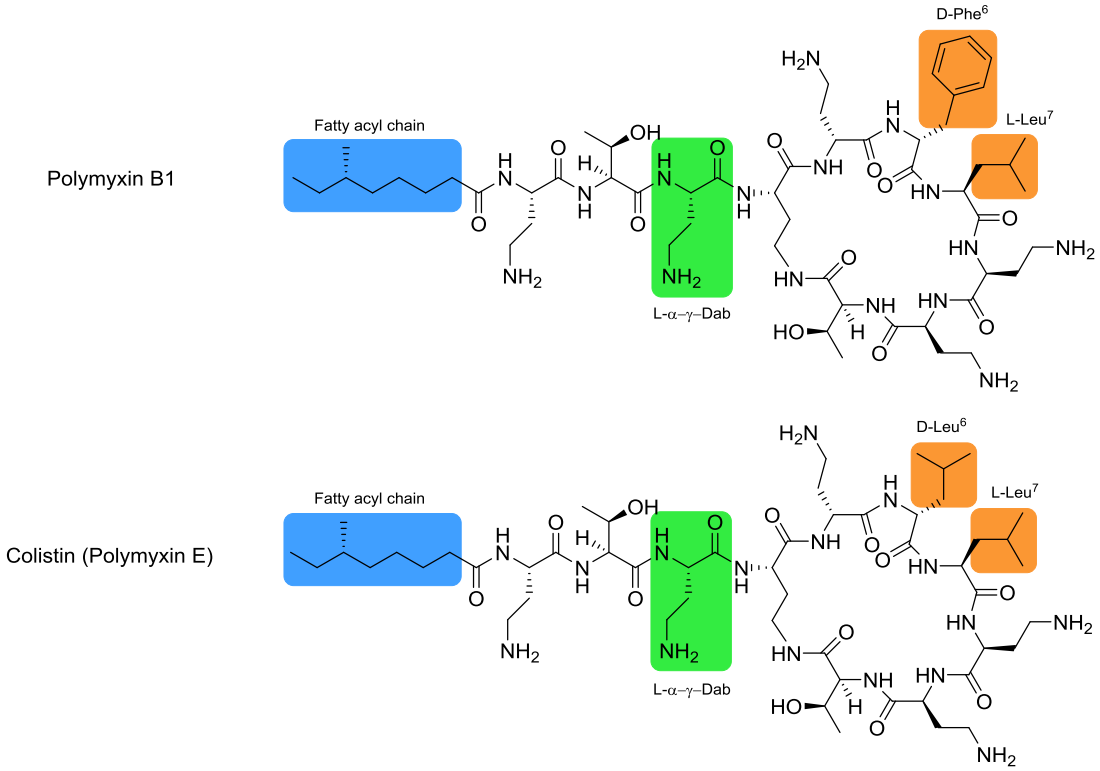

Figure 1-3: Structures of polymyxin B1 and colistin (polymyxin E).
Color coded diagram of polymyxin B1 (top) and colistin (bottom) depicting the fatty acyl chain (blue), L-α-γ-diamino-butyric acid residue (green), and D-Phe^6-L-Leu^7 segment on polymyxin B or D-Leu^6-L-Leu^7 on colistin (orange).

1.4.2 Mechanism of action of polymyxins

Polymyxins are thought to penetrate the outer membrane via self-promoted uptake where they then disrupt the inner membrane, resulting in cell lysis[10,32]. The initial target of polymyxins is the LPS component of the outer membrane[35]. Protonation of free γ-amines on positively charged L-α-γ-Dab residues on the polymyxin promotes electrostatic attraction to the negatively charged phosphate groups on lipid A, displacing Ca^{2+} and Mg^{2+} ions[35,36]. The N-terminal fatty acyl chain of the polymyxin then inserts into the outer membrane, followed by the D-Phe^6-L-Leu^7 (polymyxin B) or D-Leu^6-L-Leu^7

(colistin) segment[10]. This weakens the packaging of adjacent lipid A fatty acyl chains in the outer membrane, causing it to expand and form destabilized areas through which the polymyxin will cross[36,37]. The polymyxin then inserts into the phospholipid bilayer of the inner membrane, disrupting its structural integrity which leads to membrane lysis and cell death.

Although the membrane lysis pathway is accepted as the common mode of action of polymyxins, an alternative mechanism called the vesicle-vesicle contact pathway has also been proposed [38,39]. Following the insertion of polymyxin into the outer membrane, it is believed that polymyxin can induce lipid exchange between anionic phospholipids of the inner and outer membrane. This exchange of phospholipids between vesicles disrupts phospholipid composition, potentially causing an osmotic imbalance that leads to cell lysis. Another alternate mechanism of action is the hydroxyl radical pathway, where polymyxins may cause cell death by inducing the formation of reactive oxygen species such as superoxide (O_2^-), hydrogen peroxide (H_2O_2), and hydroxyl radicals ($^{\bullet}OH$) that damage DNA, lipids, and proteins[40,41].

1.4.3 Clinical use of polymyxins

Polymyxin B can be administered parenterally, intrathecally, or topically as polymyxin B sulfate, whereas colistin is available in two forms: colistin methanesulfonate (CMS), a sulfomethylated inactive pro-drug, for parenteral administration and colistin sulfate for oral or topical administration[42]. Additionally, both polymyxin B and CMS can be administered via inhalation.

The clinical experience with polymyxin B is less established than that of CMS. A global survey on the use of polymyxins was analyzed to show that out of 284 respondents from 56 countries; only 1.4% reported experience with polymyxin B, compared to the 50% who have used CMS[42]. Several studies have demonstrated that CMS has acceptable efficacy and toxicity when used in high-dose, extended interval treatment regimens[43–45], and that renal functions of patients returned to normal following the termination of treatment with CMS[45].

Combination therapy of polymyxins with other antibiotics such as rifamycins and carbapenems in Gram-negative bacteria has been reported to show synergy *in vitro*, although the clinical efficacy of polymyxin combination therapy remains to be proven[42]. One study involving 251 patients with MDR *Acinetobacter baumannii* bloodstream infections showed that colistin combination therapy significantly lowered patient mortality and showed higher bacteriological eradication[46], although additional future studies on polymyxin combination therapies *in vivo* are required to come to a final verdict.

1.4.4 Toxicity of polymyxins

Shortly after their discovery, the polymyxins were used clinically to treat Gram-negative infections via parenteral administration[10]. Following the use of polymyxin B and colistin for two decades, reports emerged regarding the severe nephrotoxicity and neurotoxicity associated with these antibiotics[33,47–49].

Polymyxin-induced nephrotoxicity has been shown to affect the proximal and distal tubules of the kidney, and is associated with the aggregation of polymyxins that results in apoptosis and necrosis of kidney tubular cells[44]. Following tubular uptake and accumulation, the polymyxins induce a decrease in antioxidant systems (including glutathione, catalase, and superoxide dismutase), mitochondrial dysfunction, cytochrome *c* release, increases in apoptosis inducing factor, and generation of reactive oxygen species that result in cell apoptosis and necrosis. Complications with polymyxin-related nephrotoxicity can cause increased serum creatinine and blood urea nitrogen levels, decreased creatinine clearance, as well as hematuria (presence of blood in urine) and proteinuria (presence of excess proteins in urine)[44]. A study conducted by Abdelraouf *et al.*[50] reports that the uptake of polymyxin B into renal cells is a non-passive process and that frequent dosing is associated with an earlier onset of nephrotoxicity. This may be overcome by administering the drug in a single dose that saturates the uptake, resulting in less accumulation of the drug in the kidney, versus fractionalized administration that results in repeated exposure to lower drug concentrations and therefore more drug uptake into the kidney cells. Indeed, the nephrotoxicity arising from colistin methanesulfonate use is more prevalent than that of polymyxin B[51,52], although the reasons for this are unclear.

Recent studies report a low overall incidence of neurotoxicity related to polymyxin B and colistin treatment, between 0-7%[42,44]. The neurotoxic effects include paresthesia (a burning or prickling sensation), ataxia (loss of full control of bodily movements), dizziness, psychosis, and seizures[33,42]. In more severe cases, neuromuscular

blockade can occur due to the inhibition of acetylcholine receptors or prevention of acetylcholine release, resulting in respiratory failure.

As a result of this toxicity and the availability of less toxic alternatives, the clinical use of polymyxins was halted in the 1980s[10], when treatment regimens were not well optimized. However, the increase in resistance to most classes of antibiotics in Gram-negative bacteria, especially *Pseudomonas aeruginosa*, *Acinetobacter baumannii*, and *Klebsiella pneumoniae*, as well as a shortage of new antibiotics, has renewed interest in polymyxins[35,53]. Compared with older recommended doses, current dosing of polymyxins improves the cure rate without significantly increasing the rate of polymyxin-induced toxicity[44], however, concerns regarding toxicity still remain and polymyxins need to be further characterized and optimized for clinical use.

1.4.5 Polymyxin derivatives

The toxicity surrounding the use of polymyxins has sparked interest in the development of polymyxin analogues that possess the same potent antibacterial activity but have attenuated toxicity. There has been extensive work done to characterize the structure-function relationship of polymyxins and to develop potential replacements with an improved therapeutic index[35,53]. Medicinal chemistry strategies for improving the polymyxins have included modifications to the length and size of the N-terminal fatty acyl chain, the L-α-γ-Dab residues and amino acid substitutions, the D-Phe^6-L-Leu^7 or D-Leu^6-L-Leu^7 motif, the size of the cyclic peptide ring, and the length of the N-terminal tripeptide side chain.

The reduction of nephrotoxicity is the main target for improving the polymyxin class of antibiotics[53], and most efforts to develop these new polymyxins are not employing a prodrug approach. Some of the novel synthetic variants of polymyxin are prepared with a total synthesis approach using solid-phase peptide synthesis allowing for modification of the core heptapeptide, or through semi-synthetic modification using protecting and deprotecting strategies allowing for modification of the linear tripeptide and the N-terminal fatty acyl chain.

One analogue, SPR741[53] (Figure 1-4), has a cyclic core identical to polymyxin B but contains an N-acetyl-threonine-D-serine side chain and therefore only has three positive charges compared to the five positive charges of polymyxin B. SPR741 has poor antibiotic activity, but retains the ability to synergize with rifampicin, clarithromycin, and azithromycin against *E. coli*, *K. pneumoniae*, and *A. baumanii*. In rats, renal clearance of SPR741 was also 4000-fold higher than colistin and it was not associated with nephrotoxicity when dosed up to 60 mg/kg in Cynomolgus monkeys compared to polymyxin B at 12 mg/kg which demonstrated nephrotoxicity.

Another analogue, FADDI-002[53] (Figure 1-4), consists of a polymyxin B backbone with an L-octyl-glycine residue at position 7 in addition to an *n*-octanoyl N-terminus. This compound was shown to kill polymyxin resistant strains of *Pseudomonas* and *Acinetobacter* at 2-4 μg/mL and 2-16 μg/mL concentrations, respectively, compared to 32->32 μg/mL and 8-128 μg/mL for treatment with polymyxin B. In addition, FADDI-002 showed a 2.6 $\log_{10}$ reduction in *P. aeruginosa* cell count 24 hours post infection

compared to a 0.7 $\log_{10}$ reduction observed with colistin. Although, these compounds showed high human plasma protein binding at 97% compared to 51% for polymyxin B.

Therefore, the development of polymyxin derivatives may produce a safer antibiotic that is effective at combating Gram-negative bacterial infections, although care should be taken as certain modifications that may attenuate the toxicity of the polymyxin may also modify the antimicrobial activity, pharmacodynamic or pharmacokinetic properties[35,53].

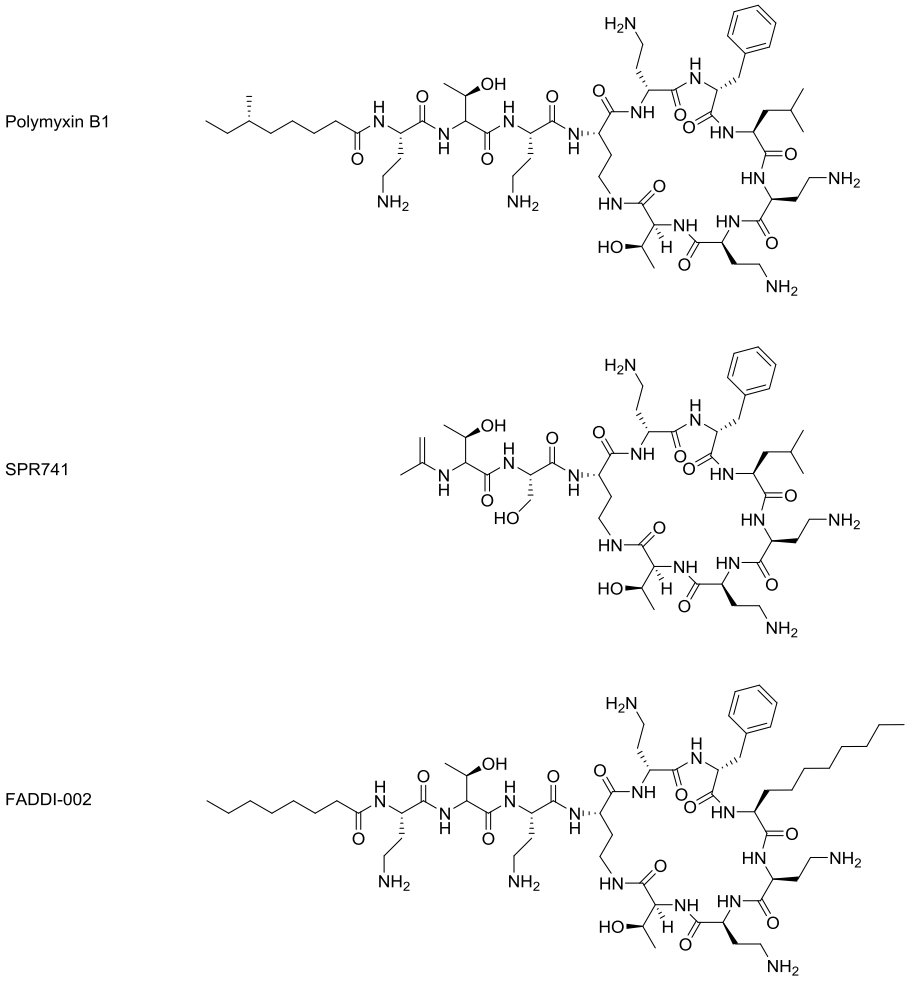

Figure 1-4: Polymyxin derivatives SPR741 and FADDI-002.
Top. Polymyxin B1. *Middle.* SPR741 has a cyclic core identical to polymyxin B but contains an N-acetyl-threonine-D-serine side chain. *Bottom.* FADDI-002 consists of a polymyxin B backbone with an L-octyl-glycine residue at position 7 in addition to an *n*-octanoyl N-terminus.

1.5 Resistance to polymyxins

With the reintroduction of polymyxins into the clinic, many antibiotic resistant infections could be treated effectively. These potent antibiotics, commonly referred to as antibiotics of last resort, were used successfully to treat MDR bacteria such as *Salmonella enterica*, *Pseudomonas aeruginosa*, *Acinetobacter baumannii*, *Klebsiella pneumoniae*,

and *Escherichia coli* that did not respond to other antibiotic therapies[54]. But, as with many of the antibiotics discovered to date, resistance to polymyxins closely followed. The last two decades have presented numerous reports regarding polymyxin resistance in the clinic worldwide[55], including resistance in bacteria which were normally susceptible to these antibiotics[54]. The current susceptibility breakpoints for polymyxin B and colistin are available from the Clinical and Laboratory Standard Institute (CLSI), but only the susceptibility breakpoint for colistin is available from the European Committee on Antimicrobial Susceptibility Testing (EUCAST), and these are summarized in Table 1-1**.**

	CLSI[56]		**EUCAST**[57]	
Microorganism	**Polymyxin B**	**Colistin**	**Polymyxin B**	**Colistin**
Pseudomonas spp.	8	8	-	4
Acinetobacter spp.	4	4	-	2
Enterobacteriaceae	-	-	-	2

Table 1-1: Susceptibility breakpoints of polymyxin B and colistin recommended by the Clinical and Laboratory Standard Institute and the European Committee on Antimicrobial Susceptibility Testing. CLSI: Clinical and Laboratory Standard Institute; EUCAST: European Committee of Antimicrobial Susceptibility Testing.

Resistance to polymyxins occurs through various mechanisms, the most common involving the two component regulatory systems PhoP-PhoQ and PmrA-PmrB that result in the modification of LPS by the addition of phosphoethanolamine or 4-amino-4-deoxy-L-arabinose to the phosphate groups on lipid A[10,11,54]. Additionally, less common modifications involving the addition of acyl chains to lipid A or mutations in genes responsible for the biosynthesis of LPS have also been characterized to confer polymyxin resistance[58–61].

1.5.1 Aminoarabinose transferases

Aminoarabinose transferases, such as ArnT, catalyse the addition of a positively charged 4-amino-4-deoxy-L-arabinose (L-Ara4N) onto the 1- and 4'-phosphate headgroups of lipid A, producing L-Ara4N-Lipid A (Figure 1-5)[62]. The L-Ara4N is provided by the lipid carrier undecaprenyl phosphate and the reaction is catalyzed on the periplasmic surface of the inner membrane by an integral membrane lipid-to-lipid glycosyltransferase.

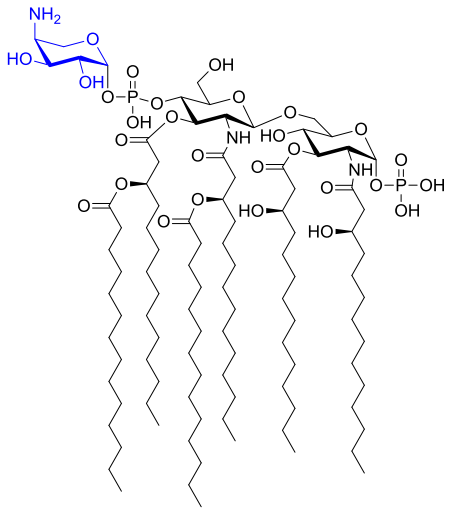

Figure 1-5: Lipid A modified with 4-amino-4-deoxy-L-arabinose on the 4'-phosphate.
The addition of 4-amino-4-deoxy-L-arabinose (in blue) onto the 1- or 4'-phosphate groups of lipid A is catalyzed by aminoarabinose transferases such as ArnT.

The addition of this positively charged residue reduces the negative charge of the outer membrane, resulting in a decreased electrostatic attraction to positively charged L-α-γ-Dab residues on polymyxin, which is believed to be the most important aspect of polymyxin bioactivity[35]. The addition of L-Ara4N also decreases the dependency of LPS

on divalent cation cross-bridging for stabilization, blocking the self-promoted uptake of polymyxins[10,35,63].

Traditionally, lipid A modifications such as the addition of L-Ara4N are chromosomally encoded, involving two component regulatory systems PhoP-PhoQ and PmrA-PmrB that respond to environmental signals such as low pH or Mg^{2+} and sub-inhibitory concentrations of cationic antimicrobial peptides (CAMPs)[10,34]. During times of cell stress, PhoQ, an inner-membrane sensor kinase, phosphorylates the cytoplasmic regulator PhoP, leading to the activation of PmrA-PmrB via PhoP-activated PmrD protein that phosphorylates PmrA[10,35]. This results in the transcription of PmrA-activated genes whose products are necessary for the covalent modification of phosphate groups on lipid A. Mutations in these two component regulatory systems have been reported in *S. enterica*, *E. coli*, *K. pneumoniae*, *A. baumanii*, and *P. aeruginosa*[64–67], and usually result in the constitutive expression of lipid A modifying enzymes that produce the polymyxin resistant phenotype[10,34].

1.5.2 Phosphoethanolamine transferases

Phosphoethanolamine (PEtN) transferases, such as MCR-1, catalyze the addition of a PEtN residue onto the 1- or 4'-phosphate of lipid A, producing PEtN-Lipid A[68,69] (Figure1-6). The PEtN residue is provided by phosphatidylethanolamine, a lipid commonly found within the inner membrane of Gram-negative bacteria, and the reaction is catalyzed on the periplasmic surface of the inner membrane by an integral membrane protein. The reaction mechanism for this process is yet to be understood[70].

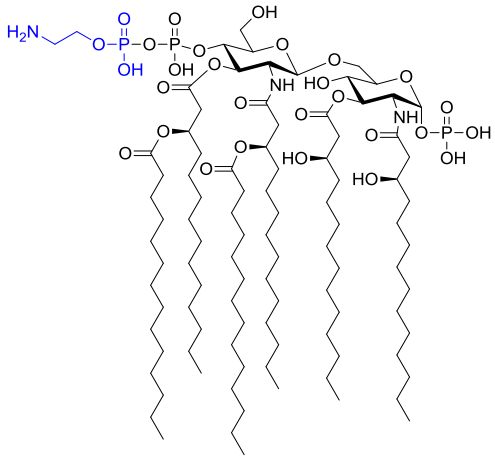

Figure 1-6: Lipid A modified with phosphoethanolamine on the 4'-phosphate.
The addition of phosphoethanolamine (in blue) onto the 1- or 4'-phosphate groups of lipid A is catalyzed by phosphoethanolamine transferases such as MCR-1.

The addition of this residue is also reported to reduce the negative charge of the outer membrane, decreasing the electrostatic attraction of positively charged L-α-γ-Dab residues on polymyxin[35,54]. The presence of PEtN still provides resistance to CAMPs and decreases the dependency of the outer membrane on divalent cations for cross-bridging and stabilizing LPS in low Mg^{2+} conditions[12,71]. As with the aminoarabinose transferases, the addition of PEtN to lipid A is also carried out by enzymes controlled by the PhoP-PhoQ and PmrA-PmrB two component regulatory systems, with the exception of mobile colistin resistance PEtN transferases such as the MCR enzymes that reside on plasmids.

1.5.3 Palmitoyl transferases

Palmitoyl transferases, such as PagP, catalyse the addition of a palmitate residue in acyloxyacyl linkage at the 2 position of lipid A, producing hepta-acylated lipid A

(Figure 1-7)[59,60]. The palmitate is provided by a phosphoethanolamine acyl donor and the reaction is catalyzed in the outer membrane by a membrane bound palmitoyl transferase[58].

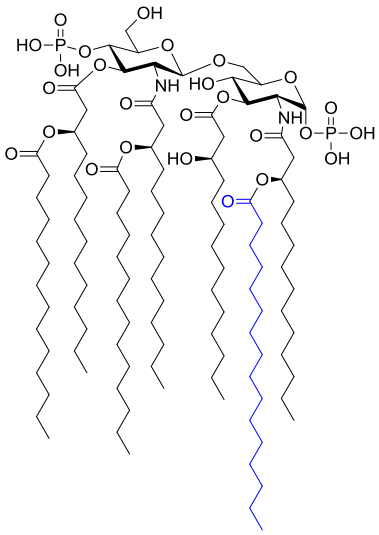

Figure 1-7: Lipid A modified with the addition of palmitate to the acyl chain at position 2.
The addition of palmitate (in blue) to the acyl chain at position 2 via acyloxyacyl linkage resulting in hepta-acylated lipid A is catalyzed by palmitoyl transferases such as PagP.

The addition of this palmitoyl ($C_{16:0}$) residue to the acyl chain of lipid A protects bacteria from CAMPs, likely due to increased van der Waals forces within the lipid bilayer that alter membrane fluidity and prevent CAMP insertion and further membrane disruption[58,60]. Indeed, the expression of PagP is mediated by the PhoP-PhoQ two component regulatory system in the presence of CAMPs. PagP-independent acylation of lipid A has also been observed in *A. baumannii*, in which acetyltransferases $LpxL_{Ab}$ and $LpxM_{Ab}$ transfer one and two lauroyl ($C_{12:0}$) acyl chains, respectively, onto lipid A during its biosynthesis, forming hepta-acylated lipid A[58].

1.5.4 LPS mutants

In rare instances, it has been reported that *A. baumannii* can become resistant to polymyxins due to the complete loss of LPS production[61,72,73]. The absence of LPS prevents the interaction of polymyxins with the outer membrane, giving rise to very high resistance profile[72]. Deletions, point mutations, or insertions have been responsible for the disruption of the first three genes in the lipid A biosynthetic pathway, *lpxA*, *lpxC*, *lpxD*. Although, these mutants tend to suffer from impaired growth and protein expression, as well as decreased virulence.

1.6 The discovery and dissemination of MCR-1

Previously, chromosomally-encoded PEtN transferases have been observed to be under the control of the PhoP-PhoQ and PmrA-PmrB pathway[71], until the recent discovery by Liu *et al.* that documented the emergence of a plasmid-mediated polymyxin resistance mechanism catalyzed by a PEtN transferase enzyme called MCR-1[34].

MCR-1 was identified in China during routine surveillance of antimicrobial resistance in *E. coli* isolated from food animals[34]. The gene was identified in 15% of *E. coli* isolates from raw meat samples, 21% from animals, and 16% from hospitalized patients in China from 2011-2014[34]. MCR-1 was proposed to be an integral inner membrane protein with a transmembrane region consisting of 5 α-helices and a periplasmic C-terminal catalytic domain, consistent with other known PEtN transferases such as *Nm*EptA from *Neisseria meningitidis* and EptC from *Campylobacter jejuni*. The crystal structure of the MCR-1 C-terminal domain revealed a confirmation similar to

*Nm*EptA and EptC (Figure 1-8), where the presence of Zn^{2+} ions and conserved residues suggest that the enzyme functions by a similar mechanism[68,74,75].

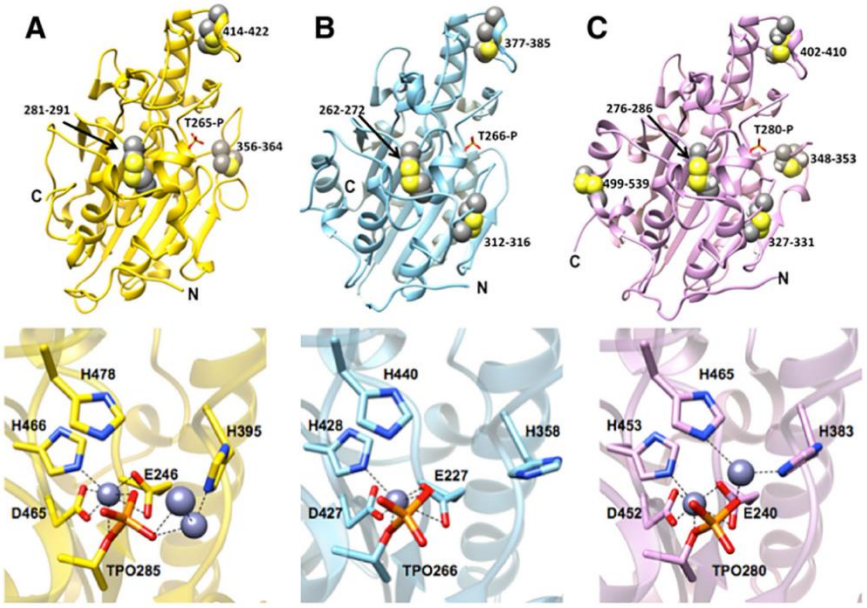

Figure 1-8: Crystal structures of MCR-1, EptC, and *Nm*EptA catalytic domains.
Top. The catalytic domains of MCR-1 (A), EptC (B), and *Nm*EptA (C) share similar tertiary structures as well as an active-site threonine in its phosphorylated form. Disulfide bonds are shown as space-filling spheres. *Bottom.* The active site residues are shown as stick models with Zn^{2+} atoms (blue spheres). The MCR-1 Zn^{2+} atom coordinated by phosphothreonine-285, E246, D465 and H466 is conserved in EptC and *Nm*EptA. This figure was acquired from a study by Stojanoski *et al.*[68] and used under the Creative Commons Attribution 4.0 International License (https://creativecommons.org/licenses/by/4.0/).

The plasmid on which *mcr-1* was identified, pHNSHP45, has a high conjugation rate at a frequency of 10^{-1} to 10^{-3} cells per recipient cell[34]. This is problematic due to the ability of Gram-negative organisms to readily take up foreign DNA, and a plasmid-mediated resistance mechanism to one of the most potent classes of antibiotics has the potential to create an enormous impact on the future use of polymyxin as an antibiotic[71,76]. In addition, the *mcr-1* gene was located downstream of an insertion sequence[34], which

indicates that horizontal gene transfer may have played a role in the acquisition of *mcr-1* by *E. coli*.

The previous year has seen an increase in surveillance for polymyxin resistance due to the discovery of *mcr-1*, and many of the resistant isolates identified came from food and animals, as well as a few human isolates[77]. The spread of *mcr-1* via horizontal gene transfer to other MDR bacteria has been observed[78], posing a threat to the longevity of polymyxins in the clinic. Additionally, *mcr-1* has been identified in *E. coli*, *S. enterica*, *K. pneumoniae*, *E. aerogenes*, and *E. cloacae*[34,77,79,80], and one report suggests that the gene has been identified in at least 16 countries[81]. Although the approximate emergence of *mcr-1* is not known as it has remained largely undetected until recently, one study identified three *mcr-1*$^{+}$ *E. coli* isolates in China from the 1980s, when polymyxins were used in food-producing animals[82].

Two studies identified *mcr-1* in 13 of 105 polymyxin resistant isolates (12.4%) from calves and piglets in Belgium from 2011-2012[83], and in 106 of 517 extended-spectrum beta-lactamase-positive isolates (21%) from veal calves in France from 2005-2014[84]. Many carried resistance determinants to several antibiotics including trimethoprim, tetracyclines, aminoglycosides, sulfonamides, and β-lactams. More instances of *mcr-1* were identified in chicken *E. coli* isolates in China from 2004, 2006, and 2009-2014, where the frequency of occurrence rose from 6 of 115 isolates (5.2%) in 2009, to 29 of 114 isolates (25.4%) in 2013[82]. The *mcr-1* gene has also been identified in 2015 in a feline *E. coli* isolate which also carried the NDM-5 β-lactamase and was resistant to 17 different antibiotics including carbapenems, aminoglycosides,

tetracyclines, quinolones, and polymyxins[85]. This suggests that the prevalence of *mcr-1* in Gram-negative bacteria is increasing, and that the worldwide spread of *mcr-1* may be underestimated.

The *mcr-1* gene has been identified in 13 *E. coli* and 3 *K. pneumoniae* isolates from hospital inpatients from 2014, and the plasmid pHNSHP45 has been identified in 25 of 1738 isolates (1.44 % - 16 *E. coli*, 9 *K. pneumoniae*), suggesting the interspecies transfer of the plasmid identified by Liu *et al.*[86]. One study explored the number of polymyxin resistant *E. coli* clinical isolates obtained in Canadian hospitals from 2008 to 2015 and found that 12 of 5571 isolates (0.2%) were resistant to polymyxin, two of which harbored *mcr-1* (0.04%)[87]. The *mcr-1* gene has also been identified in an *E. coli* isolate obtained from a human wound infection which carried the KPC-2 β-lactamase[78], an isolate cultured in 2015 from the urine of an 83-year-old man admitted to hospital for diverticulitis[88], and in 2016 from the urine of a 49-year-old female with a urinary tract infection[89]. These data suggest that although the incidence of *mcr-1* is currently not high, it has spread into Gram-negative bacteria associated with human infections, which will create a greater cause for concern as MDR pathogens carrying *mcr-1* emerge.

As a proof of concept, Liu *et al.*[90] investigated whether *mcr-1* would affect colistin susceptibility in clinical strains of the Gram-negative ESKAPE (*Enterococcus faecium*, *Staphylococcus aureus*, *Klebsiella pneumoniae*, *Acinetobacter baumannii*, *Pseudomonas aeruginosa*, and *Enterobacter* species) pathogens. They found that the introduction and expression of *mcr-1* was able to confer resistance to colistin in *E. coli*, *K. pneumoniae,* and *A. baumannii,* and only had a moderate effect in *P. aeruginosa,* despite

the PEtN modification being present in all four species. These findings portray the possibility of the dissemination of *mcr-1* into MDR ESKAPE pathogens that can stress the future use of polymyxins as an effective therapeutic agent.

To date, six variants of *mcr-1* that differ by one amino acid have been reported or annotated in the GenBank Database; one in KPC-3-producing *K. pneumoniae*, four in *E. coli*, and another in *S. enterica* serovar Typhimurium[91]. In addition, a second and third plasmid-mediated polymyxin resistance gene, *mcr-2* and *mcr-3*, have been identified[92,91]. The *mcr-2* and *mcr-3* genes show a 77.3% and 45.0% nucleotide identity to *mcr-1*, respectively, which translates to an 81.0% and 32.5% amino acid identity to MCR-1[90–92]. The *mcr-3* gene exhibits a 47.0% nucleotide identity sequence to *mcr-2*, which translates to a 31.7% amino acid identity to MCR-2.

1.7 Project objectives

The emergence of mobile polymyxin resistance enzyme MCR-1 presents an opportunity for horizontal transfer into MDR pathogens that may create a significant impact on the use of these last resort antibiotics. As previously mentioned, the use of antibiotic adjuvants is an avenue of research that is gaining traction as we look to extend the efficacy of our current arsenal of antibiotics. Therefore, the development or discovery of an antibiotic adjuvant for MCR-1 would be one method to extend the use of polymyxins within the clinic as the spread of this plasmid-mediated PEtN transferase continues.

The objective of this project was to conduct a cell-based high-throughput screen of an in-house Natural Product Library (NPL) consisting of Actinomycete-derived solid media extracts, which are rich in natural products, in order to search for an inhibitor of MCR-1. This project also aims to establish an *in vitro* enzyme assay that can be used for the detection of MCR-1 inhibitors. In addition, the structure-function relationship of MCR-1 is not well established, and this project aims to attain a better understanding of how the enzyme functions.

An inhibitor that is active against MCR-1 can relieve the potential pressure that the spread of this resistance determinant will put on the treatment of Gram-negative infections with polymyxins. In the presence of an inhibitor, MCR-1 will no longer be able to carry out the addition of PEtN onto lipid A, and the outer membrane will return to a wild-type state, allowing the interaction of polymyxin with lipid A, and the subsequent insertion of the polymyxin into the outer membrane, leading to cell death (Figure 1-9).

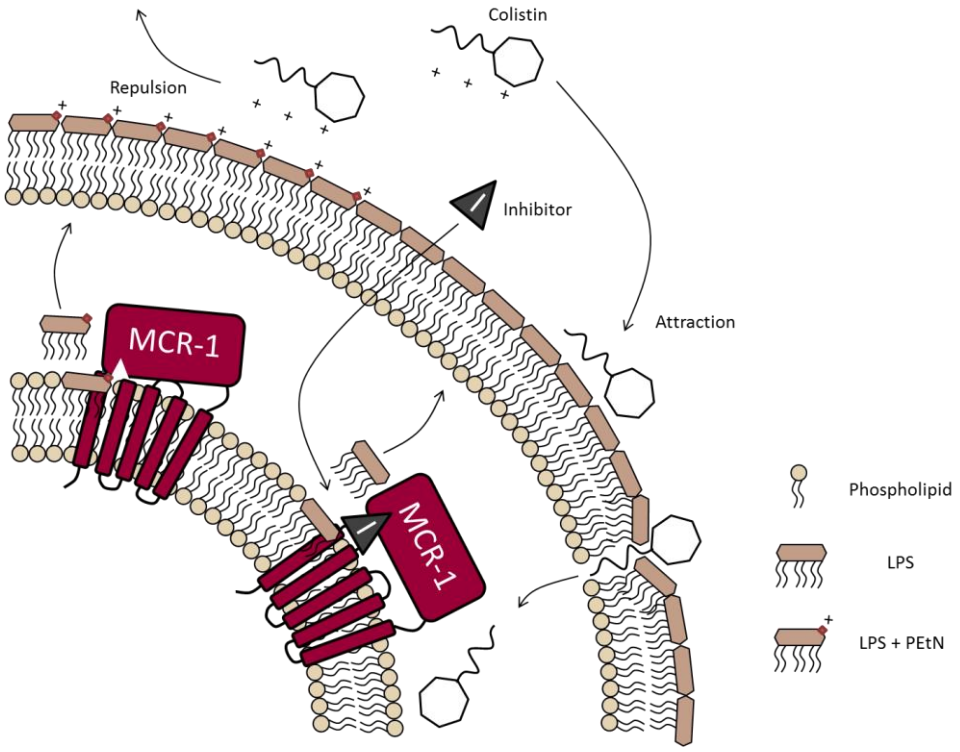

Figure 1-9: Outline of how an inhibitor of MCR-1 can rescue colistin antibiotic activity.
Cross section of a Gram-negative cell showing the inner membrane, periplasmic space, and the outer membrane. *Left.* MCR-1 modifies lipid A with a positively charged phosphoethanolamine (PEtN) residue, resulting in electrostatic repulsion of colistin, and therefore resistance. *Right.* In the presence of an inhibitor, MCR-1 no longer modifies lipid A, resulting in the electrostatic attraction of colistin to negatively charged lipopolysaccharide (LPS). This results in the self-promoted uptake of colistin and entrance into the cell, leading to cell death.

Although such an inhibitor will not alleviate other forms of polymyxin resistance, a recently discovered small molecule that downregulates the PmrA-PmrB pathway[93] and prevents lipid A modification can also be used to combat polymyxin resistance in cases where MCR-1 is absent. Targeting a common pathway for polymyxin resistance as well as an emerging mobile PEtN transferase with antibiotic adjuvants serves as an orthogonal method of controlling the outbreaks of polymyxin resistant bacteria and these options should be explored to their full potential.

Chapter 2.
Screening natural products for inhibitors of MCR-1

2.1 Introduction

The soil is considered to contain the greatest biodiversity of bacterial populations in the world[94]. Since the early 20th century, these soil microorganisms have been valued for their natural products, and have provided many important antibiotics and other bioactive compounds[95]. The use of natural products as inhibitors of antibiotic resistance determinants has been previously documented[7,9], and therefore the natural product landscape remains a point of interest to mine for an inhibitor of MCR-1.

In order to mine these natural products, the Wright Actinomycete Collection (WAC) was selected as a starting point. The WAC is a collection of predominantly Actinomycete strains isolated from soil samples gathered from various places around the world. The WAC is used to generate the Natural Product Library (NPL), which is a library consisting of WAC-derived solid media extracts dissolved in 100% DMSO, and is used in high-throughput screens to identify bioactive compounds of interest that have the potential to combat antibiotic resistance.

A system that has been recently developed to screen the NPL and assist with hit follow up is the Antibiotic Resistance Platform (ARP). The ARP is a system designed within the Wright Lab that can be used to identify new antibiotic adjuvants and dereplicate known naturally occurring antibiotic classes[8]. The process of dereplication is an important aspect of drug discovery, as identifying known chemical scaffolds produced by soil Actinomycetes is critical to reduce antibiotic rediscovery[96]. The platform consists

of a cell-based library into which are cloned individual and well characterized antibiotic resistance genes, all within the same genetic background of *E. coli* BW25113 Δ*tolC* Δ*bamB*. The use of this hyper-permeable and efflux deficient *E. coli* strain increases the sensitivity of the platform to antibacterial agents, reducing the obstacles associated with outer membrane permeability and compound efflux. The expression of antibiotic resistance genes within the ARP is controlled through the use of low copy pGDP plasmids, or through single copy gene integration into the bacterial chromosome. Further modulation of gene expression is accomplished through the use of a stronger constitutive P_{Bla} promoter (pGDP1, pGDP3) or weaker constitutive P_{Lac} promoter (pGDP2, pGDP4)[97]. Single constructs within the ARP may be used to screen the NPL for antibiotic adjuvants, and the resulting hits can be dereplicated in order to discount any antibiotic producers using the 96-well formatted ARP. The process of dereplication involves four steps (Figure 2-1): plating an Actinobacterium of interest on solid Bennett's media which is then overlaid with a mixed cellulose ester filter and incubated for 6 days at 30^{o}C, removing the filter and overlaying solid cation adjusted Mueller-Hinton II broth and incubating overnight at 4^{o}C, pinning the 96-well formatted ARP onto the solid cation adjusted Mueller-Hinton II broth using sterile 96-well pinning tools, and incubating overnight at 37^{o}C to allow the *E. coli* ARP strains to grow. The plate is then visualized for growth and the antibiotic produced can be identified due to the substrate specificity of the resistance genes present in the ARP strains, and therefore the plate would show a reduction of antibacterial activity in the presence of that antibiotic's resistance element[8].

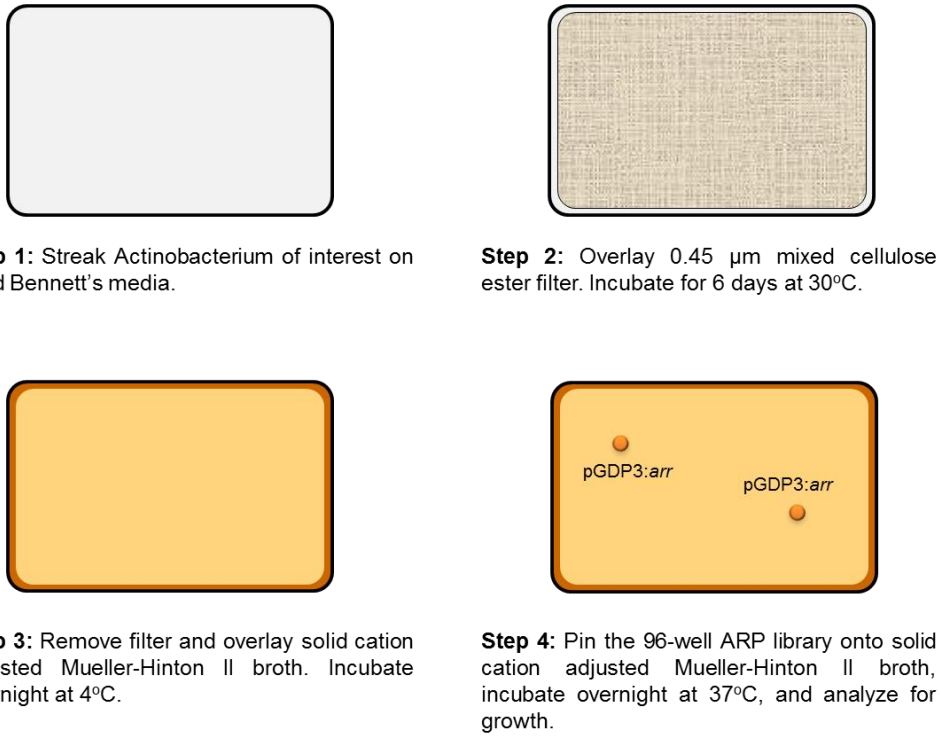

Figure 2-1: Dereplication via agar overlay method.
Dereplication allows for the identification of known antibiotics produced by an Actinobacterium of interest through the reduction of antibacterial activity in the presence of substrate specific antibiotic resistance genes present in the individual ARP strains.

In order to search for potential natural product inhibitors of MCR-1, the NPL was explored using high-throughput screening techniques. This chapter describes the creation of an *E. coli* strain harboring MCR-1 that was used to screen the NPL, as well as hit follow up and additional experiments characterizing the synergistic effects of colistin with other antibiotics.

2.2 Materials and Methods

2.2.1 Creating an *E. coli* screening strain expressing *mcr-1*

The *mcr-1* gene (GenBank accession number KP347127) was synthesized as a gBlocks® gene fragment with *Nco* I and *Xho* I restriction sites and an *Nde* I truncation site at amino acid position 179 (Integrated DNA Technologies, McMaster University). The gene fragment was cloned into pGDP1 and pGDP2 vectors[8] using restriction enzymes *Nco* I and *Xho* I (ThermoFisher) following the gBlocks® gene fragment manufacturer's protocol for cohesive-end cloning and verified by Sanger sequencing (MOBIX Lab, McMaster University). The pGDP1:*mcr-1* and pGDP2:*mcr-1* constructs were transformed into chemically competent *E. coli* BW25113 cells, plated on LB (LBL405; BioShop) agar supplemented with 50 μg/mL kanamycin (KAN201; BioShop), and incubated at 37^{o}C overnight.

2.2.2 Determining polymyxin susceptibility of the *E. coli* MCR-1 strain

Polymyxin B (P4932; Sigma) and colistin (C4461; Sigma) were dissolved in water and prepared in 2-fold serial dilutions, producing final concentrations ranging from 16 μg/mL to 0.0156 μg/mL. The minimum inhibitory concentrations (MIC) of polymyxin B and colistin were determined for *E. coli* BW25113-pGDP1:*mcr-1*, *E. coli* BW25113-pGDP2:*mcr-1*, and wild-type (WT) *E. coli* BW25113 using the microdilution broth method according to CLSI guidelines[98] with inoculum prepared using the colony suspension method. The strains were cultured in cation adjusted Mueller-Hinton II broth (CAMHB) (212322; Becton, Dickinson) at 37^{o}C with aeration (250 rpm) for 18 hours and

the absorbance at 600 nm was measured using a SpectraMax® Plus 384 Microplate Reader.

2.2.3 Determining sensitivity of *E. coli* expressing *mcr-1* to other cationic antimicrobial peptides

Cationic antimicrobial peptides (CAMPs) LL-37, 1026, 1036, and 1037 were obtained from the laboratory of Dr. Lori Burrows (McMaster University) in solution. The MICs of these CAMPs were determined for *E. coli* BW25113-pGDP2:*mcr-1* and wild-type (WT) *E. coli* BW25113 using the microdilution broth method according to CLSI guidelines[98], as previously described. The CAMPs were prepared as two-fold serial dilutions in water, producing final concentrations ranging from 128 μg/mL to 0.125 μg/mL. As a positive control, the MIC of colistin was also tested using a 2-fold serial dilution, producing final concentrations ranging from 16 μg/mL to 0.0156 μg/mL. The plates were incubated at 37°C with aeration (250 rpm) for 18 hours and the absorbance at 600 nm was measured using a SpectraMax® Plus 384 Microplate Reader.

2.2.4 Establishing screening conditions and determining the Z'

The screening conditions to identify compounds that inhibit MCR-1 were established based on the MIC data generated for *E. coli* BW25113-pGDP2:*mcr-1*. The colistin concentration for the screen was selected to be 3 μg/mL, ¾ of the MIC.

To determine the Z', a measure of the robustness of the screening conditions, a single colony of *E. coli* BW25113-pGDP2:*mcr-1* was used to inoculate 3 mL CAMHB

supplemented with 25 μg/mL kanamycin and a single colony of WT *E. coli* BW25113 was used to inoculate 3 mL CAMHB. Cultures were incubated overnight at 37°C with aeration (250 rpm), standardized to an OD_{625} of 0.1, and diluted 1/200 in CAMHB with the addition of colistin to a final concentration of 3 μg/mL in both cultures. A Beckman Biomek FX^P Laboratory Automation Workstation (Beckman Coulter) was used to dispense 49 μL of diluted *E. coli* BW25113-pGDP2:*mcr-1* culture into one half of a 384-well flat-bottom plate (3701; Corning), and 49 μL of diluted *E. coli* BW25113 culture into the remaining half of the 384-well flat-bottom plate. Each well was supplemented with an additional 1 μL of DMSO. The 384-well flat-bottom plate was incubated at 37°C with aeration (250 rpm) for 18 hours and the absorbance at 600 nm was measured using a Perkin Elmer EnVision 2102 Multilabel Plate Reader. The *Z'* was calculated according to the following formula[99]:

$$Z' = 1 - \frac{3SD\ of\ sample + 3SD\ of\ control}{|mean\ of\ sample\ - mean\ of\ control|}$$

2.2.5 Screening protocol and data analysis

A single colony of *E. coli* BW25113-pGDP2:*mcr-1* was used to inoculate 3 mL CAMHB supplemented with 25 μg/mL kanamycin and a single colony of WT *E. coli* BW25113 was used to inoculate 3 mL CAMHB. Cultures were incubated overnight at 37°C with aeration (250 rpm), standardized to an OD_{625} of 0.1, and diluted 1/200 in CAMHB with the addition of colistin to a final concentration of 3 μg/mL in both cultures. From the NPL, 7680 solid media extracts were screened in duplicate using a Beckman Biomek FX^P Laboratory Automation Workstation; 49 μL of diluted *E. coli* BW25113-

pGDP2:*mcr-1* culture was dispensed into the wells of a 384-well flat-bottom plate, followed by the addition of 1 μL of NPL extract. As a control, 49 μL of diluted *E. coli* BW25113-pGDP2:*mcr-1* and WT *E. coli* BW25113 cultures were dispensed into a subset of the wells of a 384-well flat-bottom plate, followed by the addition of 1 μL of DMSO. Plates were incubated at 37^{o}C with aeration (250 rpm) for 18 hours and the absorbance at 600 nm was measured using a Perkin Elmer EnVision 2102 Multilabel Plate Reader.

The data were normalized using the interquartile mean[100] and analyzed with TIBCO Spotfire. Screen hits were determined to be extracts that inhibited the normalized growth of *E. coli* BW25113-pGDP2:*mcr-1* to < 0.3826, a value below three times the standard deviation of the mean normalized growth of both replicates for all extracts screened. These hits were further compared to available NPL screening data for WT *E. coli* BW25113 and *E. coli* BW25113 Δ*tolC* Δ*bamB* strains in order to select hits which only inhibited growth of *E. coli* BW25113-pGDP2:*mcr-1* so that antibiotics found within the extracts could be avoided.

2.2.6 Preparation of Actinobacteria solid media extracts

Actinobacteria from the WAC corresponding to hits from the NPL screen were cultured in 3 mL *Streptomyces* Antibiotic Activity Media (SAM) (Appendix 1) for 6 days at 30^{o}C. Following incubation, 100 μL of the culture was applied as a lawn to the surface of solid Bennett's medium (Appendix 1)**,** which was then incubated at 30^{o}C for 6 days. The fermented solid Bennett's medium was pressed through a 60 mL syringe into 10 mL of 100% methanol, and incubated at 4^{o}C overnight on a shaking nutating mixer for a

minimum of 24 hours. The samples were filtered through a non-gauze milk filter (D110; KenAG) into clean glass test tubes and the solvent was evaporated in a Genevac HT-4X. The samples were dissolved in 1.5 mL 100% DMSO and incubated at room temperature for 24 hours. Following incubation, the DMSO and remaining organic matter was transferred into sterile 2 mL micro-centrifuge tubes containing one glass bead and vortexed for 5 minutes. The samples were incubated at room temperature for 24 hours, centrifuged at 17 100 g for 10 minutes, and stored at -20^{o}C.

2.2.7 Actinobacteria solid media extract assay with *E. coli* MCR-1 strain

A single colony of *E. coli* BW25113-pGDP2:*mcr-1* and WT *E. coli* BW25113 were used to inoculate 3 mL of LB, which were incubated overnight at 37^{o}C and then standardized to an OD_{625} of 0.1. Each extract was tested in duplicate against both *E. coli* strains in the presence and absence of ½ the colistin MIC for each strain (2 μg/mL and 0.125 μg/mL, respectively). The assay was conducted in a 96-well round-bottom plate (0877254; FisherScientific) where each well contained 10 μL of 10X colistin (20 μg/mL or 1.25 μg/mL) or water, 2 μL DMSO solid media extract, and 88 μL of diluted *E. coli* culture resulting in a final 1/200 dilution. The plates were incubated at 37^{o}C with aeration (250 rpm) for 18 hours and the absorbance at 600 nm was measured using a SpectraMax® Plus 384 Microplate Reader.

2.2.8 Dereplication of Actinobacteria via agar overlay

Actinobacteria from the WAC corresponding to hits from the NPL screen were cultured in 3 mL SAM for 6 days at 30°C. Following incubation, 200 µL of the culture was applied as a lawn onto the surface of 20 mL solid Bennett's medium in a rectangular Nunc™ OmniTray™ (264728; ThermoFisher). A piece of sterile 0.45 µm mixed cellulose ester filter paper (HAWP00010; EMD Millipore) was placed onto the surface and the plates were incubated at 30°C for 6 days. Following incubation, the filter paper was removed and 20 mL of CAMHB solid medium was applied onto the plate, which was then incubated at 4°C for 24 hours to allow for diffusion of compounds into the freshly overlaid medium. The previously prepared 96-well ARP library glycerol stock[8] was used to inoculate 100 µL CAMHB in a sterile 96-well round-bottom plate using a sterilized manual 96-well pinning tool, which was then incubated at 37°C overnight with aeration (250 rpm). Following incubation, the sterilized 96-well pinning tool was used to pin the ARP strains from liquid culture onto the surface of the overlaid OmniTrays. These pinned plates were incubated at 37°C for 18 hours, analyzed for growth, and imaged with an Epson Perfection V800 Photo Colour Scanner.

2.2.9 Antibiotic susceptibility testing of *E. coli* expressing *mcr-1* with sub-inhibitory colistin concentrations

Antibiotic stocks of chloramphenicol (3130; EMD Millipore) dissolved in water, spectinomycin dihydrochloride pentahydrate (S9007; Sigma) dissolved in water, hygromycin B (H3274; Sigma) dissolved in water, erythromycin hydrate (856193;

Sigma) dissolved in 25% DMSO in water, rifampicin (R3501; Sigma) dissolved in 25% DMSO in water, and clindamycin hydrochloride (PHR1159; Sigma) dissolved in 25% DMSO in water, were made at various concentrations and diluted 2-fold. Antibiotic susceptibility testing was performed in CAMHB using the microdilution broth method according to CLSI guidelines[98], with inoculum prepared using the colony suspension method. Plates were incubated at 37^{o}C with aeration (250 rpm) for 18 hours and the absorbance at 600 nm was measured using a SpectraMax® Plus 384 Microplate Reader. Strains of *E. coli* BW25113-pGDP2:*mcr-1*, WT *E. coli* BW25113, and a clinical MDR *E. coli mcr-1*$^{+}$ isolate were tested against several antibiotics in the presence and absence of sub-inhibitory concentrations of ½ MIC colistin.

2.2.10 Checkerboard MIC assay with polymyxin B nonapeptide and rifamycins

Prior to conducting checkerboard assays, the MIC of polymyxin B nonapeptide (PMBN) (P2076; Sigma) was determined for *E. coli* BW25113-pGDP2:*mcr-1* and WT *E. coli* BW25113 according to CLSI guidelines[98], as previously described. Checkerboard assays were performed in CAMHB in round-bottom 96-well plates. The assays were set up in a total volume of 100 μL per well, with 2-fold serial dilutions of PMBN in water, and rifampicin (R3501; Sigma), rifabutin, and rifapentine in 100% DMSO.

Overnight cultures of *E. coli* BW25113-pGDP2:*mcr-1* (supplemented with 2 μg/mL colistin) and WT *E. coli* BW25113 were inoculated in CAMHB from a single colony and incubated at 37^{o}C with aeration (250 rpm). The cultures were standardized to

an OD_{625} of 0.1 and diluted so that 90 μL was added into each well containing 5 μL colistin and 5 μL rifamycin, resulting in a 1/200 culture dilution. Plates were incubated at 37^{o}C with aeration (250 rpm) for 18 hours and the absorbance at 600 nm was measured using a SpectraMax® Plus 384 Microplate Reader.

2.3 Results

2.3.1 MCR-1 confers resistance to polymyxins

To examine whether expression of recombinant MCR-1 confers resistance to polymyxins, the MICs of polymyxin B and colistin were determined for *E. coli* BW25113-pGDP1:*mcr-1*, *E. coli* BW25113-pGDP2:*mcr-1*, and WT *E. coli* BW25113. The expression of *mcr-1* under the control of the stronger promoter in pGDP1 results in an MIC of 8 μg/mL for polymyxin B and colistin. The MIC of both polymyxin B and colistin for the pGDP2:*mcr-1* construct is 4 μg/mL, half of what was observed for the pGDP1:*mcr-1* construct, and consistent with the presence of a weaker promoter driving expression of *mcr-1* in pGDP2. The absence of the *mcr-1* resistance element in WT *E. coli* BW25113 results in a polymyxin B and colistin MIC of 0.25 μg/mL. Therefore, compared to the WT strain, the expression of *mcr-1* with the pGDP1 and pGDP2 vectors increases the cell's resistance to colistin 32-fold and 16-fold, respectively (Table 2-1).

Construct	MIC Polymyxin B (μg/mL)	MIC Colistin (μg/mL)
pGDP1:*mcr-1*	8	8
pGDP2:*mcr-1*	4	4
WT BW25113	0.25	0.25

Table 2-1: Polymyxin B and colistin MIC data for *E. coli* BW25113 expressing *mcr-1* and WT *E. coli* BW25113.
Minimum inhibitory concentration (MIC) data generated for polymyxin B and colistin tested against *E. coli* BW25113-pGDP1:*mcr-1*, *E. coli* BW25113-pGDP2:*mcr-1*, and WT *E. coli* BW25113. Experiments were conducted as per CLSI guidelines.

2.3.2 MCR-1 does not confer resistance to other cationic antimicrobial peptides (CAMPs)

To examine whether MCR-1 confers resistance to CAMPs other than polymyxin B and colistin, the MICs of CAMPs LL-37[101], 1026[101], 1036[101], and 1037[101] were determined for *E. coli* BW25113-pGDP2:*mcr-1* and WT *E. coli* BW25113. The MICs of LL-37, 1026, and 1036 were 32, 8, and 32 μg/mL, respectively, for both *E. coli* BW25113-pGDP2:*mcr-1* and WT *E. coli* BW25113. Testing CAMP 1037, the MIC was determined to be 8 μg/mL for *E. coli* BW25113-pGDP2:*mcr-1* and 4 μg/mL for WT *E. coli* BW25113. These results are summarized in Table 2-2 and indicate that MCR-1 is not able to confer significant resistance to the CAMPs tested.

CAMP	Sequence	*E. coli* Strain	MIC (μg/mL)
LL-37	LLGDFFRKSKEKIGKEFKR IVQRIKDFLRNLVPRTES	*E. coli* BW25113-pGDP2:*mcr-1*	32
		WT *E. coli* BW25113	32
1026	VQWRIRVRVIKK	*E. coli* BW25113-pGDP2:*mcr-1*	8
		WT *E. coli* BW25113	8
1036	VQFRIRVRIVIRK	*E. coli* BW25113-pGDP2:*mcr-1*	32
		WT *E. coli* BW25113	32
1037	KRFRIRVRV	*E. coli* BW25113-pGDP2:*mcr-1*	8
		WT *E. coli* BW25113	4

Table 2-2: MIC data of CAMPs for *E. coli* BW25113 expressing *mcr-1* and WT *E. coli* BW25113. Minimum inhibitory concentration (MIC) data generated for cationic antimicrobial peptides LL-37, 1026, 1036, and 1037 tested against *E. coli* BW25113-pGDP2:*mcr-1* and WT *E. coli* BW25113. Experiments were conducted as per CLSI guidelines.

2.3.3 Z' and screening data analysis

The robustness of the screening conditions was determined based on 192 samples with a positive signal (cell growth) and 192 samples with negative signal (cell death). The optical density measurements at 600 nm indicate a noticeable difference in growth between the *E. coli* BW25113-pGDP2:*mcr-1* strain and the WT *E. coli* BW25113 control in the presence of 3 μg/mL colistin. The Z' was calculated to be 0.75 (Figure 2-2), reflecting an excellent assay and acceptable screening conditions.

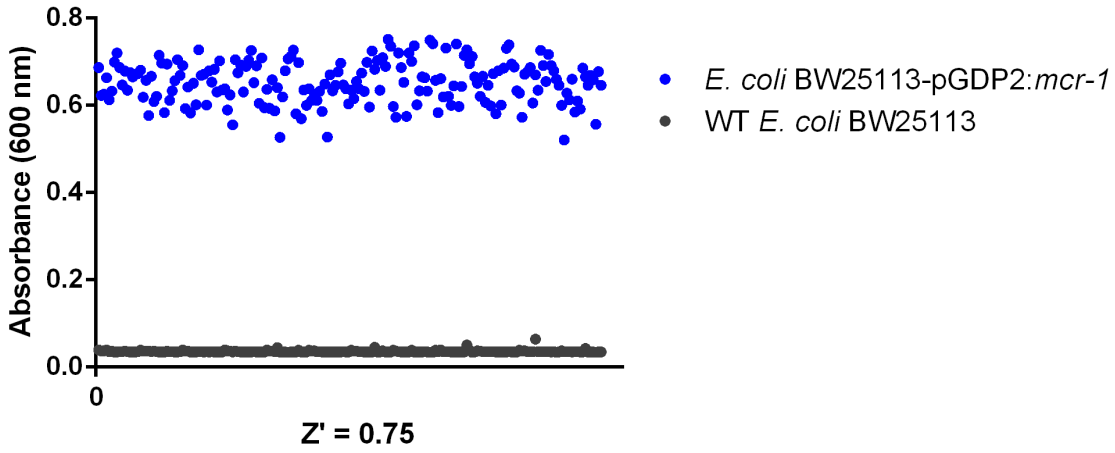

Figure 2-2: Z' for MCR-1 NPL screen at 3 µg/mL colistin.
The Z' test was conducted in a 384-well flat-bottomed plate, with half of the plate containing the positive signal (*E. coli* BW25113-pGDP2:*mcr-1* at 3 µg/mL colistin) and the other half containing the negative signal (*E. coli* BW25113 at 3 µg/mL colistin). The plate was incubated at 37°C for 18 hours with aeration (250 rpm) and the absorbance at 600 nm was measured. The Z' was determined to be 0.75.

The Natural Product Library was screened for inhibitors of MCR-1. The screening data collected for 7680 solid media extracts was normalized based on the interquartile mean, and analyzed with TIBCO Spotfire. Extracts that resulted in an average normalized growth value of both replicates to less than 0.3826 were identified as hits. This cutoff identified a total of 80 hits, a hit rate of 1.04%. These results were plotted as a replicate plot (Figure 2-3) and a histogram (Figure 2-4) to visualize both replicates of normalized growth as well as the number of hits that produced various values of normalized growth below the cutoff.

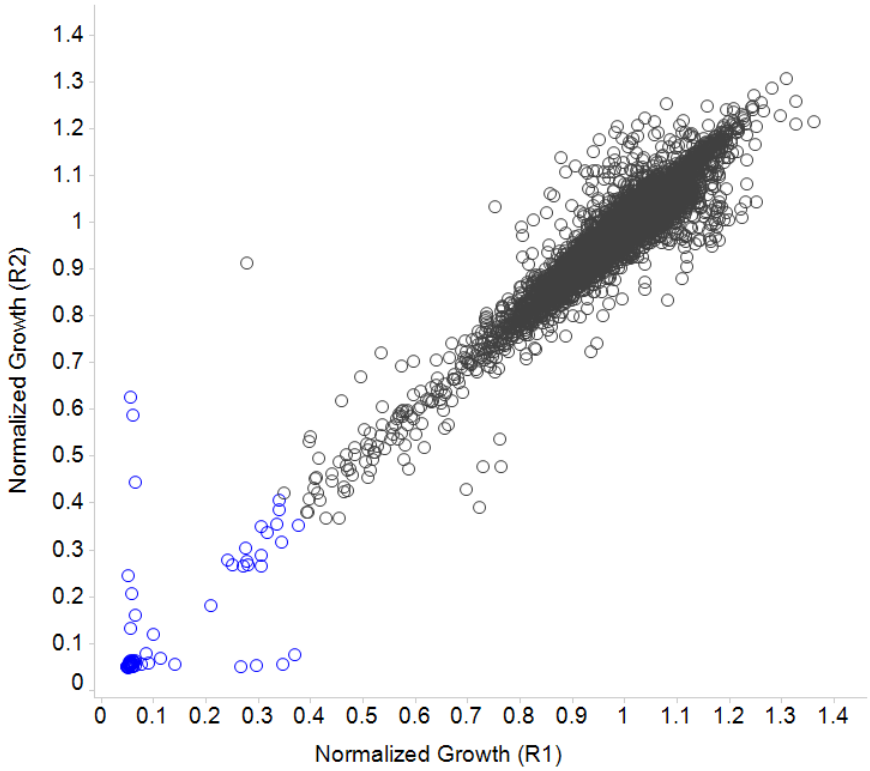

Figure 2-3: Interquartile mean normalized growth replicate plot of the MCR-1 NPL screen.
Screening data for both replicates of 7680 NPL extracts screened against *E. coli* BW25113-pGDP2:*mcr-1* at 3 µg/mL colistin were normalized based on the interquartile mean. The data were compiled and analyzed in TIBCO Spotfire. The blue color highlights hits whose average normalized growth value of two replicates falls below 0.3826.

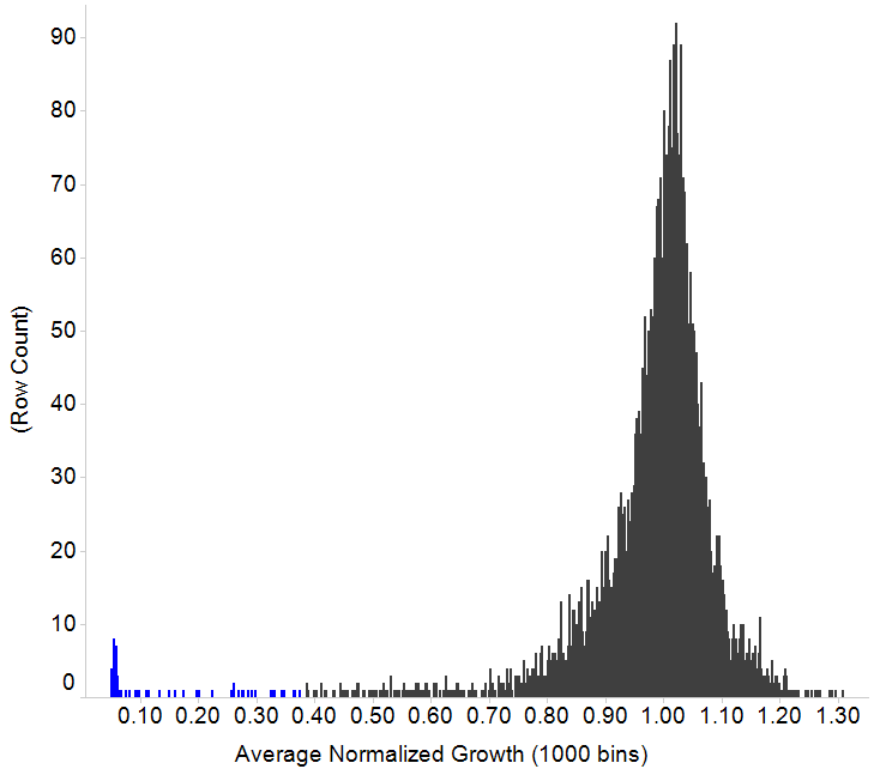

Figure 2-4: Interquartile mean normalized growth histogram of the MCR-1 NPL screen.
Screening data for both replicates of 7680 NPL extracts screened against *E. coli* BW25113-pGDP2:*mcr-1* at 3 µg/mL colistin were normalized based on the interquartile mean. For each extract tested, the average normalized growth of both replicates was plotted as a histogram to indicate the number of extracts (row count) that produced the various average normalized growth values. The average normalized growth was separated into 1000 bins and analyzed in TIBO Spotfire.

The data from resulting hits were compared with screening data available for WT *E. coli* BW25113 and *E. coli* BW25113 Δ*tolC* Δ*bamB* which were previously screened against the NPL in the absence of drug. Hits were narrowed down to include extracts that inhibited the growth of *E. coli* BW25113-pGDP2:*mcr-1* at 3 µg/mL colistin but had no growth inhibitory effects on WT *E. coli* BW25113 and *E. coli* BW25113 Δ*tolC* Δ*bamB*. Comparing the screening data to data generated for WT *E. coli* BW25113 revealed the hits that exhibited standalone antimicrobial activity. The hyper-permeable and efflux

deficient *E. coli* BW25113 Δ*tolC* Δ*bamB* strain is more sensitive to antibiotics that have weak activity against Gram-negative bacteria, and therefore it was possible to discount antibiotics found within these extracts that are likely to synergize with colistin, but could not initially pass through the outer membrane of WT *E. coli* BW25113. This narrowed down the data to 11 hits (WAC 2633, 4321, 2201, 4675, 8802, 7463, 6261, 7295, 6216, 7376, 2536), which were selected for further experiments.

2.3.4 Actinobacteria solid media extract assay with *E. coli* MCR-1

The solid media extracts isolated from WAC strains were tested against *E. coli* BW25113-pGDP2:*mcr-1* and WT *E. coli* BW25113 in the presence and absence of colistin at ½ MIC of each strain (Figure 2-5).

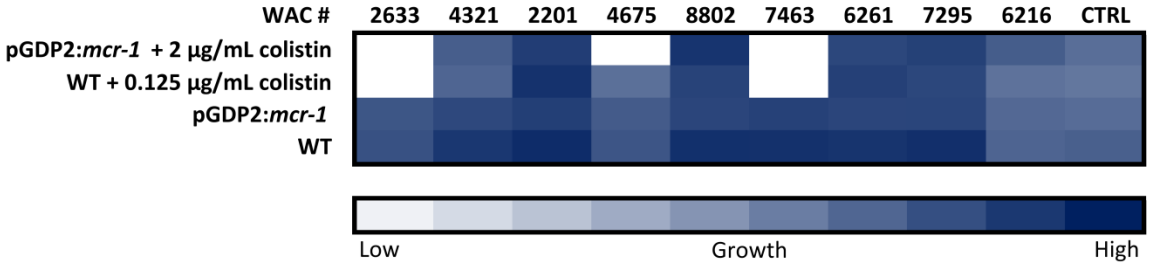

Figure 2-5: Solid media extract assay for *E. coli* BW25113-pGDP2:*mcr-1* and WT *E. coli* BW25113. Heat plot generated for solid media extracts of WAC strains (numbered) tested against *E. coli* BW25113-pGDP2:*mcr-1* and WT *E. coli* BW25113 in the presence and absence of colistin at ½ MIC. The blue color represents cell growth, and the white color represents no cell growth.

The solid media extracts tested did not inhibit the growth of *E. coli* BW25113-pGDP2:*mcr-1* or WT *E. coli* BW25113 in the absence of colistin. Extracts of WAC 4321, 2201, 8802, 6261, 7295, and 6216 did not show the ability to inhibit growth of either

strain of *E. coli* in the presence of ½ MIC colistin, and are henceforth referred to as false positives. The extracts from WAC 2633 and 7463 inhibited growth of *E. coli* BW25113-pGDP2:*mcr-1* at 2 μg/mL colistin and WT *E. coli* BW25113 at 0.125 μg/mL colistin, but did not inhibit growth of both *E. coli* strains in the absence of colistin, and therefore likely contain an unknown antibiotic. The solid media extract from WAC 4675 only inhibited the growth of *E. coli* BW25113-pGDP2:*mcr-1* at 2 μg/mL colistin, and did not inhibit the growth of WT *E. coli* BW25113 at 0.125 μg/mL colistin, or *E. coli* BW25113-pGDP2:*mcr-1* and WT *E. coli* BW25113 in the absence of colistin. Therefore, WAC 4675 was of interest as it potentially contained an MCR-1 inhibitor. The results from this assay are summarized in Table 2-3.

WAC #	Solid Media Extract Assay Result
2633	Unknown antibiotic
4321	False positive
2201	False positive
4675	Potential inhibitor
8802	False positive
7463	Unknown antibiotic
6261	False positive
7295	False positive
6216	False positive

Table 2-3: Summary of solid media extract assay.
Extracts from WAC 2633 and 7463 contained an unknown antibiotic, as evidenced by their ability to inhibit growth of *E. coli* BW25113-pGDP2:*mcr-1* and WT *E. coli* BW25113 at ½ MIC colistin. Extracts from WAC 4321, 2201, 8802, 6261, 7295, and 6216 were labelled as false positives because they did not show the ability to inhibit growth of either *E. coli* strain in the presence of ½ MIC colistin. Extract from WAC 4675 potentially contained an inhibitor as it only inhibited the growth of *E. coli* BW25113-pGDP2:*mcr-1* at ½ MIC.

The extracts from WAC 7376 and WAC 2536 were not tested in this assay, as these WAC strains were dereplicated and observed to produce antibiotics (see section 2.3.5).

2.3.5 Dereplication of Actinobacteria via agar overlay reveals many antibiotic producers

The 11 WAC strains that were narrowed down as hits from the MCR-1 screen were dereplicated using the ARP via agar overlay in order to discount any antibiotic producers (Figure 2-6). Stamping the ARP onto plates that were cultured with WAC 2633, 4321, 4675, 6261, and 6216 did not result in any visible *E. coli* growth, suggesting that they all are antibiotic producers. Dereplication of WAC 2201, 7463, and 2536 resulted in partial *E. coli* growth, and WAC 8802 resulted in full ARP *E. coli* growth. Dereplication of WAC 7295 and WAC 7376 resulted in the growth of an ADP-ribosyltransferase (pGDP3:*arr*) ARP strain which confers resistance to rifamycins.

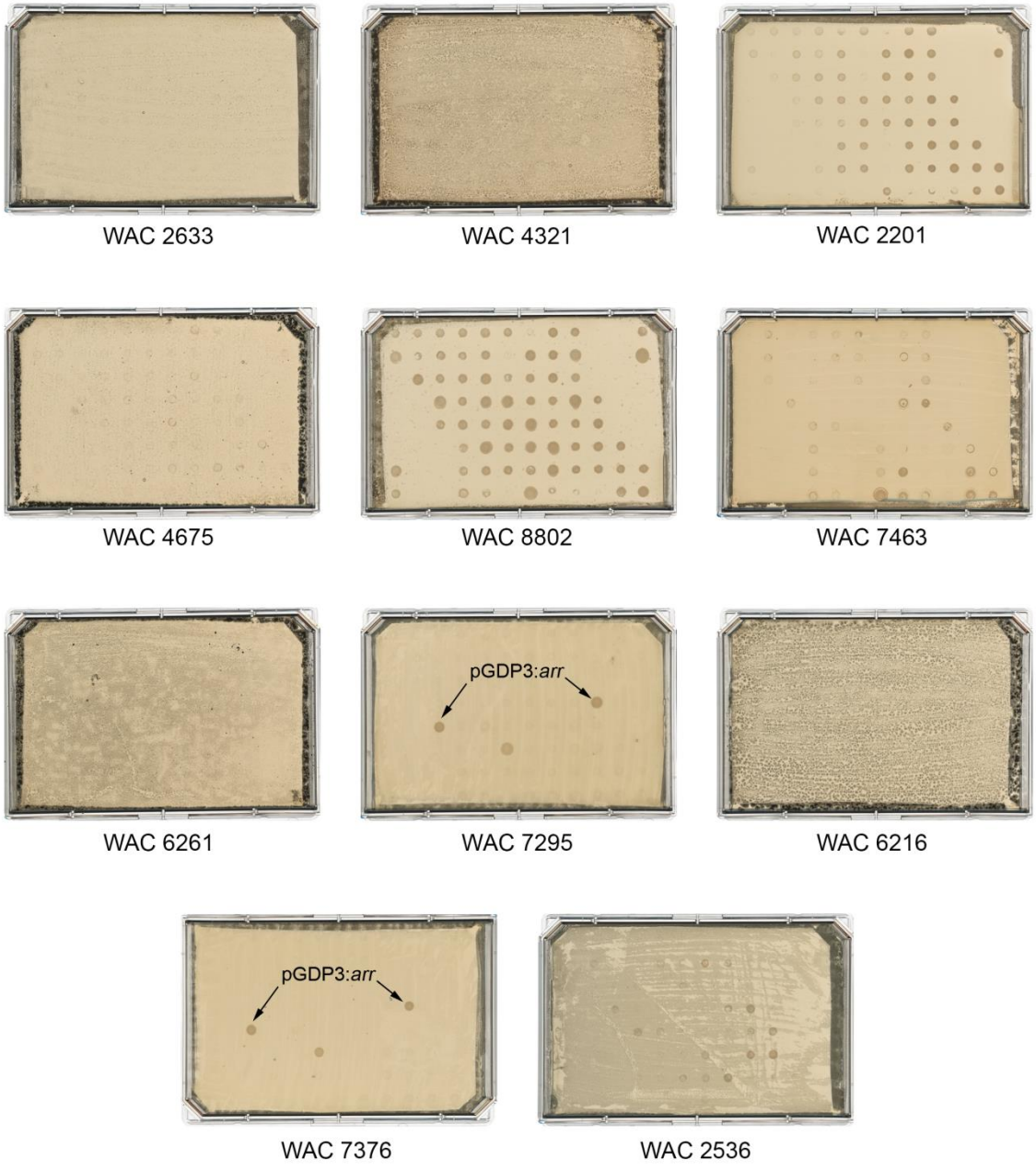

Figure 2-6: Dereplication of WAC strains corresponding to hits from the MCR-1 NPL screen.
Dereplication of 11 WAC strains reveals many plates that exhibit no growth of any ARP strains. WAC 2201, 7463, and 2536 show partial *E. coli* growth, and WAC 8802 showed whole ARP library growth. WAC 7295 and 7376 show colony growth in duplicate corresponding to the pGDP3:*arr* ARP strain, conferring resistance to rifamycins, and a single colony corresponding to the pGDP2:$bla_{\text{TEM-1}}$ ARP strain, which is believed to be a contaminant.

2.3.6 Sub-inhibitory concentrations of colistin potentiate antibiotics in colistin resistant bacteria

Following the results observed during dereplication, the possibility of colistin potentiating antibiotics in the resistant strain expressing *mcr-1* warranted further exploration. The susceptibility of *E. coli* BW25113-pGDP2:*mcr-1*, WT *E. coli* BW25113, and a clinical MDR *E. coli mcr-1*$^{+}$ isolate (colistin resistant, MIC of 4 μg/mL) to several antibiotics was determined in the presence and absence of sub-inhibitory concentrations of colistin at ½ MIC (Figure 2-7). In many cases, the presence of sub-inhibitory colistin drastically decreased the MIC of the other antibiotic, even in strains harboring *mcr-1*.

Chloramphenicol

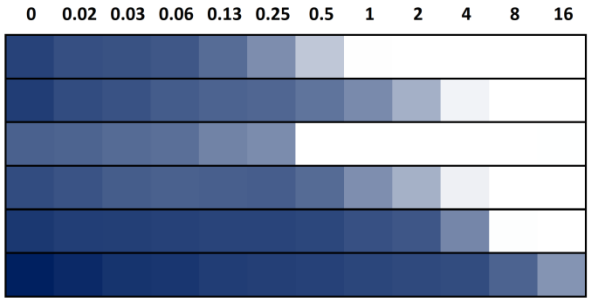

(µg/mL)	MIC (µg/mL)
pGDP2:*mcr-1* + 2 µg/mL colistin	1
pGDP2:*mcr-1*	8
WT + 0.125 µg/mL colistin	0.5
WT	8
Clinical isolate + 2 µg/mL colistin	8
Clinical isolate	>16

Spectinomycin

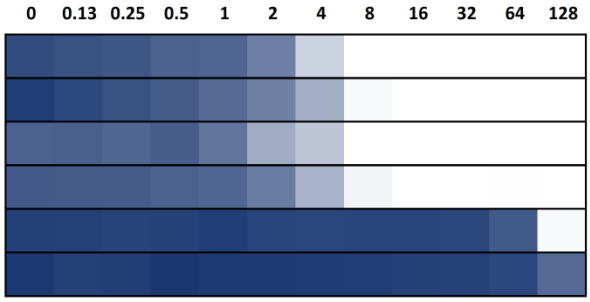

(µg/mL)	MIC (µg/mL)
pGDP2:*mcr-1* + 2 µg/mL colistin	8
pGDP2:*mcr-1*	8
WT + 0.125 µg/mL colistin	8
WT	8
Clinical isolate + 2 µg/mL colistin	128
Clinical isolate	>128

Hygromycin B

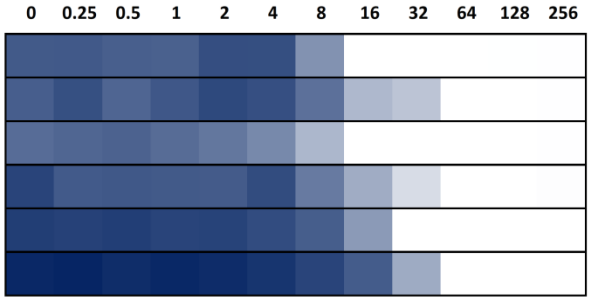

(µg/mL)	MIC (µg/mL)
pGDP2:*mcr-1* + 2 µg/mL colistin	16
pGDP2:*mcr-1*	64
WT + 0.125 µg/mL colistin	16
WT	64
Clinical isolate + 2 µg/mL colistin	32
Clinical isolate	64

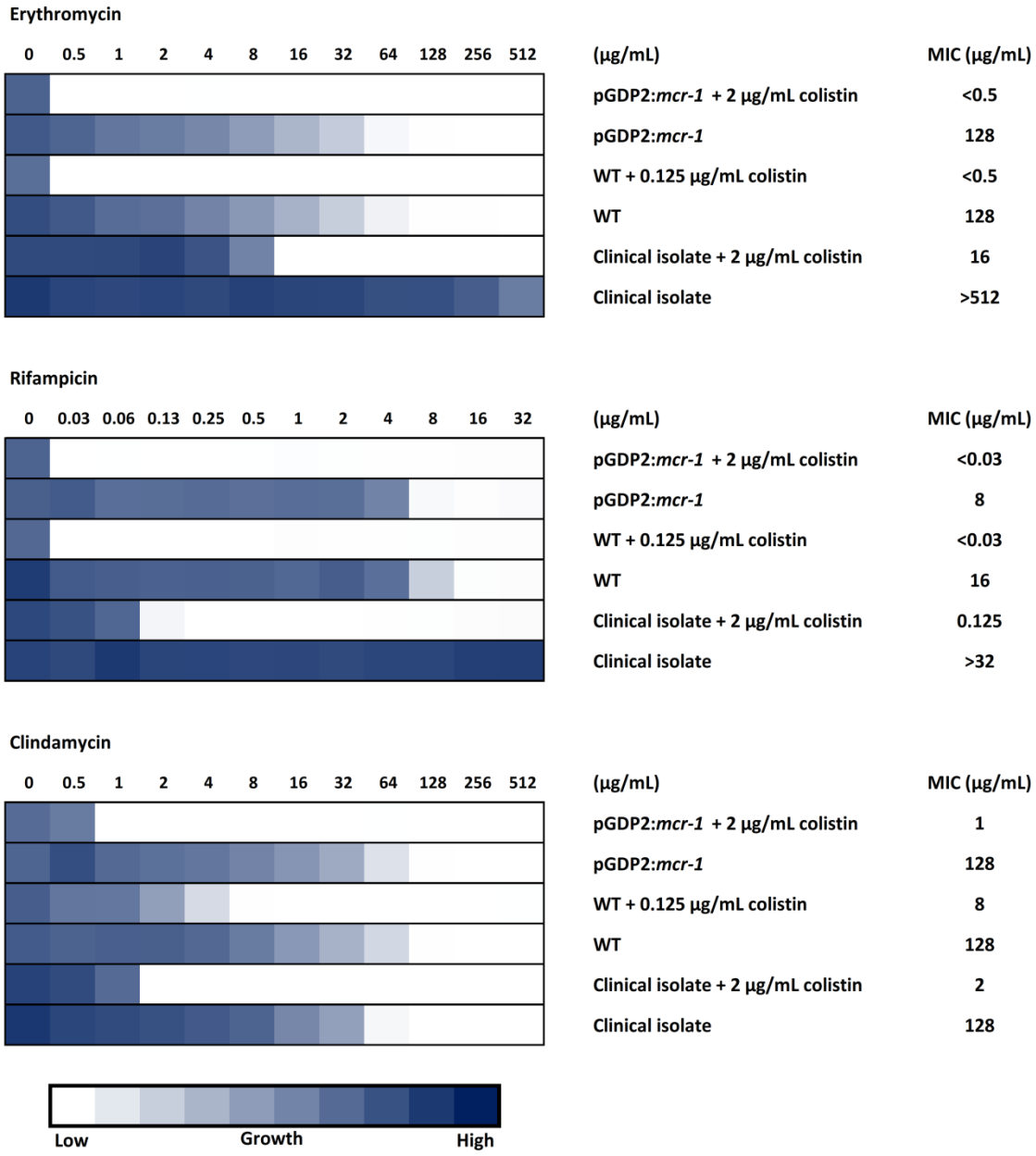

Figure 2-7: Colistin synergy with other antibiotics in *E. coli.*
Several antibiotics were tested in the presence and absence of ½ MIC colistin to determine the potentiating effects of colistin in a colistin-resistant strain. A heat plot was generated for antibiotics tested against *E. coli* BW25113-pGDP2:*mcr-1*,WT *E. coli* BW25113, and a clinical MDR *E. coli mcr-1*$^{+}$ isolate. The blue color represents cell growth, and the white color represents no cell growth.

Sub-inhibitory concentrations of colistin decreased the MIC of chloramphenicol in *E. coli* BW25113-pGDP2:*mcr-1* (8 μg/mL), WT *E. coli* BW25113 (8 μg/mL), and the clinical MDR *E. coli mcr-1*$^{+}$ isolate (>16 μg/mL) to 1, 0.5, and 8 μg/mL, respectively. Colistin did not have a great effect on the MIC of spectinomycin in *E. coli* BW25113-pGDP2:*mcr-1* and WT *E. coli* BW25113, but it decreased the MIC of the clinical MDR *E. coli mcr-1*$^{+}$ isolate from >128 μg/mL to 128 μg/mL. The effect of colistin potentiation on hygromycin B was similar to that of chloramphenicol, and the MIC of the antibiotic in *E. coli* BW25113-pGDP2:*mcr-1* (64 μg/mL), WT *E. coli* BW25113 (64 μg/mL), and the clinical MDR *E. coli mcr-1*$^{+}$ isolate (64 μg/mL) was reduced to 16, 16, and 32 μg/mL, respectively.

The ability of colistin to potentiate antibiotics was most notably observed with erythromycin, rifampicin, and clindamycin. In the case of erythromycin, the MIC in *E. coli* BW25113-pGDP2:*mcr-1* (128 μg/mL), WT *E. coli* BW25113 (128 μg/mL), and the clinical MDR *E. coli mcr-1*$^{+}$ isolate (>512 μg/mL) was reduced to <0.5, <0.5, and 16 μg/mL, respectively. This represents a 64-fold change in the *E. coli* BW25113 strains, and at least a 32-fold change in the clinical MDR *E. coli mcr-1*$^{+}$ isolate. A similar pattern was observed with rifampicin and clindamycin, where additions of sub-inhibitory concentrations of colistin reduced the MIC of each drug in each strain of *E. coli*, to varying degrees. The MIC of rifampicin in *E. coli* BW25113-pGDP2:*mcr-1* (8 μg/mL) and WT *E. coli* BW25113 (16 μg/mL) was reduced to <0.025 μg/mL, at least a 320-fold decrease, and >32 μg/mL to 0.125 μg/mL in the clinical MDR *E. coli mcr-1*$^{+}$ isolate, a >256-fold decrease. Lastly, the MIC of clindamycin in *E. coli* BW25113-pGDP2:*mcr-1*

(128 μg/mL), WT *E. coli* BW25113 (128 μg/mL), and the clinical MDR *E. coli mcr-1*$^{+}$ isolate (128 μg/mL) was reduced to 1, 8, and 2 μg/mL, respectively, indicating a 128-, 16-, and 64-fold decrease.

2.3.7 Polymyxin B nonapeptide synergizes with rifamycins in the presence of a polymyxin resistance element

The MIC of PMBN was determined to be >128 μg/mL for *E. coli* BW25113-pGDP2:*mcr-1* and WT *E. coli* BW25113. The synergistic effect of PMBN with rifamycins in *E. coli* BW25113-pGDP2:*mcr-1* was explored due to the strong synergy observed with colistin and rifampicin in the same strain. The checkerboard MIC studies confirmed synergy between PMBN and rifamycins (Figure 2-8). PMBN synergizes with all three rifamycins tested in *E. coli* BW25113-pGDP2:*mcr-1*, and to a greater degree in WT *E. coli* BW25113. All three rifamycins share similar synergistic profiles in the colistin-resistant *E. coli* strain, but rifabutin appears to have the strongest synergy in WT *E. coli* BW25113.

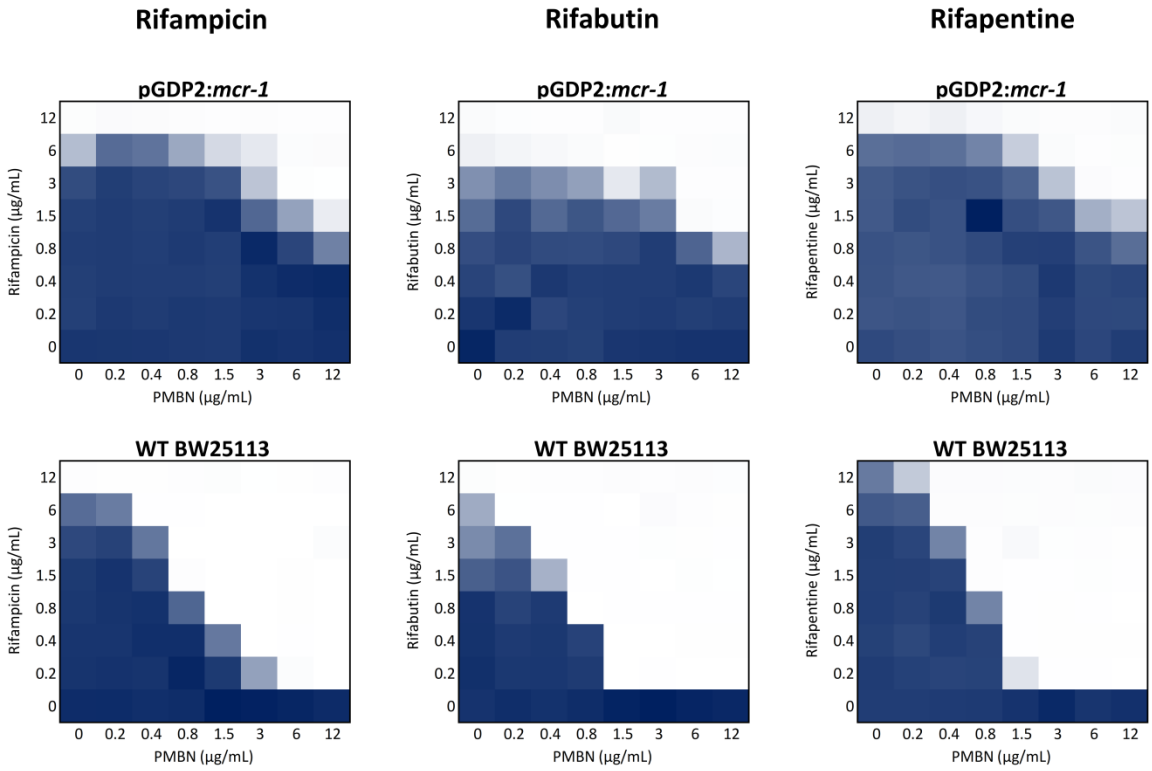

Figure 2-8: Checkerboard assay of polymyxin B nonapeptide synergy with rifamycins.
Checkerboard analysis showing the synergistic effects of polymyxin B nonapeptide (PMBN) with rifampicin, rifabutin, and rifapentine in *E. coli* BW25113-pGDP2:*mcr-1* and WT *E. coli* BW25113. Synergy of colistin with these rifamycins is present in the MCR-1 *E. coli* strain, although the synergy is stronger in the WT *E. coli* strain. Blue represents high cell growth and white represents no cell growth.

2.4 Discussion

The extent to which the pGDP1:*mcr-1* and pGDP2:*mcr-1* constructs confer resistance to polymyxins is comparable to that determined by Liu *et al.*[34] upon the discovery of *mcr-1*. Indeed, this level resistance is relatively low in the overall landscape of polymyxin resistance, as evidenced by the identification of bacterial isolates such as *Acinetobacter baumannii* that have been characterized with polymyxin resistance as high as 128 µg/mL[72] and greater[61], due to mutations in the genes responsible for lipid A biosynthesis. Although, a plasmid mediated resistance mechanism to polymyxins has the

potential to mobilize to other Gram-negative pathogens and/or integrate into MDR species, posing a greater cause for concern in the ability to battle bacterial infections.

MCR-1 confers resistance to polymyxins, which are a class of CAMPs, and the experiments conducted in this chapter aimed to explore whether this resistance would translate to other CAMPs such as LL-37, 1026 (synthetic), 1036 (synthetic), and 1037 (synthetic). The list of CAMPs that were tested was not extensive, but the data suggests that MCR-1 does not possess universal ability to confer cross-resistance to other CAMPs. If the case had been that MCR-1 did confer cross-resistance to CAMPs, the emergence and dissemination of MCR-1 could have been hypothesized to have occurred as a result of selective pressures of the immune system during infection. Resistance to CAMPs would offer a fitness advantage to bacterial pathogens that were establishing infection, providing them with a greater chance of survival.

In addition, a recent study conducted a similar experiment in order to determine MCR-1 CAMP cross-resistance[102]. Their study did not involve the same CAMPs tested in this chapter, but their results point to the same outcome that there is no evident cross-resistance. A separate study[103] tested several antimicrobial peptides including LL-37, and identified cathelicidins that had potent bactericidal activity against colistin resistant bacteria harboring MCR-1. These experiments lead us to conclude that MCR-1 is specific in its ability to confer resistance to polymyxins.

These results also question our understanding of how the addition of PEtN to the phosphate group of lipid A protects the Gram-negative bacteria from polymyxins. It is often stated that the addition of a PEtN group increases the overall positive charge of the

outer membrane in order to reduce electrostatic attraction between polymyxins and the outer membrane. However, the structure of PEtN is zwitterionic, a dipolar ion containing both positive and negative electrical charges, resulting in a neutral molecule (Figure 2-9).

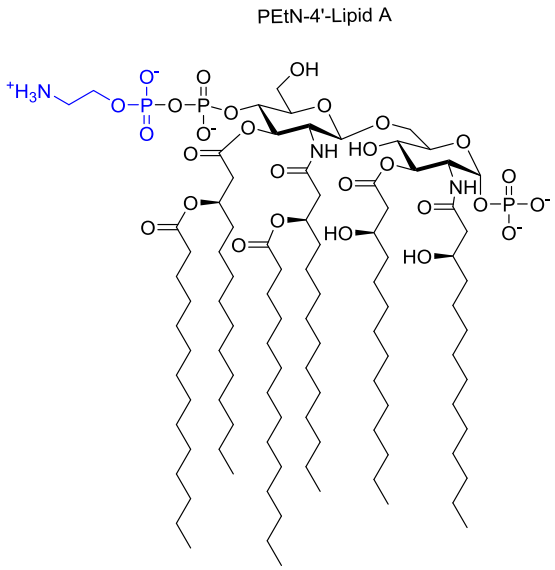

Figure 2-9: Zwitterionic phosphoethanolamine-4'-lipid A.
A phosphoethanolamine residue (blue) attached to the 4'-phosphate group of lipid A. The phosphoethanolamine residue is a zwitterion, containing both positive and negative charges that result in a net charge of zero.

Therefore, if the PEtN in the outer membrane contains a neutral net charge, perhaps it protects the cells from polymyxins by blocking the physical interaction of the polymyxin and the outer membrane, rather than by electrostatic repulsion. This provides a possible explanation as to why MCR-1 confers resistance to polymyxins but leaves the cells susceptible to other CAMPs. Because the data generated in this chapter and other studies point to this same CAMP susceptibility, the current hypothesis of the emergence of mobile colistin resistance from overuse of polymyxins within the agricultural industries in

various parts of the world still holds significance, and is a recent example of what may result from misuse of antibiotics[104–107].

The solid media extracts of WAC strains that were identified as hits in the MCR-1 screen were tested against *E. coli* BW25113-pGDP2:*mcr-1* and WT *E. coli* BW25113 and many of the extracts tested were identified as false positives as they were unable to inhibit the growth of either *E. coli* strain in the presence or absence of colistin (Figure 2-5). These hits were identified within the screening data due to their growth inhibition effects on *E. coli* BW25113-pGDP2:*mcr-1* in the presence of colistin, so it is unexpected that they did not exhibit the same activity in this assay. This could have been the result of a production issue by the Actinobacteria, producing a sub-optimal concentration of compounds compared to the extract within the NPL. The dereplication that followed was conducted in order to understand what these WAC strains were producing, and to discount any antibiotic producers.

Analyzing the dereplication plates for growth revealed several plates that did not appear to have any visible ARP *E. coli* growth. This suggests that the Actinobacteria that were cultured on these plates produce an antibiotic which has not been accounted for in the ARP. Some of the plates revealed partial and spotty growth of *E. coli* colonies, which may arise from non-uniform Actinobacteria growth on the plates resulting in fluctuating concentrations of active compounds within the agar.

Following the identification of antibiotic producers in the dereplication experiments, sub-inhibitory concentrations of colistin were tested with other antibiotics in order to determine the extent of synergy in a polymyxin resistant background. The results

indicated that colistin was able to potentiate antibiotics in the colistin-sensitive *E. coli* strain, as well as the colistin-resistant *E. coli* strains, which was unexpected. Although there have been reports published that explored the use of colistin in synergy with other antibiotics to treat bacteria that were resistant to those respective non-colistin antibiotics, where colistin would potentiate the effect of the other antibiotic in the resistant strain[108–110], those findings have been widely explored and differ from what was observed in this chapter. Another two reports identified a strong synergistic effect between polymyxins and rifampicin in polymyxin-resistant carbapenem β-lactamase-producing *Klebsiella pneumoniae*[111,112]. These two reports discuss the synergistic effect of colistin with other antibiotics in colistin-resistant strains, similar to the trend that was observed in the work conducted in this chapter. Many of the hits identified in the MCR-1 NPL screen contained antibiotics that were potentiated by colistin in order to kill the colistin resistant strain, as they were not identified as hits in the WT *E. coli* BW25113 or *E. coli* BW25113 Δ*tolC* Δ*bamB* NPL screening data. This may have been due to a low concentration of antibiotic within these extracts, but enough to inhibit the growth of the MCR-1 strain in the presence of colistin, which was demonstrated by the extent of synergy observed for colistin and rifampicin in this chapter.

These observations beg the question of how polymyxins are able to potentiate antibiotics in strains that should be resistant, especially when treated with sub-inhibitory concentrations of polymyxins. Studies conducted with polymyxin B nonapeptide, a cyclic heptapeptide with an N-terminal Thr-Dab dipeptide component[35] (Figure 2-10), note that it has decreased antimicrobial activity against *E. coli* (MIC >128 μg/mL in *E. coli*

BW25113-pGDP2:*mcr-1* and WT *E. coli* BW25113) and can still perturb the Gram-negative outer membrane, but does not cause major disruption of membrane integrity like the native antibiotic does[113,10].The PMBN expands the surface area of the outer membrane[114], and permits entry of certain hydrophobic antibiotics that are normally impermeable to an intact outer membrane[35].

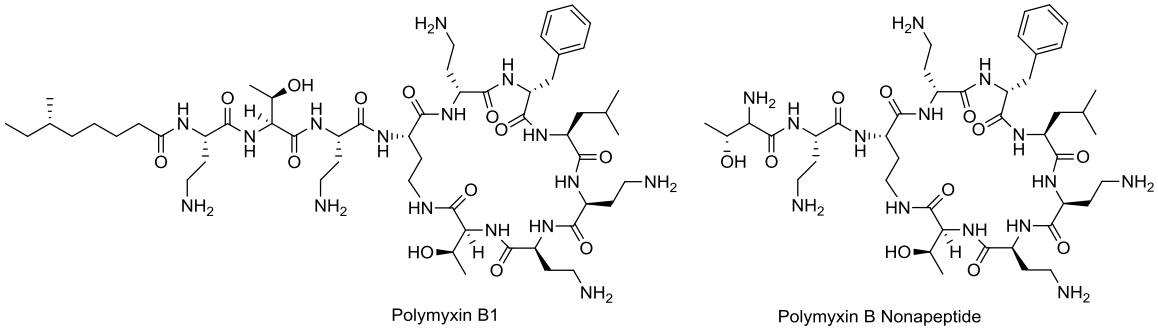

Figure 2-10: Polymyxin B1 and polymyxin B nonapeptide.
Left: Polymyxin B1 is a cyclic heptapeptide ring with a tripeptide side chain acylated by a fatty acid tail. *Right:* Polymyxin B nonapeptide is composed of a cyclic heptapeptide and an N-terminal Thr-Dab dipeptide component.

This study has shown that PMBN can also potentiate rifamycins in *E. coli* BW25113-pGDP2:*mcr-1*, although the combination is more synergistic in WT *E. coli* BW25113. Relating this back to polymyxins and the synergy observed in the MCR-1 *E. coli* strain, the data suggests that in regards to potentiating other antibiotics, the bactericidal activity of polymyxins is less important than their ability to perturb the outer membrane, even in the presence of a polymyxin resistance element. Therefore, it appears that it is not the hydrophobic tail of polymyxin that is responsible for the synergy, but rather the heptapeptide ring and tri-peptide side chain, which have negligible antibiotic characteristic on their own. Looking at the synergy between colistin and rifampicin, even

with MCR-1 producing PEtN-modified lipid A, it appears that the bactericidal effect of colistin was muted, but it was able to perturb the membrane to a degree where rifampicin was able to cross the outer membrane.

The extent of lipid A modification by MCR-1 is unknown, in the sense that it is not well understood how much of the lipid A population is modified with a PEtN residue. Within the dynamic outer membrane, there may be 'weak points' where the overall number of modified lipid A residues is low enough to permit the interaction of polymyxin with the outer membrane, just enough to allow smaller hydrophobic antibiotics to pass through. Therefore, when looking back at the results obtained during dereplication following our screen, it is probable that colistin was potentiating miniscule concentrations of antibiotics within these extracts, which would have appeared as a hit in the NPL screen of *E. coli* BW25113-pGDP2:*mcr-1* with colistin, but not the WT *E. coli* BW25113 parent strain or the hyper-permeable and efflux deficient strain in the absence of antibiotic.

Chapter 3.
Developing an *in vitro* biochemical assay to test for MCR-1 activity

3.1 Introduction

One of the most common mechanisms of resistance to polymyxins involves the addition of a phosphoethanolamine (PEtN) residue onto lipid A[10,11]. MCR-1 catalyzes this reaction by the transfer of a PEtN from phosphatidylethanolamine onto the 1 or 4' phosphate of lipid A[68,69]. Although the entire reaction mechanism is yet to be understood, the transfer of PEtN onto lipid A is believed to be catalyzed by the Thr285 nucleophile[70]. One study conducted on *Nm*EptA, an MCR-1 homolog found in *Neisseria meningitides* in which the active site residues are conserved, identified the formation of a Thr280-PEtN enzyme intermediate, which was similar to those that have been observed in other alkaline phosphatase-type phosphate transferases[74]. This suggests that *Nm*EptA, and therefore MCR-1, function via ping-pong mechanism.

A ping-pong reaction, also known as a double-displacement reaction or covalent catalysis, is a catalytic pathway in which the enzyme oscillates between two stable forms. In the first reaction, a part of the substrate forms a covalent bond with the free enzyme to create an enzyme-substrate intermediate[115,116]. In a second step, the enzyme-substrate intermediate undergoes another reaction to form a product, which regenerates the original free enzyme (Figure 3-1).

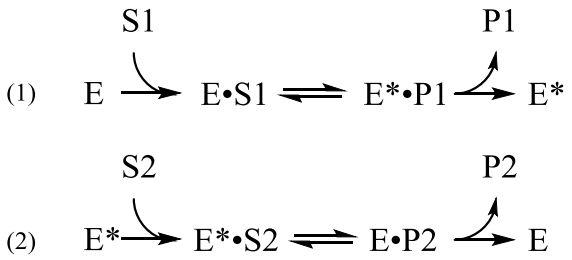

Figure 3-1: Ping-pong reaction mechanism.
The two step mechanism of a ping-pong reaction where E – free enzyme; E* – enzyme-substrate intermediate; S1 – substrate one; S2 – substrate two; P1 – product one; P2 – product two.

In the case of MCR-1, the first step of the reaction involves a Thr285 nucleophilic attack on the PEtN moiety of phosphatidylethanolamine, producing an MCR-1-PEtN enzyme-substrate intermediate, and expelling the diacylglycerol product. In the second step of the reaction, the phosphate group of lipid A behaves as the nucleophile and attacks the PEtN residue attached to MCR-1 to produce an MCR-1-(PEtN-Lipid A) complex. Following this step, the PEtN-Lipid A is released and the free MCR-1 enzyme is regenerated to repeat the reaction. The proposed scheme for the mono-zinc ping-pong mechanism of MCR-1 is outlined in Figure 3-2.

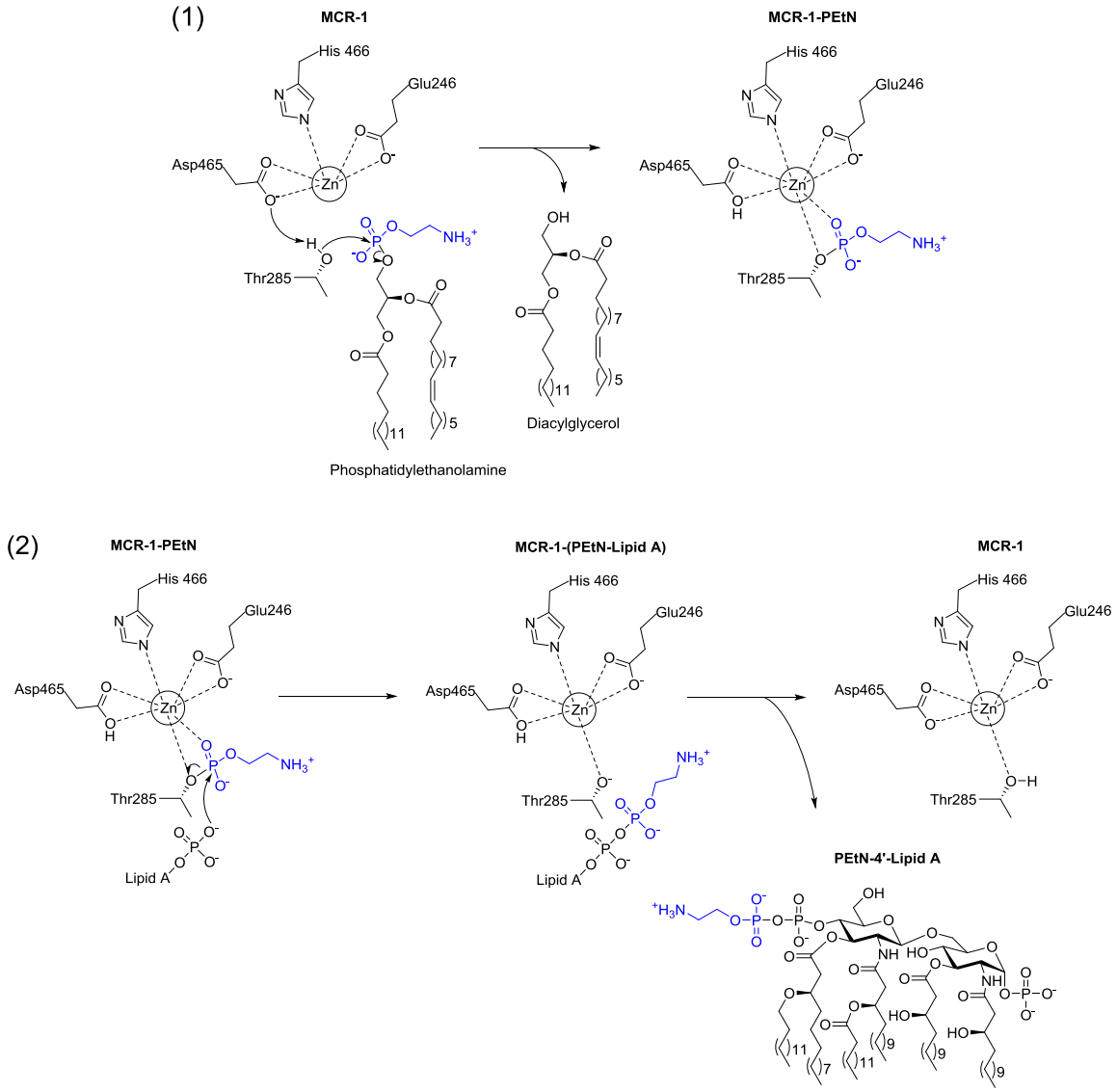

Figure 3-2: Ping-pong reaction mechanism of MCR-1.
The proposed two step ping-pong mono-zinc mechanism for MCR-1 with Thr285 acting as the nucleophile. The schematic depicts the active site of MCR-1 and the reactions that take place. The first step (1) involves the nucleophilic attack of MCR-1 onto phosphatidylethanolamine, producing an MCR-1-PEtN intermediate. The second step (2) involves the nucleophilic attack of lipid A on PEtN, regenerating free MCR-1. PEtN is depicted in blue.

Crystal structures of the C-terminal domain of MCR-1 have identified one, two, three, or four zinc ions present in the active site[68,69]. In one of the crystallographic studies, density

functional theory models of MCR-1-catalysed PEtN transfer identified minimum-energy structures for all intermediates along putative mechanistic pathways requiring either one or two zinc ions[69]. These models proposed that within the mono-zinc mechanism shown above, both Glu246 and Asp465 are able to act as general bases to deprotonate Thr285, and the products generated from deprotonation were isoenergetic.

In Chapter 2, many antibiotics were identified within the NPL extracts that were used to screen for inhibitors of MCR-1. This chapter describes the purification of the MCR-1 C-terminal catalytic domain and the synthesis of a chromogenic compound to test for activity of MCR-1 *in vitro*. Using a chromogenic compound that may be a substitute of the natural substrate provides an orthogonal approach to whole cell screening when searching for inhibitors of MCR-1.

3.2 Materials and Methods

3.2.1 Cloning, expression, and purification of MCR-1 C-terminal domain

The MCR-1 C-terminal domain (amino acids 209-541) was amplified by PCR from purified pGDP2:*mcr-1* plasmid using forward primer MCR-1_CTD_Fwd (Appendix 2) which incorporated an *Nde* I restriction site, and reverse primer MCR-1_CTD_Rev (Appendix 2) which incorporated an *Xho* I restriction site. The size of the amplified *mcr-1* C-terminal domain (209-541) PCR product was approximately 1 kb, which was the expected size of the gene.

The amplified *mcr-1* C-terminal domain (209-541) was cloned into the pET28a expression vector using restriction enzymes *Nde* I and *Xho* I, introducing an N-terminal

$His_{(6)}$-tag for Ni-NTA purification. The final construct was verified by Sanger sequencing (MOBIX Lab, McMaster University). The construct was transformed into chemically competent *E. coli* Rosetta-gami(DE3)pLysS (70956; Novagen) cells for overexpression. A single colony was used to inoculate 600 mL 2ZYM-2X Lac media (Appendix 1) supplemented with 50 μg/mL kanamycin and 35 μg/mL chloramphenicol, which was then incubated at 25°C with aeration (180 rpm) for 64 hours.

Following incubation, the cell culture was separated by centrifugation at 6400 g for 30 minutes at 4°C. The supernatant was discarded and the remaining pellet was re-suspended in 50 mL lysis buffer (25 mM HEPES pH 7.5, 300 mM NaCl, 10 mM imidazole) and frozen at -80°C overnight. To lyse the cells, the frozen cultures were thawed and passed through a Constant Systems continuous-flow cell-disruptor at 20 000 psi at 4°C. Lysed cells were collected into a chilled container with ½ crushed EDTA-free Pierce™ protease inhibitor tablet (88266; ThermoScientific), egg white lysozyme (LYS702; BioShop), and bovine pancreas DNAse I (DN25; Sigma). The lysate was incubated on ice for 5 minutes and separated by centrifugation at 30 000 g for 30 minutes at 4°C to remove cellular debris. The supernatant was collected and purified using standard affinity chromatography Ni-NTA resin (30210; Qiagen). At 4°C, approximately 5 mL of resin was equilibrated by running one column volume of lysis buffer through the column. The lysate was added to the column and it was set to incubate for 30 minutes. Following incubation, the flow through was collected, and the column was then washed three times with one column volume of wash buffer (25 mM HEPES pH 7.5, 300 mM NaCl, 25 mM imidazole), followed by four separate elutions with one column volume of

25%, 50%, 75% elution buffer (25 mM HEPES pH 7.5, 300 mM NaCl, 250 mM imidazole) in wash buffer, and 100% elution buffer.

The pellet, flow through, wash, and elution samples were applied onto a 12 % SDS-polyacrylamide gel, run at 80 V for 20 min, followed by 100 V for 40 min, and then visualized with Coomassie blue stain. Elution fractions were combined and dialyzed against 2 L of dialysis buffer (25 mM HEPES pH 7.5, 300 mM NaCl, 1 mM DTT) at 4^{o}C overnight. The protein sample was concentrated using an Amicon Ultra-15 filter unit with Ultracel-10 membrane (UFC901024;EMD Millipore) centrifugal filter at 4000 g for 25 minute intervals at 4^{o}C. Glycerol was added to a final concentration of 20 %, the concentrations of several aliquots were determined using the Pierce BCA protein assay kit (23227; ThermoFisher), and the samples were stored at -80^{o}C.

3.2.2 Synthesis of *O*-(*p*-nitrophenylphosphoryl)ethanolamine TFA salt (*p*NP-PEtN)

Unless otherwise stated, reactions were carried out at room temperature.

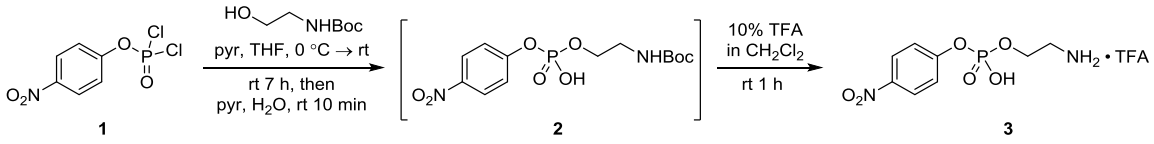

Figure 3-3: Schematic of the synthesis of *O*-(*p*-nitrophenylphosphoryl)ethanolamine TFA salt

A solution of 1.10 mL (7.11 mmol) *N*-Boc-ethanolamine in 20 mL THF was slowly added to a mixture containing 3.65 g (14.3 mmol) of *p*-nitrophenyl dichlorophosphate and 2.30 mL (28.4 mmol) pyridine in 35 mL dry THF at 0^{o}C over 1

hour. Following the addition, the ice bath was removed and the solution was allowed to warm to room temperature, where the mixture was stirred for 7 hours. A solution of 2.30 mL (28.4 mmol) pyridine in 10.2 mL water was added to the reaction mixture, which was then stirred for 10 minutes. Following this incubation period, the mixture was concentrated under vacuum, producing a yellow oil with an approximate volume of 10 mL. The yellow oil was diluted with 50 mL distilled water and washed three times with 50 mL EtOAc. The aqueous phase was acidified with two 50 mL volumes of 5% aqueous $KHSO_4$ to pH 3-4 and extracted with three 50 mL volumes of CH_2Cl_2. The combined CH_2Cl_2 extracts were washing with 50 mL brine, dried over Na_2SO_4, and concentrated under vacuum to produce a 37:7:12:43 mixture (860 mg) of the Boc-protected intermediate (2), *p*-nitrophenol, *p*-nitrophenyl phosphate, and pyridine, respectively. This was determined by dissolving a small amount of product in deuterated chloroform and submitting for NMR experiments on a Bruker AVIII 700 MHz instrument equipped with a cryoprobe. A portion of the crude mixture was used in the next step without further purification.

A volume of 0.1 mL TFA was added to a solution containing 72 mg of the crude Boc-protected phosphonate mixture in 1 mL CH_2Cl_2, which was then stirred at room temperature for 1 hour. The reaction mixture was concentrated under vacuum and the residue was triturated with two 1 mL volumes of EtOAc to produce 35 mg (0.093 mmol) of the TFA salt of the free amine as a fine white powder. This was determined by dissolving a small amount of product in deuterated DMSO and submitting for NMR experiments as previously described (Appendix 3).

3.2.3 Chromogenic assay with MCR-1 C-terminal domain

In order to determine if *O*-(*p*-nitrophenylphosphoryl)ethanolamine (*p*NP-PEtN) was a substrate for the MCR-1 C-terminal domain, a reaction containing the purified MCR-1 C-terminal domain and *p*NP-PEtN was set up in a 96-well flat-bottom plate. A 25 mM and 12.5 mM stock of *p*NP-PEtN substrate was prepared in assay buffer (50 mM HEPES pH 7.5, 150 mM NaCl, 5 mM $MgCl_2$, 20 μM $ZnSO_4$). In 100 μL reactions, wells were filled to 90 μL with assay buffer and purified MCR-1 C-terminal domain to a total of 2 μg and 4 μg enzyme, as well as a no enzyme control. The plate was incubated at 30^{o}C in a SpectraMax® Plus 384 Microplate Reader for 10 minutes prior to reaction initiation by the addition of 10 μL of *p*NP-PEtN stocks, resulting in final concentrations of 2.5 mM and 1.25 mM. The plate was read at 30^{o}C for 30 minutes at 12 second intervals, with absorbance measured at 405 nm using a SpectraMax® Plus 384 Microplate Reader.

3.3 Results

3.3.1 Cloning, expression, and purification of MCR-1 C-terminal domain

The N-terminal $His_{(6)}$-tagged C-terminal catalytic domain of MCR-1 (amino acids 209-541) was successfully purified using Ni-NTA affinity chromatography. The purification fractions were analyzed on an SDS-polyacrylamide gel to confirm the size of the protein. A band consistent with the predicted molecular weight of 39.4 kDa was observed in wash fractions 1-3, and elution fractions 1 and 2 (Figure 3-4). Elution fraction 1 also contained some residual proteins that were eluted from the column.

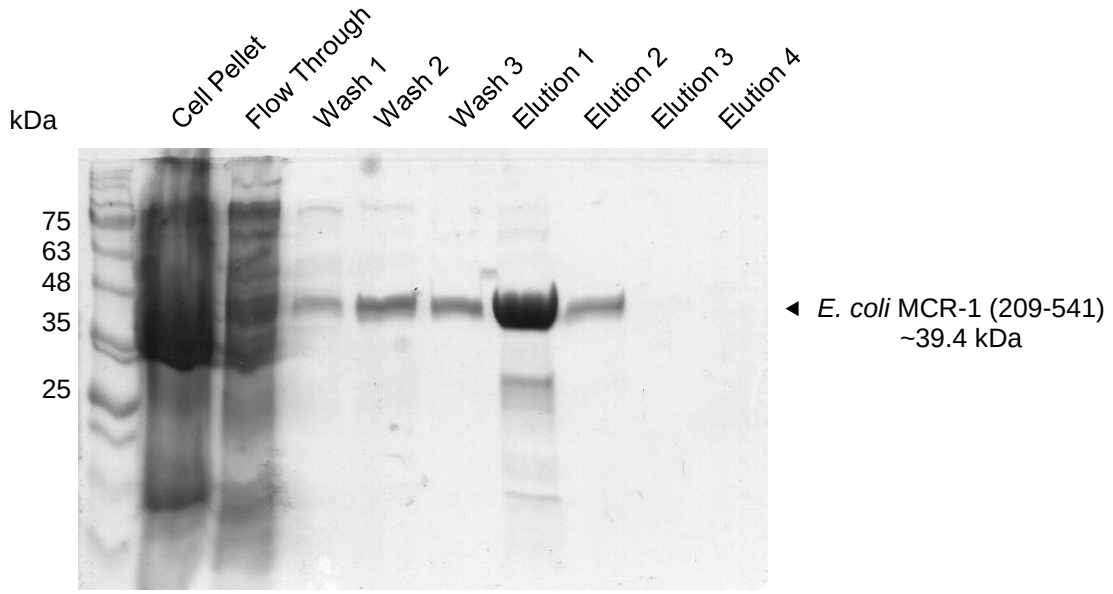

Figure 3-4: Overexpression and purification of MCR-1 C-terminal domain.
Fractions from the overexpression and purification of MCR-1 (209-541) run on an SDS-polyacrylamide gel. The presence of MCR-1 (209-541) is visible in wash 1-3 fractions and elution 1-2 fractions. The protein was purified by Ni-NTA affinity chromatography.

3.3.2 Synthesis of *O*-(*p*-nitrophenylphosphoryl)ethanolamine TFA salt

The chromogenic *p*NP-PEtN compound was synthesized through modification of a known method[117] and confirmed via ^{1}H and ^{13}C NMR (Appendix 3). The known method involves a one-step reaction of 4-nitrophenyl dichlorophosphate with ethanolamine, and a several day crystallization step which resulted in a low yield. With this method, there was the possibility of nucleophilic attack by the amine group of ethanolamine rather than the desired hydroxyl group, resulting in a mixture of products that would be troublesome to purify. In addition, the long crystallization step was not optimal, and therefore a more reliable method was desired. A two-step reaction involving *N*-Boc-ethanolamine was conducted and the additional deprotection step with TFA allowed for the isolation of pure product from a mixture obtained from the first reaction.

3.3.3 Chromogenic assay with MCR-1 C-terminal domain

In order to determine whether the purified MCR-1 C-terminal catalytic domain (209-541) could catalyze the cleavage of PEtN from *p*NP-PEtN, an enzyme assay was conducted. Presuming the mechanism (Figure 3-2) is true, and *p*NP-PEtN is an acceptable substrate for the C-terminal catalytic domain of MCR-1, the first half of the overall ping-pong reaction should generate *p*-nitrophenol (*p*NP) and MCR-1-PEtN enzyme-substrate intermediate (Figure 3-5).

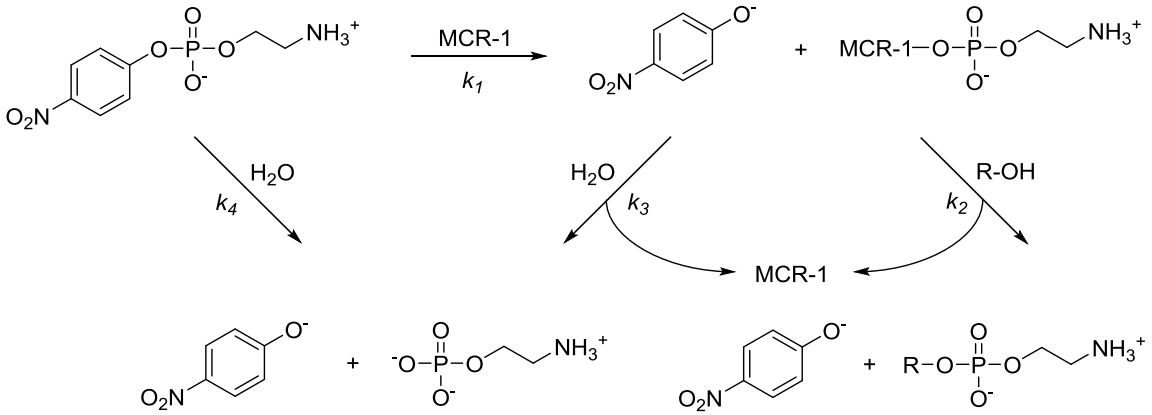

Figure 3-5: *O*-(*p*-Nitrophenylphosphoryl)ethanolamine assay reaction diagram.
Diagram depicting possible reactions involved in the MCR-1 *p*NP-PEtN assay.

The possibility of competing reactions in the assay may add some complexity to understanding the overall results that are observed. The competing reactions involve the interaction of *p*NP-PEtN with MCR-1 (k_1) versus the hydrolysis of this compound by water (k_4), which generates *p*NP, and the removal of PEtN from MCR-1 by a PEtN acceptor such as lipid A, depicted as R-OH (k_2), versus water (k_3), which regenerates MCR-1. Since only the first half of the overall ping-pong reaction mechanism was tested,

the generation of MCR-1-PEtN (k_1) and the removal of PEtN from MCR-1 by water (k_3) were competing with the background hydrolysis of *p*NP-PEtN by water (k_4), both of which would generate *p*NP and produce a change in absorbance at 405 nm.

Assuming $k_3 > k_4$ for this application, if $k_1 > k_4$ then it's expected to observe a quick burst of *p*NP generation until the free enzyme is saturated with PEtN, followed by a linear change in absorbance due to generation of *p*NP by MCR-1, whereas the no enzyme control would show a small increase in absorbance over time due to background hydrolysis of *p*NP-PEtN. If $k_4 > k_1$, it's expected to observe a linear increase in absorbance over time due to the dominating background hydrolysis of *p*NP-PEtN, with the possibility of observing a greater absorbance in the samples containing enzyme due to their reaction with the substrate. Assuming k_1 is not hindering the progression of the reaction, if $k_4 > k_3$ then it's expected to observe a burst of *p*NP generation until all of the available active sites become occupied by PEtN, following which any change in absorbance will be largely due to the background hydrolysis of *p*NP-PEtN.

The reactions containing a no enzyme control, 2 μg MCR-1 (209-541), and 4 μg MCR-1 (209-541) were initiated with 2.5 mM *p*NP-PEtN and 1.25 mM *p*NP-PEtN. The increases in absorbance at 405 nm over the course of the reactions appear to be very similar throughout the experimental trials at each respective substrate concentration (Figure 3-6).

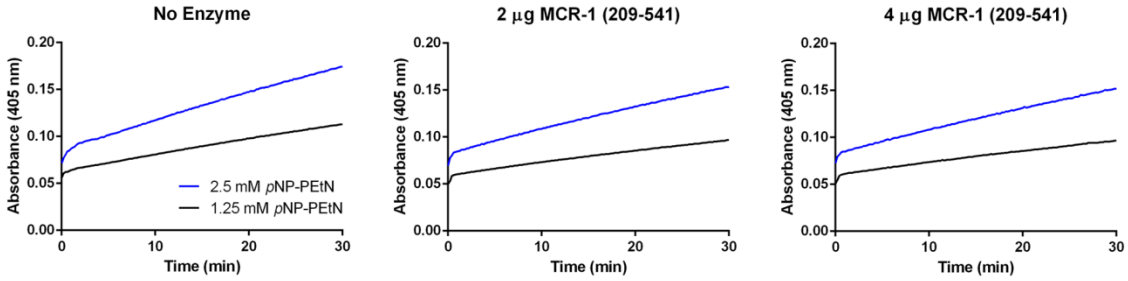

Figure 3-6: Assay of *p*NP-PEtN with the C-terminal domain of MCR-1
The reaction was carried out with 2.5 mM (blue) and 1.25 mM (black) *p*NP-PEtN in the presence of 0 µg, 2 µg, and 4 µg MCR-1 (209-541). The reactions were incubated at 30°C for 30 minutes and the absorbance was measured at 405 nm.

For the 2.5 mM *p*NP-PEtN reaction over the course of 30 minutes, the no enzyme control shows an increase in absorbance at 405 nm to approximately 0.17 units, and the 2 µg MCR-1 (209-541) and 4 µg MCR-1 (209-541) reactions read approximately 0.15 units. In the reaction initiated with 1.25 mM *p*NP-PEtN, the increase in absorbance following the 30 minute reaction reads approximately 0.11 units in the no enzyme control, and approximately 0.10 in the 2 µg MCR-1 (209-541) and 4 µg MCR-1 (209-541) reactions.

3.4 Discussion

The reactions carried out with *p*NP-PEtN and MCR-1 (209-541) showed minimal differences from the no enzyme control over a period of 30 minutes. A study published by Wanty *et al.*[118] discussed the use of this substrate in an assay with the C-terminal soluble domain of *Nm*EptA at 37°C for 50 hours. The authors report the ability of the enzyme to cleave PEtN from *p*NP-PEtN, as dictated by the blank-adjusted absorbance values at 405 nm following incubation: 0.65 for the reaction with enzyme, and 0.19 for the no-enzyme

control. The change in absorbance in the no-enzyme control suggests background hydrolysis of the *p*NP-PEtN, which is similar to the results observed in the experiment conducted in this chapter. The no-enzyme control reaction conducted in this chapter showed an absorbance value of approximately 0.17 following the 30 minute incubation, with no indication of approaching a plateau, although the absorbance readings were not blank-adjusted.

A classic example of the ping-pong mechanism involving the hydrolysis of *p*-nitrophenyl acetate (*p*NP-Ac) by chymotrypsin, which was carried out by Hartley and Kilby[115], may suggest what is occurring in our MCR-1 reaction. Chymotrypsin is a protease which catalyzes the hydrolysis of peptides. It employs a nucleophilic serine residue, similar to the proposed threonine nucleophile in MCR-1. The reaction observed between chymotrypsin and *p*NP-Ac proceeded with a burst of *p*NP generation, followed by a linear generation of *p*NP by the enzyme. This suggested that the overall reaction proceeded with an initial rapid reaction of *p*NP-Ac with the enzyme, followed by a slower reaction that was responsible for hydrolysis of acetate from the enzyme-substrate intermediate, allowing the enzyme to continue its reaction and generate more *p*NP. In other terms, the initial reaction involved the rapid formation of a substrate-enzyme complex until all the available enzyme was occupied, following which the substrate could be slowly hydrolyzed from the enzyme, allowing the free enzyme to repeat the reaction.

Comparing the reaction of chymotrypsin with *p*NP-Ac to MCR-1 (209-531) with *p*NP-PEtN, the first step of the reaction could be the rapid nucleophilic attack by Thr285 to produce the MCR-1-PEtN intermediate. The second step of the reaction traditionally

requires the presence of lipid A, in which a phosphate group acts as the nucleophile to remove the PEtN from MCR-1, regenerating free enzyme. In the reaction carried out in this chapter, water was the only potential nucleophile for the second step of the overall reaction. The data showed an overall linear increase in absorbance over time that was similar in the no enzyme control and the reactions containing enzyme, which was due to the background hydrolysis of *p*NP-PEtN. Indeed, it is uncertain whether *p*NP-PEtN is an adequate substrate for MCR-1, and therefore due to the absence of a definitive change in absorbance when enzyme was present, it is difficult to suggest the relationship that k_1 has with respect to the first reaction. To determine whether any interaction between MCR-1 and *p*NP-PEtN exists, matrix-assisted laser desorption/ionization time-of-flight mass spectrometry (MALDI-TOF-MS) experiments can be conducted to observe if an MCR-1-PEtN enzyme-substrate intermediate is able to form.

It is possible that the first reaction occurred very quickly, and that $k_4 > k_3$ which resulted in the measurement of *p*NP production due to hydrolysis rather than cleavage of *p*NP-PEtN by MCR-1. Water may have not been an adequate nucleophile to remove PEtN from MCR-1, so following the initial reaction of MCR-1 with *p*NP-PEtN, all the enzymes may have had their active sites occupied and background hydrolysis of the *p*NP-PEtN compound was responsible for the overall change in absorbance that was observed. In the early burst reaction, the concentration of the enzyme is equal to the concentration of product that can form, and therefore assuming that 100% of MCR-1 was capable of reacting with the substrate, k_3 was insignificant, and water was unable to efficiently remove PEtN from MCR-1, then it is possible to calculate the expected change in

absorbance during the burst phase using the Beer-Lambert law, $A = \varepsilon cl$, where A is the absorbance, ε is the molar extinction coefficient of the product, c is the molar concentration of the limiting reactant, and l is the path length. If the molecular weight of the enzyme is known, and 1 kDa = 1 g/mol, then the mass of the enzyme used in the assay can be divided by the weight in g/mol to obtain the number of moles of enzyme present in the reaction, which can then be converted to a molar concentration. The molar concentration of substrate in the reaction can also be determined, and the following calculations using the Beer-Lambert law require the use of the limiting reagent's concentration in order to calculate the expected absorbance values. Therefore, if we look at the reaction involving 2 μg MCR-1 (5.08×10^{-11} mol) with 2.5 mM *p*NP-PEtN (2.50×10^{-7} mol), we can see that the enzyme is the limiting reagent and therefore it is only possible to generate 5.08×10^{-11} moles of *p*NP ($\varepsilon = 18\,000\ M^{-1}\ cm^{-1}$). Following the conversion into molar concentrations and using the Beer-Lambert law with a path length of 0.3 cm for a 100 μL volume in a flat-bottom 96-well plate, the expected absorbance is calculated to be 0.00274, a value that is too small to have been observed in the experiment. Doubling the amount of enzyme used in the reaction would have doubled the expected absorbance value during the burst reaction, but it still would have been too small to distinguish when compared to the no enzyme control. Therefore, it is possible that the first reaction with MCR-1 and *p*NP-PEtN occurred quickly, but once the enzyme was saturated with PEtN, the background hydrolysis of *p*NP-PEtN dominated the reaction and attributed to the linear change in absorbance that was observed across the three conditions that were tested. The experiment should be repeated with a much greater concentration of MCR-1

that will produce a greater expected absorbance value, assuming *p*NP-PEtN is a substrate for the enzyme. Additionally, the zinc concentration in the reaction buffer may have not been adequate, and the use of higher zinc concentrations should be explored in future experiments.

Although the presence of a PEtN acceptor such as lipid A was not included in this assay, it could allow for the regeneration of free MCR-1 in the second half of the overall reaction which would allow the initial reaction to repeat, effectively completing the catalytic cycle. As it appears that water was a poor PEtN acceptor and was unable to hydrolyze PEtN from the active site of MCR-1, then perhaps the reaction should be attempted with lipid A present, but as this may complicate the assay, the use of a lipid A surrogate should be explored beforehand. The addition of the PEtN residue is believed to occur at the 4'-phosphate of lipid A[68,119], however it has also been proposed to occur at the 1-phosphate group[68,69] depending on the orientation of lipid A. Therefore, the use of a potential surrogate such as N-acetyl-α-D-glucosamine 1-phosphate (Figure 3-7) may be the key to successful turnover of *p*NP-PEtN.

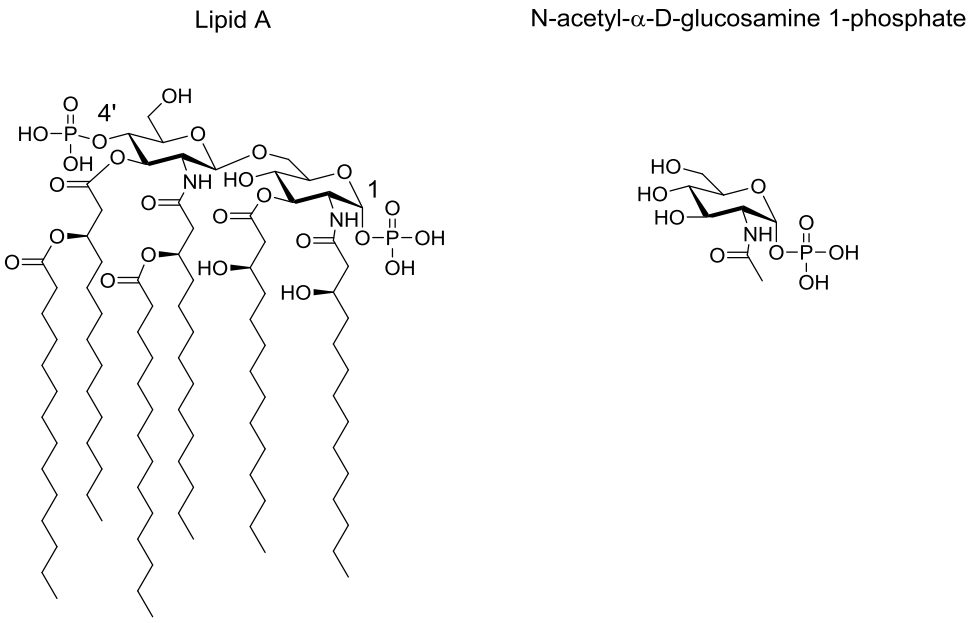

Figure 3-7: Structure of lipid A and N-acetyl-α-D-glucosamine 1-phosphate.
Left: Lipid A with numbered 4'- and 1-phosphate groups. *Right:* N-acetyl-α-D-glucosamine 1-phosphate that may serve as a potential surrogate to lipid A in a reaction with the MCR-1 C-terminal soluble domain and *p*NP-PEtN.

The N-acetyl-α-D-glucosamine 1-phosphate makes up what is essentially the right half of lipid A, minus the acyl chains, and therefore may potentially serve as a surrogate for lipid A in the reaction involving the C-terminal soluble domain of MCR-1 and *p*NP-PEtN.

A more recent study by Anandan *et al.*[74], published the full-length crystal structure of *Nm*EptA. The paper discusses the ability of full-length *Nm*EptA to remove PEtN from a fluorescently labelled lipid substrate resembling phosphatidylethanolamine, 1-acyl-2-{12-[(7-nitro-2-1,3-benzoxadiazol-4-yl)amino]dodecanoyl}-*sn*-glycero-3-phosphoethanolamine (Figure 3-8), as was measured by thin-layer chromatography (TLC) and mass spectrometry.

Phosphatidylethanolamine

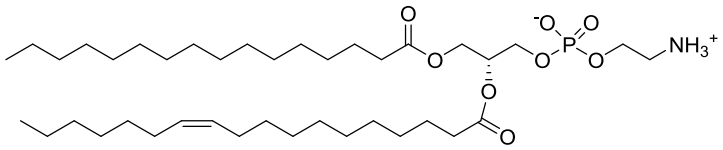

1-acyl-2-{12-[(7-nitro-2-1,3-benzoxadiazol-4-yl)amino]dodecanoyl}-*sn*-glycero-3-phosphoethanolamine

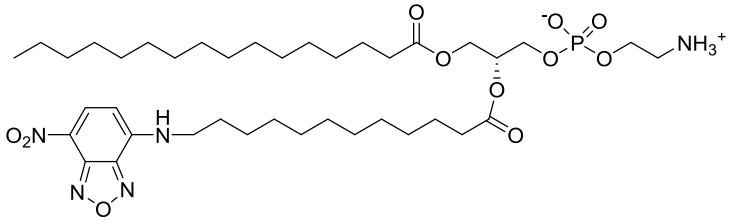

Figure 3-8: Phosphatidylethanolamine and a fluorescent homologue.
Top: Phosphatidylethanolamine, the native substrate for MCR-1. *Bottom*: The fluorescently labelled lipid substrate used in the study published by Anandan *et al.*[74] to characterize full length *Nm*EptA activity.

The paper also discusses the inability of the C-terminal soluble domain of *Nm*EptA to catalyze the hydrolysis of PEtN from this compound, suggesting that the transmembrane domain is required for its activity on a lipid substrate. Perhaps the use of full length MCR-1 or MCR-1 with truncated transmembrane regions, as well as a lipid substrate, will produce a successful result. Although this will not be a chromogenic assay and will have a longer turnaround time, it may prove to be a useful secondary assay for determining whether compounds of interest have any inhibitory effect on MCR-1.

Chapter 4.
Characterizing the structure-function relationship of MCR-1

4.1 Introduction

The integral inner membrane protein MCR-1 contains a transmembrane domain consisting of 5 major α-helices, and a C-terminal catalytic domain which adopts an α/β/α fold characteristic of the alkaline phosphatase superfamily[68]. These PEtN transferases are targeted to the inner membrane by the signal anchor sequence located in the first transmembrane domain which is recognized by the signal recognition particle and targets the protein to the inner membrane in a co-translational fashion[120]. Although their exact enzymatic mechanism of action is not completely understood, the crystal structure of the C-terminal catalytic domain of MCR-1 identified the presence of zinc ions, suggesting that it functions as a zinc metalloenzyme.

Zinc metalloenzymes rely on an essential zinc cofactor to carry out their biological function[121]. The zinc ion behaves as a Lewis acid to accept a pair of electrons and can act as a catalyst for reactions such as protein hydrolysis and the hydration of carbon dioxide. Within the zinc-binding sites of proteins, the ion is coordinated by different amino acid side chains, including the oxygen of aspartate or glutamate, the sulfur of cysteine, and the more commonly observed nitrogen of histidine. In rare cases it is also possible for the carbonyl oxygen of asparagine or glutamine to interact with the zinc ion. In a catalytic zinc site, the zinc ion directly participates in bond making or bond breaking reactions, whereas in a co-catalytic zinc site, several metal ions bound in proximity to one another enhance the catalytic activity of the site where one zinc ion

plays a catalytic role. Additionally, the removal of the zinc ion(s) can lead to a loss of enzyme activity.

Several crystal structures of the MCR-1 C-terminal catalytic domain have emerged, identifying a core hydrolase fold similar to that of alkaline phosphatase[68–70] which contains a co-catalytic zinc site[121]. Although, the crystal structures of MCR-1 indicate the presence of 1, 2, 3, and 4 zinc ions in the active site, as well as a phosphorylated Thr285 nucleophile and non-phosphorylated Thr285 nucleophile. These results are likely due to the various crystallization conditions, and therefore it is unknown exactly how many active zinc ions reside within MCR-1. The findings are summarized in Table 4-1.

PDB	No. of Zincs in Active Site	Phosphorylated Thr285? (Y/N)
5LRN[69]	1	Y
5LRM[69]	2	N
5GOV (Protein A)[70]	4	Y
5GOV (Protein B)[70]	2	N
5K4P[68]	3	Y

Table 4-1: List of MCR-1 crystal structures.
A list of PDB files containing MCR-1 crystal structures with varying quantities of active site zinc ions, as well as a phosphorylated and non-phosphorylated threonine nucleophiles.

In MCR-1, the presence of a phosphorylated and non-phosphorylated threonine nucleophile is hypothesized as the existence of two states of MCR-1 in its physiological environment which may reflect the existence of multiple reaction states during catalysis[70], although this hypothesis warrants further exploration. To compare these crystal structures to other PEtN transferase C-terminal domain crystal structures, *Nm*EptA (PDB: 4KAV)

from *Neisseria meningitides* contains 1 zinc ion and a phosphorylated threonine, *Nm*EptA (PDB: 4KAY) contains 2 zinc ions and a phosphorylated threonine, and EptC from *Campylobacter jejuni* (PDB: 4TN0) contains 1 zinc ion and a phosphorylated threonine. The full length crystal structure of *Nm*EptA which includes the transmembrane domain (PDB: 5FGN) contains 1 zinc ion and a non-phosphorylated threonine.

The MCR-1 crystal structures agree upon the placement of the one zinc ion coordinated by Asp465, His466, Glu246, and Thr285 in a tetrahedral geometry[68–70]. With respect to that zinc ion, it is plausible that MCR-1 employs a catalytic zinc site to accomplish its PEtN transfer onto lipid A[121]. Although, if MCR-1 has the potential to employ a second zinc in the active site, then perhaps it contains a co-catalytic zinc site[121], similar to that of alkaline phosphatase[68].

The structure and function relationship of MCR-1 and the *Moraxella catarrhalis* PEtN transferase, which shares 59% amino acid sequence identity with MCR-1[34], have not been extensively documented. This chapter describes the creation of *E. coli* MCR-1 and *M. catarrhalis* PEtN transferase truncations and a chimeric protein, as well as the generation of single amino acid substitutions and transmembrane domain truncations of *E. coli* MCR-1. These experiments were conducted to determine the functions of several amino acids that are conserved among PEtN transferases (Appendix 4) and whether it was possible to generate a shorter functioning variant of MCR-1 that could be used in an enzyme assay.

4.2 Materials and Methods

All primer sequences used in the following protocols can be found in Appendix 2.

4.2.1 Determining polymyxin susceptibility of *E. coli* MCR-1 and *Moraxella catarrhalis* phosphoethanolamine transferase truncations

The constructs described in this section have been obtained from the laboratory of Dr. Alexei Savchenko (University of Toronto). The full length *E. coli mcr-1* gene from pGDP2:*mcr-1* was cloned into the pNIC-CH expression vector, and the C-terminal domains of *E. coli* MCR-1 as well as the *M. catarrhalis* PEtN transferase (amino acids 217-541 and 235-578, respectively) were cloned into the pET22b expression vector incorporating an N-terminal PelB leader sequence. The transmembrane domain of *E. coli* MCR-1 (amino acids 1-207) and the C-terminal domain of the *M. catarrhalis* PEtN transferase (amino acids 235-578) were joined into one gene and cloned into pNIC-CH. These pET22b and pNIC-CH constructs were transformed into chemically competent *E. coli* BL21(DE3) cells and plated on LB agar supplemented with 100 μg/mL ampicillin (AMP201; BioShop) and LB agar supplemented with 50 μg/mL kanamycin, respectively. The MIC of colistin was determined for these *E. coli* strains using the microdilution broth method according to CLSI guidelines[98], with inoculum prepared using the colony suspension method. The strains were cultured in CAMHB at 37^{o}C with aeration (250 rpm) for 18 hours and the absorbance at 600 nm was measured using a SpectraMax® Plus 384 Microplate Reader.

4.2.2 Determining polymyxin susceptibility of *E. coli* MCR-1 harbouring single amino acid substitutions

The pNIC-CH plasmids containing *mcr-1* mutants were obtained from the laboratory of Dr. Alexei Savchenko (University of Toronto). Single amino acid substitutions were generated in MCR-1 via site-directed mutagenesis. The PCR reactions were carried out using pNIC-CH:*mcr-1* template DNA to create the mutants listed in Table 4-2, which also lists the primers that were used. Following the PCR reaction, the product was digested with the addition of 1 μL *Dpn* I at 37^{o}C for 1 hour. The digestion reaction was then repeated for an additional hour. A volume of 4 μL from the PCR/*Dpn* I digest was transformed into 80 μL of chemically competent *E. coli* DH5α cells, which were then plated on an LB agar plate supplemented with 50 μg/mL kanamycin and incubated at 37^{o}C overnight. Plasmid DNA from successful transformants was isolated, sequence verified, transformed into chemically competent *E. coli* BL21(DE3) cells, plated on LB agar plates supplemented with 50 μg/mL kanamycin, and incubated at 37^{o}C overnight. The MIC of colistin was determined for the *E. coli* BL21(DE3) MCR-1 mutants according to CLSI guidelines, as previously described.

MCR-1 Mutant	Proposed Function	Primer Set
Glu246Ala	Zn^{2+} binding	MCR-1_E246A
His395Ala	Zn^{2+} binding	MCR-1_H395A
Asp465Ala	Zn^{2+} binding	MCR-1_D465A
His478Ala	Zn^{2+} binding	MCR-1_H478A
Glu468Ala	Zn^{2+} binding	MCR-1_E468A
Thr285Ala	Nucleophile	MCR-1_T285A
Arg402Ala	Sulfate binding site	MCR-1_R402A
Glu363Ala	Sulfate binding site	MCR-1_E363A
Cys281Ala	Disulfide bond	MCR-1_C281A
Cys364Ala	Disulfide bond	MCR-1_C364A
Cys414Ala	Disulfide bond	MCR-1_C414A
Asn328Ala	Active site	MCR-1_N328A
Asn329Ala	Active site	MCR-1_N329A
Ser330Ala	Active site	MCR-1_S330A
Lys348Ala	Active site	MCR-1_K348A
His390Ala	Active site	MCR-1_H390A
Met392Ala	Active site	MCR-1_M392A
His466Ala	Active site	MCR-1_H466A
Thr112Ala	TMH3-TMH4 periplasmic loop	MCR-1_T112A
Asn108Ala	TMH3-TMH4 periplasmic loop	MCR-1_N108A
Gln107Ala	TMH3-TMH4 periplasmic loop	MCR-1_Q107A
Glu116Ala	TMH3-TMH4 periplasmic loop	MCR-1_E116A
Pro195Asp	TMH5-Catalytic domain linker	MCR-1_P195D

Table 4-2: List of MCR-1 mutants generated by site-directed mutagenesis.
The MCR-1 mutants generated via site directed mutagenesis, as well as the respective primers for the creation of each mutant.

4.2.3 Cloning MCR-1 transmembrane truncation mutants in *E. coli*

The following protocol adopts the nomenclature of the various motifs found within the full length *Nm*EptA crystal structure[74] (Figure 4-1 and Appendix 4) and applies it to MCR-1. Unless otherwise specified, plasmid DNA isolated from a clinical MDR *E. coli mcr-1*$^{+}$ isolate was used as template DNA for all PCR reactions.

The full length *mcr-1* gene was amplified by PCR using primers MCR-1_Fwd and MCR-1_Rev, incorporating *Nde* I and *Xho* I restriction sites. The size of the PCR product

coincided with the expected size of approximately 1600 bp, and was cloned into the pET22b expression vector using restriction enzymes *Nde* I and *Xho* I, generating a construct with a C-terminal $His_{(6)}$-tag. The construct was sequenced (MOBIX Lab, McMaster University) and transformed into chemically competent *E. coli* BL21(DE3) cells.

The segment of MCR-1 containing the signal anchor sequence for inner membrane targeting[120], spanning from the start of the protein including TMH1 as well as TMH1' (amino acids 1-45), which from hereon is referred to as TM1, was amplified by PCR using primers MCR-1_TM1_Fwd and MCR-1_TM1_Rev, incorporating *Nde* I and *Hind* III restriction sites. The size of the PCR product coincided with the expected size of approximately 135 bp, was cloned into the pET22b expression vector using restriction enzymes *Nde* I and *Hind* III, and was transformed into chemically competent *E. coli* TOP 10 cells. The plasmids of six transformants were purified and screened for the presence of the TM1 insert by PCR using primers MCR-1_TM1_Fwd and MCR-1_TM1_Rev. A plasmid that produced an amplicon at approximately 135 bp was selected and verified by Sanger sequencing (MOBIX Lab, McMaster University). The new plasmid that was generated, pET22b-TM1, was used as the vector backbone for subsequent cloning.

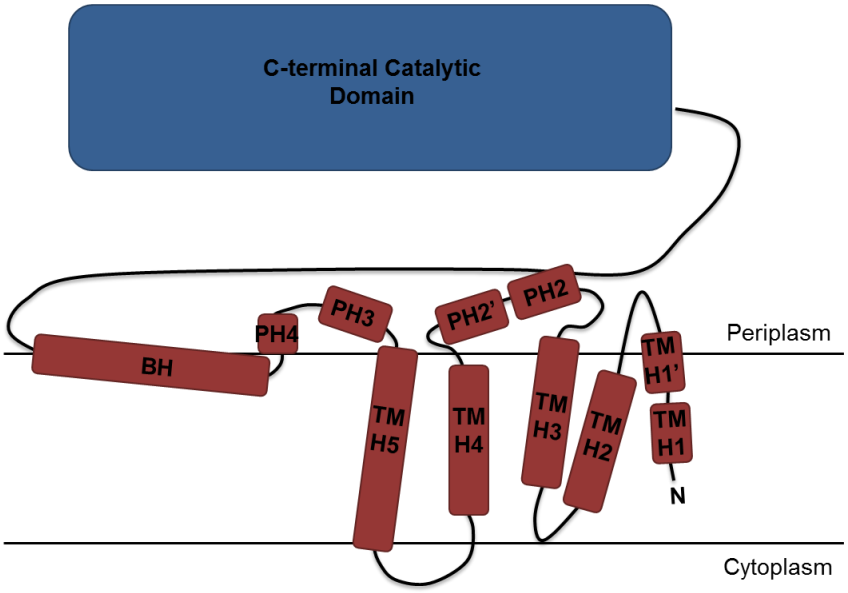

Figure 4-1: Transmembrane domains of MCR-1 based on *Nm*EptA.
A diagram depicting the transmembrane domain motifs of MCR-1, based on the schematic of full length *Nm*EptA. Adapted from Anandan *et al.*[74].

The MCR-1 transmembrane truncations were created by generating several amplicons from various positions within the gene to the end of the gene via PCR. The primers used to amplify these truncations require different forward primers and reverse primer GA_MCR-1_Rev, as outlined in Table 4-3.

Primer	First Motif of Amplicon
GA_MCR-1_46	TMH2
GA_MCR-1_73	TMH3
GA_MCR-1_99	PH2
GA_MCR-1_123	TMH4
GA_MCR-1_147	TMH5
GA_MCR-1_175	PH3
GA_MCR-1_194	BH
GA_MCR-1_215	C-terminal Domain
GA_MCR-1_Rev	-

Table 4-3: List of primers used to generate transmembrane truncations of *E. coli* MCR-1.
The primers used to generate transmembrane truncations of *E. coli* MCR-1 and the name of the first motif in the amplicon (Figure 4-1 and Appendix 4).

Each PCR amplicon was cloned into pET22b-TM1 by Gibson assembly, producing a final product containing a C-terminal $His_{(6)}$-tag. In a 20 μL reaction, 10 μL of 2X Gibson master mix (Appendix 1) was combined with 100 ng of *Hind* III- and *Xho* I-digested pET22b-TM1 vector and purified PCR amplicons in a 3:1 pmol insert:vector ratio. The reaction was incubated at 50°C for 20 minutes and 5 μL of the reaction was transformed into chemically competent *E. coli* TOP10 cells, which were then plated on LB plates supplemented with 100 μg/mL ampicillin and incubated overnight at 37°C. Transformants were screened for successful assembly by colony PCR with forward primers specific to each insert, and reverse primer MCR-1_Rev, as outlined in Table 4-4.

Construct	Colony PCR Primers
pET22b-TM1:*mcr-1*(46-541)	MCR-1_TM1_Fwd and MCR-1_Rev
pET22b-TM1:*mcr-1*(73-541)	MCR-1_73 and MCR-1_Rev
pET22b-TM1:*mcr-1*(99-541)	MCR-1_99 and MCR-1_Rev
pET22b-TM1:*mcr-1*(123-541)	MCR-1_123 and MCR-1_Rev
pET22b-TM1:*mcr-1*(147-541)	MCR-1_147 and MCR-1_Rev
pET22b-TM1:*mcr-1*(175-541)	MCR-1_175 and MCR-1_Rev
pET22b-TM1:*mcr-1*(194-541)	MCR-1_194 and MCR-1_Rev
pET22b-TM1:*mcr-1*(215-541)	MCR-1_215 and MCR-1_Rev

Table 4-4: *E. coli* MCR-1 transmembrane truncation constructs and primers for colony PCR.
A list of primers used to verify successful Gibson assembly in each respective MCR-1 transmembrane truncation construct.

The constructed plasmids were isolated from colonies that displayed amplicons of the correct size for each insert and were verified by Sanger sequencing (MOBIX Lab, McMaster University). The plasmids were then transformed into chemically competent *E. coli* BL21(DE3) cells and the MIC of colistin was determined for these strains according to CLSI guidelines, as previously described.

4.3 Results

4.3.1 Polymyxin susceptibility of *E. coli* MCR-1 and *Moraxella catarrhalis* phosphoethanolamine transferase truncations

To determine whether the transmembrane domain of the *E. coli* MCR-1 and *M. catarrhalis* PEtN transferase were necessary to confer resistance to polymyxins, the C-terminal domains were expressed from pET22b following a PelB periplasmic localization signal peptide. The expression of the MCR-1 (217-541) and *M. catarrhalis* PEtN transferase (235-578) C-terminal domains did not confer resistance to colistin, with an MIC of 0.125 μg/mL. The construct expressing the chimeric protein made of the *E. coli* MCR-1 transmembrane domain and the *M. catarrhalis* PEtN transferase C-terminal domain, pNIC-CH:*mcr-1(1-207)-moraxPEtN(235-578)*, as well as the full length *E. coli* MCR-1 construct, pNIC-CH:*mcr-1*, were able to confer colistin resistance, resulting in an MIC of 8 μg/mL. As expected, the pET22b and pNIC-CH controls did not promote colistin resistance, with an MIC of 0.125 μg/mL. These results are summarized in Table 4-5.

Construct	Colistin MIC (μg/mL)
pET22b	0.125
pNIC-CH	0.125
pNIC-CH:*mcr-1*	8
pET22b:*mcr-1(217-541)*	0.125
pET22b:*moraxPEtN(235-578)*	0.125
pNIC-CH:*mcr-1(1-207)-moraxPEtN(235-578)*	8

Table 4-5: Colistin MIC data for *E. coli* MCR-1 and *M. catarrhalis* PEtN transferase constructs.
Minimum inhibitory concentration (MIC) data generated for colistin tested against the C-terminal catalytic domains of *E. coli* MCR-1 and *M. catarrhalis* PEtN transferase, a chimeric protein consisting of the transmembrane domain of *E. coli* MCR-1 and the C-terminal catalytic domain of *M. catarrhalis* PEtN transferase, and an MCR-1 control. All constructs were tested in *E. coli* BL21(DE3) cells.

4.3.2 Polymyxin susceptibility of *E. coli* MCR-1 harbouring single amino acid substitutions

A collection of *E. coli* MCR-1 mutants were generated to understand which residues were essential for enzyme function. The constructs were expressed in *E. coli* BL21(DE3) and the MIC of colistin was determined for each mutant. A graph was generated to display the results (Figure 4-2).

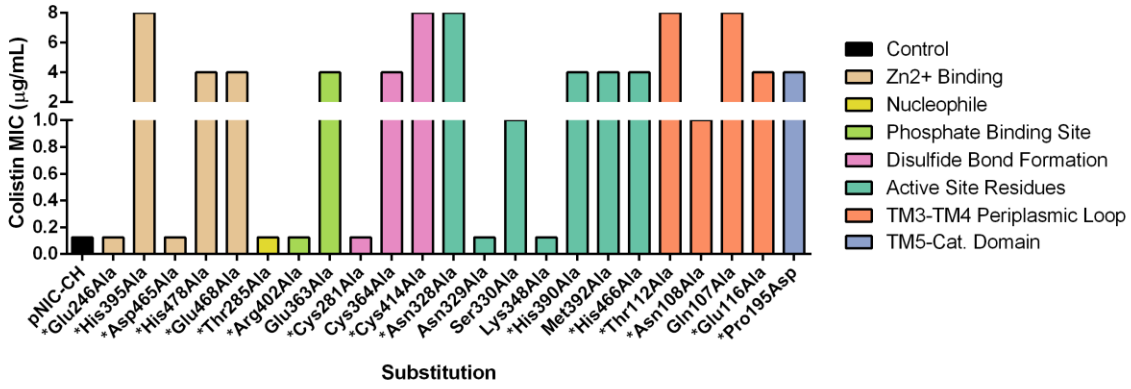

Figure 4-2: Colistin MIC data for *E. coli* MCR-1 amino acid substitutions.
Minimum inhibitory concentration (MIC) data generated for colistin tested against *E. coli* MCR-1 mutants in *E. coli* BL21(DE3) cells. Residues marked with a * indicate 100% conservation between 7 different PEtN transferases[74] (Appendix 4).

Most of the substitutions had little to no impact on the ability of MCR-1 to confer resistance to colistin, resulting in an MIC of 4 μg/mL or 8 μg/mL, where 8 μg/mL is the MIC of the native *E. coli* MCR-1 strain. Substitutions in two residues suggested to be involved in zinc binding, Glu246 and Asp465, showed a loss of enzyme activity and increased susceptibility to colistin with an MIC of 0.125 μg/mL, which is identical to the MIC of the empty vector control. Substitution of His395, which coordinates an additional zinc residue in the active site[68], did not affect the function of the enzyme, whereas

substitution of His478, which does not interact with zinc, appeared to have a slight effect on the enzyme with an MIC of 4 μg/mL. The MCR-1 nucleophile, Thr285, is critical for enzyme function, as substitution of this residue resulted in the loss of enzyme activity and an MIC of 0.125 μg/mL. A proposed phosphate binding residue, Arg402, which may make contact with the phosphate group of lipid A, was found to be important for enzyme function, as substitution of this residue also resulted in loss of enzyme activity and an MIC identical to that of the empty vector control. A structure of the active site of MCR-1 with these residues is portrayed in Figure 4-3.

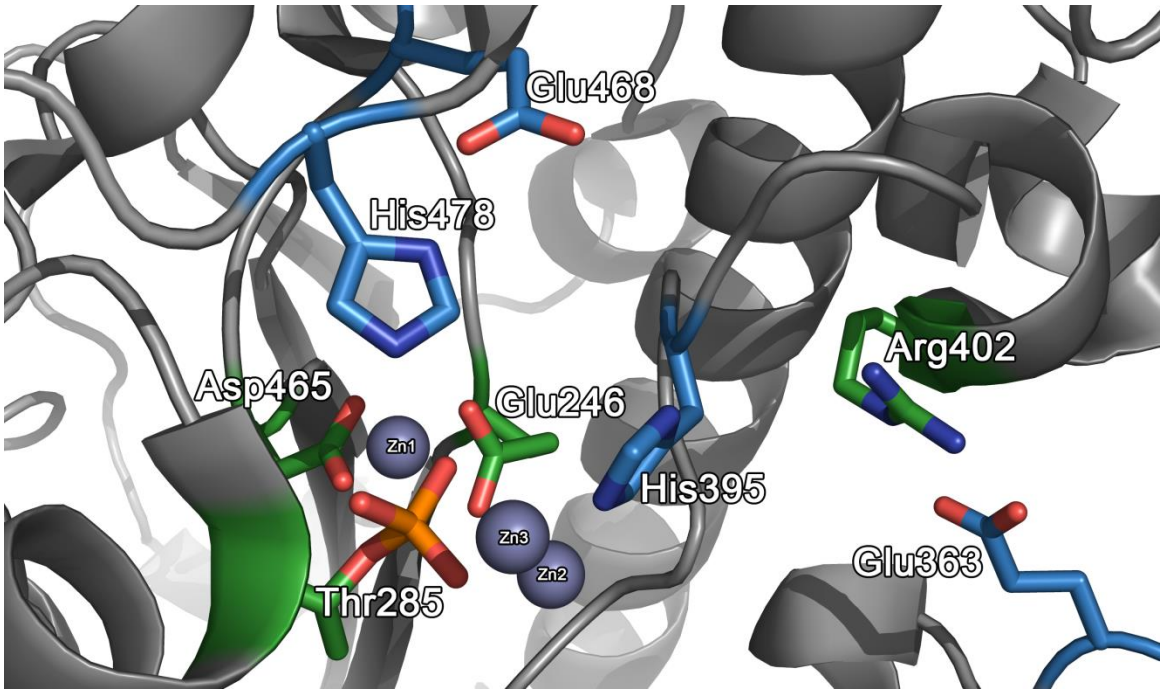

Figure 4-3: Crystal structure of the MCR-1 active site.
Crystal structure of MCR-1 with a phosphorylated threonine-285 nucleophile. Zinc ions are represented in purple. Residues represented by a green color are essential to enzyme function, where substitutions of these residues results in a colistin MIC of 0.125 μg/mL. Residues represented by a blue color are less essential to enzyme function, where substitutions of these residues results in a colistin MIC of ≥ 4 μg/mL. (PDB 5K4P).

The cysteine residues present in MCR-1 that form disulfide bonds between Cys281/Cys291, Cys356/Cys364, and Cys414/Cys422[68], were targeted for substitutions. Substitution of Cys281 resulted in a loss of colistin resistance, with an MIC of 0.125 μg/mL, whereas substitution of Cys364 had a less severe impact on MCR-1, with an MIC of 4 μg/mL. Substitution of Cys414 did not appear to impact enzyme function, with an MIC of 8 μg/mL. The structure of these cysteine residues within the overall MCR-1 C-terminal domain are portrayed in Figure 4-4.

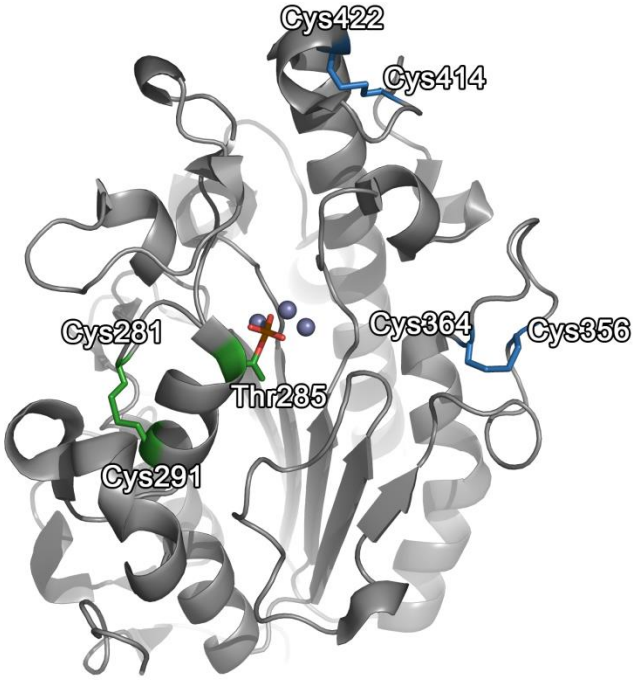

Figure 4-4: Crystal structure of MCR-1 with disulfide bonds.
Crystal structure of MCR-1 with a phosphorylated threonine-285 nucleophile. Zinc ions are represented in purple. The cysteine bond represented by a green color is essential to enzyme function, where substitution in a residue responsible for this bond results in a colistin MIC of 0.125 μg/mL. Cysteine bonds represented by a blue color are less essential to enzyme function, where substitution of these residues results in a colistin MIC of ≥ 4 μg/mL. (PDB 5K4P).

Active site residues Asn329 and Lys348 appeared to be essential to MCR-1, as substitutions of these residues resulted in an MIC of 0.125 μg/mL. A substitution of Ser330 appeared to be slightly less severe than the substitution of Asn329, but still impeded enzyme function as this reduced the MIC of colistin to 1 μg/mL and had clear impairment of enzyme function. The substitution of an adjacent residue, Asn328, did not affect MCR-1. Substitutions of His390, Met392, and His466 had little impact on the function of MCR-1, resulting in an MIC of 4 μg/mL. A structure of the active site of MCR-1 with these residues is portrayed in Figure 4-5.

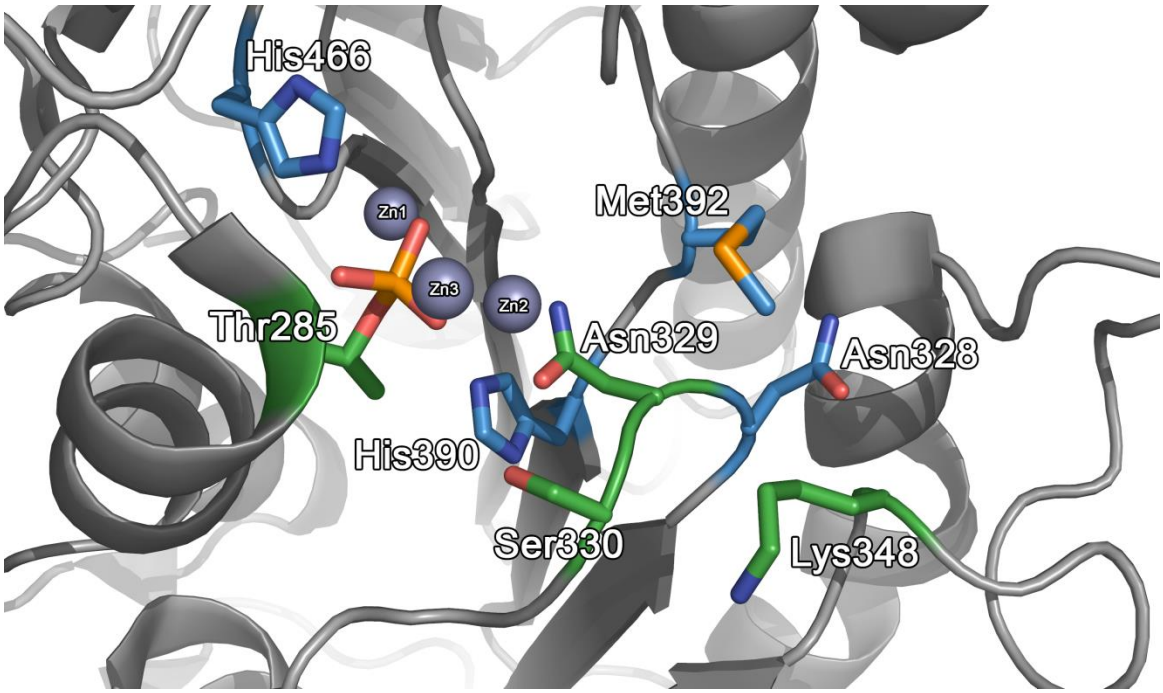

Figure 4-5: Crystal structure of the MCR-1 active site.
Crystal structure of MCR-1 with a phosphorylated threonine-285 nucleophile. Zinc ions are represented in purple. Residues represented by a green color are essential to enzyme function, where substitution of these residues results in a colistin MIC of ≤ 1 μg/mL. Residues represented by a blue color are less essential to enzyme function, where substitution of these residues results in a colistin MIC of ≥ 4 μg/mL. (PDB 5K4P).

A few substitutions were generated in the PH2 and PH2' periplasmic helices between the 3rd and 4th transmembrane helices of MCR-1 (Figure 4-1 and Appendix 4). One substitution in PH2 at a conserved residue within PEtN transferases, Asn108, lowered the MIC of colistin to 1 μg/mL. Substitutions in PH2 residues Gln107 and Thr112 did not seem to impair enzyme function, with an MIC of 8 μg/mL. The substitution of residue Glu116 within PH2' had a slight effect on enzyme activity, resulting in an MIC of 4 μg/mL. A substitution in Pro195, a conserved residue before the BH motif and C-terminal domain, lowered the MIC to 4 μg/mL.

4.3.3 Polymyxin susceptibility of the *E. coli* MCR-1 transmembrane truncation mutants

Truncations within the *E. coli* MCR-1 transmembrane domain were generated to understand the function of the transmembrane domain, and to determine the possibility of generating a shorter MCR-1 variant that conferred resistance to colistin. The pET22b-TM1:*mcr-1*(46-541) construct, which contains the TM1 fragment stitched to the remaining full length gene, conferred resistance to colistin with an MIC of 8 μg/mL. The other constructs that were generated were not successful in conferring resistance to colistin, resulting in an MIC of 4 μg/mL, which was identical to the no insert pET22b-TM1 control. As expected, the pET22b:*mcr-1* construct conferred resistance to colistin with an MIC of 8 μg/mL. A summary of the MIC data generated is displayed in Table 4-6.

Construct	First Motif Following TM1 (Signal Sequence)	Colistin MIC (μg/mL)
pET22b:*mcr-1*	-	8
pET22b-TM1	-	4
pET22b-TM1:*mcr-1*(46-541)	TMH2	8
pET22b-TM1:*mcr-1*(73-541)	TMH3	4
pET22b-TM1:*mcr-1*(99-541)	PH2	4
pET22b-TM1:*mcr-1*(123-541)	TMH4	4
pET22b-TM1:*mcr-1*(147-541)	TMH5	4
pET22b-TM1:*mcr-1*(175-541)	PH3	4
pET22b-TM1:*mcr-1*(194-541)	BH	4
pET22b-TM1:*mcr-1*(215-541)	C-terminal Domain	4

Table 4-6: Colistin MIC data for *E. coli* MCR-1 transmembrane truncation mutants.
Minimum inhibitory concentration (MIC) data generated for colistin tested against *E. coli* MCR-1 transmembrane truncation mutants, as well as an MCR-1 control. All constructs were tested in *E. coli* BL21(DE3) cells.

4.4 Discussion

The inability of the periplasmic-localized *E. coli* MCR-1 or *M. catarrhalis* PEtN transferase C-terminal domains to confer resistance to colistin is not surprising. A study conducted on *Nm*EptA discusses the inability of the soluble C-terminal domain to transfer PEtN onto the headgroup of *E. coli* lipid A, as analyzed by MALDI-TOF-MS[118]. These results suggest that the transmembrane domain of the PEtN transferase is necessary to apply the PEtN addition to lipid A. The reintroduction of the *E. coli* MCR-1 transmembrane domain to the C-terminal soluble domain of the *M. catarrhalis* PEtN transferase restored activity of the chimeric enzyme, allowing the modification of lipid A to confer resistance to colistin. As the *M. catarrhalis* PEtN transferase shares 59% amino acid sequence identity with MCR-1[34], the chimeric construct demonstrates the cross-compatibility of both domains and further supports the notion that the transmembrane domain is necessary for enzyme activity.

Several of the MCR-1 amino acid substitutions did not have an effect on the ability of the enzyme to confer resistance to colistin, and so these residues may be considered non-essential to the function of the enzyme. The two zinc-binding residues, Glu246 and Asp465, are considered essential to enzyme function as substitution of either residue resulted in a loss of enzyme activity. These two residues are conserved in several PEtN transferases[74] (Appendix 4), including EptC and *Nm*EptA[70,75], and are believed to be responsible for the deprotonation of the Thr285 nucleophile[69] (Chapter 3, Figure 3-2). Substituting of these residues may therefore result in the inability of MCR-1 to acquire the PEtN moiety and modify lipid A. Hinchliffe *et al.*[69] reported that Glu246 or Asp465 could be responsible for the deprotonation of Thr285, so it is interesting that substitutions in either residue abolish enzyme activity. This may be caused by the disruption of the (co-)catalytic zinc site when one of the residues is substituted, and may cause the enzyme to no longer be able to carry out the nucleophilic attack on PEtN.

As expected, substituting the Thr285 nucleophile resulted in loss of enzyme activity. This residue is required to generate the MCR-1-PEtN intermediate, and without this residue the reaction cannot proceed. The Arg402 residue may be responsible for coordinating the phosphate groups of lipid A, so substituting this residue would affect the ability of MCR-1 to coordinate the transfer of PEtN from Thr285 onto the phosphate group of lipid A. This impact to modification of lipid A would directly influence the resistance to colistin, increasing susceptibility.

The formation of three disulfide bonds in the C-terminal domain of MCR-1, which is typical of alkaline phosphatase enzymes[69], form between Cys281/Cys291,

Cys356/Cys364, and Cys414/Cys422[68]. The disulfide bond of Cys281/Cys291 bridges a loop region with the α-helix on which the Thr285 nucleophile resides, and the loss of this disulfide bond by substituting Cys281 likely cause a change in the tertiary structure of the C-terminal domain. This can cause the configuration of the active site to become disrupted which would impair the function of the Thr285 nucleophile. Substitutions of the other cysteine residues had a small impact on the MIC of colistin, which may be due to their farther distance from the active site resulting in a more tolerated change in tertiary structure. Substitutions of Asn329, Ser330, and Lys348 decreased the MIC of colistin, although the function of these residues is unknown. It is possible that they may assist with stabilizing the substrate in the enzyme.

Substitution of Asn108 reduced the MIC of colistin to 1 μg/mL, so this residue must be important for the catalytic activity of PEtN, as it is also 100% conserved between 7 different PEtN transferases[74] (Appendix 4). This residue falls within the PH2 motif, a periplasmic facing helix which could be partially buried or embedded in the membrane, and it is believed to complete the substrate binding site along with PH2', a neighboring helix. The study conducted by Anandan *et a.l*[74] used molecular dynamics simulations to study the orientation of *Nm*EptA in the lipid bilayer, and in one simulation a phosphatidylethanolamine headgroup spontaneously bound between the PH2 and PH2' helices. Disruption of the PH2 motif may impede the ability of MCR-1 to stabilize the substrate in the active site. Modifying Glu116, a residue within PH2' that may hydrogen bond with the amine of PEtN and is 100% conserved in 7 PEtN transferases (Appendix 4), slightly affected enzyme function and resulted in an MIC of 4 μg/mL. These

substitutions confirm the importance of the transmembrane domain in the ability of MCR-1 to function correctly.

A study by Hu *et al.*[70] generated several amino acid substitutions in MCR-1 and tested the ability of the resulting enzymes to confer resistance to colistin. The results they generated for substitutions Glu246Ala, Thr285Ala, Asp465Ala, and His395Ala are in-line with the data generated in this chapter. Their results for four substitutions, His466Ala, His478Ala, Asn329Ala, and Ser330Ala do not coincide with the data generated in this chapter. The study reports that His466Ala and His478Ala substitutions results in an MIC identical to the control strain, 2 μg/mL, whereas this chapter reports an MIC of 4 μg/mL, a 32-fold increase from the control strain MIC of 0.125 μg/mL. Their Asn329Ala and Ser330Ala substitutions did not affect the enzyme's ability to confer resistance to colistin (MIC of 8 μg/mL), whereas this chapter reports the decrease in MIC to 0.125 μg/mL and 1 μg/mL, respectively.

The MCR-1 transmembrane truncations were generated to determine if it was possible to generate a shorter functional MCR-1 variant that could be used in an enzyme assay. The constructs were designed to include the TMH1 and TMH1' regions at the N-terminus of each truncation so that the protein would be localized into the inner membrane. The only construct that conferred resistance was pET22b-TM1:*mcr-1*(46-541), which is the full length *mcr-1* gene containing the TMH1 and TMH1' region stitched to the remaining *mcr-1* gene. The other constructs were not able to confer resistance to colistin, suggesting that the entire protein structure is required for proper enzyme function.

Chapter 5.
Conclusions and future directions

5.1 Conclusions and future directions

The aim of this work was to conduct a high-throughput screen of Actinomycete-derived solid media extracts to search for a natural product inhibitor of MCR-1. The screen revealed many hits that were found to contain antibiotics that synergized with the sub-inhibitory concentration of colistin to kill the *E. coli* BW25113-pGDP2:*mcr-1* strain. The synergy of colistin with other antibiotics was explored and it was determined that sub-inhibitory concentrations of colistin can synergize with hydrophobic antibiotics such as rifamycins, even in the presence of a polymyxin resistance element, explaining the large number of antibiotics that were identified in the screen.

The goal of developing an *in vitro* enzyme assay was to test for inhibitors of MCR-1 without the worry of polymyxin synergizing with other antibiotics. A chromogenic substrate, *p*NP-PEtN, was synthesized but it was not turned over the by the C-terminal catalytic domain of MCR-1. The assay did not show any change in absorbance over the course of the reaction compared to the no enzyme control, suggesting the incompatibility of the substrate, or the possible lack of a PEtN acceptor to remove the PEtN from the active site of MCR-1. The addition of a lipid A surrogate such as the proposed N-acetyl-α-D-glucosamine 1-phosphate should be explored in the future. Additionally, recreating the reaction with full length MCR-1 and lipid substrates may prove to be a useful strategy to determine if a compound inhibits MCR-1, although the process would not be as facile as a chromogenic assay.

Lastly, this work aimed to explore the structure-function relationship of MCR-1 through the introduction of single amino acid substitutions and the generation of MCR-1 transmembrane truncation mutants. The substitutions provide insight into key residues that are essential for the catalysis of the transfer of PEtN onto lipid A. Although not many MCR-1 mutants were generated, further work should be done to generate more substitutions in residues that are 100% conserved among the seven PEtN transferases (Appendix 4), in order to further understand how they affect the enzyme. Future work should focus on the transmembrane domain, where substitutions of other key conserved residues may aid in the understanding of the importance of the transmembrane domain, as well as how it functions in stabilizing the substrates and bringing them into the active site. The generation of transmembrane truncation mutants did not result in a functional MCR-1 variant, further suggesting the importance of that domain.

References

1. Black, S. R. *et al.* Regional infection control assessment of antibiotic resistance knowledge and practice. *Infect. Control Hosp. Epidemiol.* **36,** 1–6 (2015).
2. Arias, C. A. & Murray, B. E. A new antibiotic and the evolution of resistance. *N. Engl. J. Med.* **372,** 1168–1170 (2015).
3. Palumbi, S. R. Humans as the world's greatest evolutionary force. *Science.* **293,** 1786–1790 (2001).
4. Spellberg, B. *et al.* Combating antimicrobial resistance: policy recommendations to save lives. *Clin. Infect. Dis.* **52,** 397–428 (2011).
5. Infectious Diseases Society of America. Bad Bugs, No Drugs. 37 (2004).
6. Kim, S. K. *et al.* Antibiotic resistance in bacteria: novel metalloenzyme inhibitors. *Chem. Biol. Drug Des.* **74,** 343–348 (2009).
7. King, A. M. *et al.* Aspergillomarasmine A overcomes metallo-β-lactamase antibiotic resistance. *Nature* **510,** 503–6 (2014).
8. Cox, G. *et al.* A common platform for antibiotic dereplication and adjuvant discovery. *Cell Chem. Biol.* **24,** 98–109 (2017).
9. Reading, C. & Cole, M. Clavulanic acid: a beta-lactamase-inhibiting beta-lactam from *Streptomyces clavuligerus. Antimicrob. Agents Chemother. N.J* **11,** 852–857 (1977).
10. Yu, Z., Qin, W., Lin, J., Fang, S. & Qiu, J. Antibacterial mechanisms of polymyxin and bacterial resistance. *Biomed Res. Int.* 1–11 (2015). doi:10.1155/2015/679109
11. Wang, X. & Quinn, P. J. Lipopolysaccharide: biosynthetic pathway and structure modification. *Prog. Lipid Res.* **49,** 97–107 (2010).
12. Kim, S. H., Jia, W., Parreira, V. R., Bishop, R. E. & Gyles, C. L. Phosphoethanolamine substitution in the lipid A of *Escherichia coli* O157:H7 and its association with PmrC. *Microbiology* **152,** 657–666 (2006).
13. Raetz, C. R. H. & Whitfield, C. Lipopolysaccharide endotoxins. *Annu. Rev. Biochem.* **71,** 635–700 (2002).
14. Nikaido, H. Molecular basis of bacterial outer membrane permeability revisited. *Microbiol. Mol. Biol. Rev.* **67,** 593–656 (2003).
15. Kabanov, D. S. & Prokhorenko, I. R. Structural analysis of lipopolysaccharides from Gram-negative bacteria. *Biochem.* **75,** 383–404 (2010).
16. Babinski, K. J., Kanjilal, S. J. & Raetz, C. R. H. Accumulation of the lipid A precursor UDP-2,3-diacylglucosamine in an *Escherichia coli* mutant lacking the *lpxH* gene. *J. Biol. Chem.* **277,** 25947–25956 (2002).
17. Babinski, K. J., Ribeiro, A. A. & Raetz, C. R. H. The *Escherichia coli* gene encoding the UDP-2,3-diacylglucosamine pyrophosphatase of lipid A biosynthesis. *J. Biol. Chem.* **277,** 25937–25946 (2002).
18. Crowell, D. N., Reznikoff, W. S. & Raetz, C. R. H. Nucleotide sequence of the *Escherichia coli* gene for lipid A disaccharide synthase. *J. Bacteriol.* **169,** 5727–5734 (1987).
19. Crowell, D. N., Anderson, M. S. & Raetz, C. R. H. Molecular cloning of the genes for lipid A disaccharide synthase and UDP-N-acetylglucosamine acyltransferase in *Escherichia coli. J. Bacteriol.* **168,** 152–159 (1986).

20. Garrett, T. A., Que, N. L. S. & Raetz, C. R. H. Accumulation of a lipid A precursor lacking the 4'-phosphate following inactivation of the *Escherichia coli lpxK* gene. *J. Biol. Chem.* **273,** 12457–12465 (1998).
21. Garrett, T. A., Kadrmas, J. L. & Raetz, C. R. H. Identification of the gene encoding the *Escherichia coli* lipid A 4'-kinase. Facile phosphorylation of endotoxin analogs with recombinant LpxK. *J. Biol. Chem.* **272,** 21855–21864 (1997).
22. Brozek, K. A., Hosakas, K., Robertsong, A. D., Raetzll, C. R. H. & Chern, K. J. B. Biosynthesis of lipopolysaccharide in *Escherichia coli.* Cytoplasmic enzymes that attach 3-deoxy-D-manno-octulosonic acid to lipid A. *J. Biol. Chem.* **264,** 6956–6966 (1988).
23. Brozek, K. A. & Raetz, C. R. H. Biosynthesis of lipid A in *Escherichia coli.* Acyl carrier protein-dependent incorporation of laurate and myristate. *J. Biol. Chem.* **265,** 15410–15417 (1990).
24. Doerrler, W. T., Gibbons, H. S. & Raetz, C. R. H. MsbA-dependent translocation of lipids across the inner membrane of *Escherichia coli*. *J. Biol. Chem.* **279,** 45102–45109 (2004).
25. Doerrler, W. T. & Raetz, C. R. H. ATPase activity of the MsbA lipid flippase of *Escherichia coli. J. Biol. Chem.* **277,** 36697–36705 (2002).
26. Sperandeo, P. *et al.* Characterization of *lptA* and *lptB*, two essential genes implicated in lipopolysaccharide transport to the outer membrane of *Escherichia coli. J. Bacteriol.* **189,** 244–253 (2007).
27. Sperandeo, P. *et al.* Functional analysis of the protein machinery required for transport of lipopolysaccharide to the outer membrane of *Escherichia coli. J. Bacteriol.* **190,** 4460–4469 (2008).
28. Ruiz, N., Gronenberg, L. S., Kahne, D. & Silhavy, T. J. Identification of two inner-membrane proteins required for the transport of lipopolysaccharide to the outer membrane of *Escherichia coli*. *PNAS* **105,** 5537–5542 (2008).
29. Wu, T. *et al.* Identification of a protein complex that assembles lipopolysaccharide in the outer membrane of *Escherichia coli. PNAS* **103,** 11754–11759 (2006).
30. Benedict, R. G. & Langlykke, A. F. Antibiotic activity of *Bacillus polymyxa*. *J. Bacteriol.* **54,** 24 (1947).
31. Ainsworth, G. C., Brown, A. M. & Brownlee, G. 'Aerosporin', an antibiotic produced by *Bacillus aerosporus* Greer. *Nature* **160,** 878 (1947).
32. Berglund, N. A. *et al.* Interaction of the antimicrobial peptide polymyxin B1 with both membranes of *E. coli*: a molecular dynamics study. *PLoS Comput. Biol.* **11,** 1–17 (2015).
33. Michalopoulos, A. & Falagas, M. E. Colistin and polymyxin B in critical care. *Crit. Care Clin.* **24,** 377–391 (2008).
34. Liu, Y. Y. *et al.* Emergence of plasmid-mediated colistin resistance mechanism MCR-1 in animals and human beings in China: A microbiological and molecular biological study. *Lancet Infect. Dis.* **16,** 161–168 (2015).
35. Velkov, T., Thompson, P. E., Nation, R. L. & Li, J. Structure-activity relationships of polymyxin antibiotics. *J. Med. Chem.* **53,** 1898–1916 (2010).

36. Velkov, T., Roberts, K. D., Nation, R. L., Thompson, P. E. & Li, J. Pharmacology of polymyxins: new insights into an 'old' class of antibiotics. *Future Microbiol.* **8,** 711–724 (2013).
37. Hancock, R. E. Peptide antibiotics. *Lancet* **349,** 418–422 (1997).
38. Cajal, Y., Rogers, J., Berg, O. G. & Jain, M. K. Intermembrane molecular contacts by polymyxin B mediate exchange of phospholipids. *Biochemistry* **35,** 299–308 (1996).
39. Clausell, A. *et al.* Gram-negative outer and inner membrane models: insertion of cyclic cationic lipopeptides. *J. Phys. Chem.* **111,** 551–563 (2007).
40. Imlay, J. A. The molecular mechanisms and physiological consequences of oxidative stress: lessons from a model bacterium. *Nat. Rev. Microbiol.* **11,** 443–454 (2013).
41. Kohanski, M. A., Dwyer, D. J., Hayete, B. & Lawrence, C. A. A common mechanism of cellular death induced by bactericidal antibiotics. *Cell* **130,** 797–810 (2007).
42. Cai, Y., Lee, W. & Kwa, A. L. Polymyxin B versus colistin: an update. *Expert Rev. Anti. Infect. Ther.* **13,** 1481–1497 (2015).
43. Biswas, S., Brunel, J., Dubus, J., Reynaud-Gaubert, M. & Rolain, J. Colistin: an update on the antibiotic of the 21st century. *Expert Rev. Anti. Infect. Ther.* **10,** 917–934 (2012).
44. Shahbazi, F. & Dashti-Khavidaki, S. Colistin: efficacy and safety in different populations. *Expert Rev. Clin. Pharmacol.* **8,** 423–448 (2015).
45. Dal, L. *et al.* High-dose, extended-interval colistin administration in critically ill patients: is this the right dosing strategy? A preliminary study. *Clin. Infect. Dis.* **54,** 1720–1726 (2012).
46. Batirel, A. *et al.* Comparison of colistin–carbapenem, colistin–sulbactam, and colistin plus other antibacterial agents for the treatment of extremely drug-resistant *Acinetobacter baumannii* bloodstream infections. *Eur. J. Clin. Microbiol. Infect. Dis.* **33,** 1311–1322 (2014).
47. Elwood, C. M., Lucas, G. D. & Muehrcke, R. C. Acute renal failure associated with sodium colistimethate treatment. *Arch. Intern. Med.* **118,** 326–334 (1966).
48. Fekety, R. F., Norman, P. S. & Cluff, L. E. The treatment of Gram-negative bacillary infections with colistin: the toxicity and efficacy of large doses in forty-eight patients. *Ann. Intern. Med.* **57,** 214–229 (1962).
49. Parisi, A. F. & Kaplan, M. H. Apnea during treatment with sodium colistimethate. *JAMA* **194,** 184–185 (1965).
50. Abdelraouf, K. *et al.* Characterization of polymyxin B-induced nephrotoxicity: implications for dosing regimen design. *Antimicrob. Agents Chemother.* **56,** 4625–4629 (2012).
51. Akajagbor, D. S. *et al.* Higher incidence of acute kidney injury with intravenous colistimethate sodium compared with polymyxin B in critically ill patients at a tertiary care medical center. *Clin. Infect. Dis.* **57,** 1300–1303 (2013).

52. Phe, K. *et al.* In vitro assessment and multicenter cohort study of comparative nephrotoxicity rates associated with colistimethate versus polymyxin B therapy. *Antimicrob. Agents Chemother.* **58,** 2740–2746 (2014).
53. Brown, P. & Dawson, M. J. Development of new polymyxin derivatives for multi-drug resistant Gram-negative infections. *J. Antibiot. (Tokyo).* 1–9 (2017). doi:10.1038/ja.2016.146
54. Olaitan, A. O., Morand, S. & Rolain, J. Mechanisms of polymyxin resistance : acquired and intrinsic resistance in bacteria. *Front. Microbiol.* **5,** 1–18 (2014).
55. Falagas, M. E., Rafailidis, P. I. & Matthaiou, D. K. Resistance to polymyxins: mechanisms, frequency and treatment options. *Drug Resist. Updat.* **13,** 132–138 (2010).
56. Wayne, P. A. Clinical and laboratory standards institute. Performance standards for antimicrobial susceptibility testing; Twenty-fifth informational supplement. CLSI document M100-25. (2015).
57. European committee on antimicrobial susceptibility testing. Breakpoint tables for interpretation of MICs and zone diameters. Version 7.1. (2017).
58. Boll, J. M. *et al.* Reinforcing lipid A acylation on the cell surface of *Acinetobacter baumannii* promotes cationic antimicrobial peptide resistance and desiccation survival. *MBio* **6,** 1–11 (2015).
59. Guo, L. *et al.* Lipid A acylation and bacterial resistance against vertebrate antimicrobial peptides. *Cell* **95,** 189–198 (1998).
60. Bishop, R. E. *et al.* Transfer of palmitate from phospholipids to lipid A in outer membranes of Gram-negative bacteria. *EMBO J.* **19,** 5071–5080 (2000).
61. Moffatt, J. H. *et al.* Colistin resistance in *Acinetobacter baumannii* is mediated by complete loss of lipopolysaccharide production. *Antimicrob. Agents Chemother.* **54,** 4971–4977 (2010).
62. Petrou, V. I. *et al.* Structures of aminoarabinose transferase ArnT suggest a molecular basis for lipid A glycosylation. *Science* **351,** 608–612 (2016).
63. Gunn, J. S. *et al.* PmrA-PmrB-regulated genes necessary for 4-aminoarabinose lipid A modification and polymyxin resistance. *Mol. Microbiol.* **27,** 1171–1182 (1998).
64. Lee, J. Y. & Ko, K. S. Mutations and expression of PmrAB and PhoPQ related with colistin resistance in *Pseudomonas aeruginosa* clinical isolates. *Diagn. Microbiol. Infect. Dis.* **78,** 271–276 (2014).
65. Beceiro, A. *et al.* Phosphoethanolamine modification of lipid A in colistin-resistant variants of *Acinetobacter baumannii* mediated by the *pmrAB* two-component regulatory system. *Antimicrob. Agents Chemother.* **55,** 3370–3379 (2011).
66. Cheng, H., Chen, Y. & Peng, H. Molecular characterization of the PhoPQ-PmrD-PmrAB mediated pathway regulating polymyxin B resistance in *Klebsiella pneumoniae* CG43. *J. Biomed. Sci.* **17,** 1–16 (2010).
67. Trent, M. S., Ribeiro, A. A., Lin, S., Cotter, R. J. & Raetz, C. R. H. An inner membrane enzyme in *Salmonella* and *Escherichia coli* that transfers 4-amino-4-deoxy- L-arabinose to lipid A. *J. Biol. Chem.* **276,** 43122–43131 (2001).

68. Stojanoski, V. *et al.* Structure of the catalytic domain of the colistin resistance enzyme MCR-1. *BMC Biol.* **14,** 1–10 (2016).
69. Hinchliffe, P. *et al.* Insights into the mechanistic basis of plasmid-mediated colistin resistance from crystal structures of the catalytic domain of MCR-1. *Sci. Rep.* **7,** 1–10 (2017).
70. Hu, M. *et al.* Crystal Structure of *Escherichia coli* originated MCR-1, a phosphoethanolamine transferase for colistin resistance. *Sci. Rep.* **6,** 1–7 (2016).
71. Arroyo, L. A. *et al.* The *pmrCAB* operon mediates polymyxin resistance in *Acinetobacter baumannii* ATCC 17978 and clinical isolates through phosphoethanolamine modification of lipid A. *Antimicrob. Agents Chemother.* **55,** 3743–3751 (2011).
72. Beceiro, A. *et al.* Biological cost of different mechanisms of colistin resistance and their impact on virulence in *Acinetobacter baumannii*. *Antimicrob. Agents Chemother.* **58,** 518–526 (2014).
73. Moffatt, J. H. *et al.* Insertion sequence ISAba11 is involved in colistin resistance and loss of lipopolysaccharide in *Acinetobacter baumannii. Antimicrob. Agents Chemother.* **55,** 3022–3024 (2011).
74. Anandan, A. *et al.* Structure of a lipid A phosphoethanolamine transferase suggests how conformational changes govern substrate binding. *PNAS* **114,** 2218–2223 (2017).
75. Fage, C. D., Brown, D. B., Boll, J. M., Keatinge-clay, A. T. & Trent, M. S. Crystallographic study of the phosphoethanolamine transferase EptC required for polymyxin resistance and motility in *Campylobacter jejuni*. *Acta Crystallogr.* **70,** 2730–2739 (2014).
76. Mell, J. C. & Redfield, R. J. Natural competence and the evolution of DNA uptake specificity. *J. Bacteriol.* **196,** 1471–1483 (2014).
77. Hu, Y., Liu, F., Lin, I. Y., Gao, G. F. & Zhu, B. Dissemination of the *mcr-1* colistin resistance gene. *Lancet Infect. Dis.* **16,** 292–293 (2016).
78. Falgenhauer, L. *et al.* Colistin resistance gene *mcr-1* in extended-spectrum β-lactamase-producing and carbapenemase-producing Gram-negative bacteria in Germany. *Lancet Infect. Dis.* **16,** 282–283 (2016).
79. Zeng, K., Doi, Y., Patil, S., Huang, X. & Tian, G. Emergence of the plasmid-mediated *mcr-1* gene in colistin-resistant *Enterobacter aerogene*s and *Enterobacter cloacae*. *Antimicrob. Agents Chemother.* **60,** 3862–3863 (2016).
80. Quesada, A. *et al.* Detection of plasmid mediated colistin resistance (MCR-1) in *Escherichia coli* and *Salmonella enterica* isolated from poultry and swine in Spain. *Res. Vet. Sci.* **105,** 134–135 (2016).
81. Ye, H. *et al.* Diversified *mcr-1*-harbouring plasmid reservoirs confer resistance to colistin in human gut microbiota. *MBio* **7,** 1–7 (2016).
82. Shen, Z., Wang, Y., Shen, Y., Shen, J. & Wu, C. Early emergence of *mcr-1* in *Escherichia coli* from food-producing animals. *Lancet Infect. Dis.* **16,** 293 (2016).
83. Malhotra-Kumar, S. *et al.* Colistin resistance gene *mcr-1* harboured on a multidrug resistant plasmid. *Lancet Infect. Dis.* **16,** 283–284 (2016).

84. Haenni, M. *et al.* Co-occurrence of extended spectrum β lactamase and MCR-1 encoding genes on plasmids. *Lancet Infect. Dis.* **16,** 281–282 (2016).
85. Sun, J. *et al.* Co-transfer of bla NDM-5 and *mcr-1* by an IncX3 – X4 hybrid plasmid in *Escherichia coli*. *Nat. Microbiol.* **1,** 1–4 (2016).
86. Stoesser, N., Mathers, A. J., Moore, C. E., Day, N. P. J. & Crook, D. W. Colistin resistance gene *mcr-1* and pHNSHP45 plasmid in human isolates of *Escherichia coli* and *Klebsiella pneumoniae*. *Lancet Infect. Dis.* **16,** 285–286 (2016).
87. Walkty, A. *et al.* Frequency of MCR-1-mediated colistin resistance among *Escherichia coli* clinical isolates obtained from patients in Canadian hospitals. *C. Open* **4,** 641–645 (2016).
88. Poirel, L., Kieffer, N., Liassine, N., Thanh, D. & Nordmann, P. Plasmid-mediated carbapenem and colistin resistance in a clinical isolate of *Escherichia coli*. *Lancet Infect. Dis.* **16,** 281 (2016).
89. McGann, P. *et al. Escherichia coli* harboring *mcr-1* and bla CTX-M on a novel IncF plasmid: first report of *mcr-1* in the United States. *Antimicrob. Agents Chemother.* **60,** AAC.01103-16 (2016).
90. Liu, Y. *et al.* Structural modification of lipopolysaccharide conferred by *mcr-1* in Gram-negative ESKAPE pathogens. *Antimicrob. Agents Chemother.* **61,** 1–9 (2017).
91. Yin, W. *et al.* Novel plasmid-mediated colistin resistance gene *mcr-3* in *Escherichia coli*. *MBio* **8,** 1–6 (2017).
92. Xavier, B. B. *et al.* Identification of a novel plasmid-mediated colistin resistance gene, *mcr-2*, in *Escherichia coli*, Belgium, June 2016. *Eurosurveillance* **21,** 1–6 (2016).
93. Harris, T. L. *et al.* Small molecule downregulation of PmrAB reverses lipid A modification and breaks colistin resistance. *ACS Chem. Biol.* **9,** 122–127 (2014).
94. Roesch, L. F. W. *et al.* Pyrosequencing enumerates and contrasts soil microbial diversity. *ISME J.* 283–290 (2007). doi:10.1038/ismej.2007.53
95. Daniel, R. The soil metagenome – a rich resource for the discovery of novel natural products. *Curr. Opin. Biotechnol.* **15,** 199–204 (2004).
96. Crevelin, E. J., Crotti, A. E. M., Zucchi, T. D., Melo, I. S. & Moraes, L. A. B. Dereplication of *Streptomyces* sp. AMC 23 polyether ionophore antibiotics by accurate-mass electrospray tandem mass spectrometry. *J. Mass Spectrom.* **49,** 1117–1126 (2014).
97. Deuschle, U., Kammerer, W., Gentz, R. & Bujard, H. Promoters of *Escherichia coli*: a hierarchy of in vivo strength indicates alternate structures. *EMBO J.* **5,** 2987–94 (1986).
98. CLSI. Methods for dilution antimicrobial susceptibility tests for bacteria that grow aerobically; approved standard - ninth edition. **32,** M07-A9 (2012).
99. Zhang, J., Chung, T. D. Y. & Oldenburg, K. R. A simple statistical parameter for use in evaluation and validation of high throughput screening assays. *J. Biomol. Screen.* **4,** 67–73 (1999).

100. Mangat, C. S., Bharat, A., Gehrke, S. S. & Brown, E. D. Rank ordering plate data facilitates data visualization and normalization in high-throughput screening. *J. Biomol. Screen.* **19,** 1314–1320 (2014).
101. Fuente-núñez, C. *et al.* Inhibition of bacterial biofilm formation and swarming motility by a small synthetic cationic peptide. *Antimicrob. Agents Chemother.* **56,** 2696–2704 (2012).
102. Dobias, J., Poirel, L. & Nordmann, P. Cross-resistance to human cationic antimicrobial peptides and to polymyxins mediated by the plasmid-encoded MCR-1? *Clin. Microbiol. Infect.* 1–5 (2017). doi:10.1016/j.cmi.2017.03.015
103. Kao, C. *et al.* Cathelicidin antimicrobial peptides with reduced activation of toll-like receptor signaling have potent bactericidal activity against colistin-resistant bacteria. *Am. Soc. Microbiol.* **7,** 1–10 (2016).
104. Agency, E. M. *Use of colistin products in animals within the European Union : development of resistance and possible impact on human and animal health*. (2013).
105. Jiang, H. *et al.* High prevalence and widespread distribution of multi-resistant *Escherichia coli* isolates in pigs and poultry in China. *Vet. J.* **187,** 99–103 (2011).
106. Witte, W. Medical consequences of antibiotic use in agriculture. *Science* **279,** 996–997 (2017).
107. Durso, L. M. & Cook, K. L. Impacts of antibiotic use in agriculture: what are the benefits and risks? *Curr. Opin. Microbiol.* **19,** 37–44 (2014).
108. Pankey, G. A. & Ashcraft, D. S. The detection of synergy between meropenem and polymyxin B against meropenem-resistant *Acinetobacter baumannii* using Etest and time-kill assay. *Diagn. Microbiol. Infect. Dis.* **63,** 228–232 (2009).
109. Bratu, S. *et al.* Carbapenemase-producing *Klebsiella pneumoniae* in Brooklyn , NY: molecular epidemiology and in vitro activity of polymyxin B and other agents. *J. Antimicrob. Chemother.* **56,** 128–132 (2005).
110. Pankey, G. A. & Ashcraft, D. S. Detection of synergy using the combination of polymyxin B with either meropenem or rifampin against carbapenemase-producing *Klebsiella pneumoniae. Diagn. Microbiol. Infect. Dis.* **70,** 561–564 (2011).
111. Tascini, C. *et al.* Synergistic activity of colistin plus rifampicin against colistin-resistant KPC-producing *Klebsiella pneumoniae*. *Am. Soc. Microbiol.* **57,** 3990–3993 (2013).
112. Elemam, A., Rahimian, J. & Doymaz, M. In vitro evauation of antibiotic synergy for polymyxin B-resistant carbapenemase-producing *Klebsiella pneumoniae*. *Am. Soc. Microbiol.* **48,** 3558–3562 (2010).
113. Dixon, R. A. & Chopra, I. Leakage of periplasmic proteins from *Escherichia coli* mediated by polymyxin B nonapeptide. *Antimicrob. Agents Chemother.* **29,** 781–788 (1986).
114. Viljanen, P. & Vaara, M. Susceptibility of Gram-negative bacteria to polymyxin B nonapeptide. *Antimicrob. Agents Chemother. N.J* **25,** 701–705 (1984).
115. Abeles, R. H., Frey, P. A. & Jencks, W. P. *Biochemistry*. (Jones and Bartlett Publishers, 1992).

116. Cleland, W. W. The kinetics of enzyme-catalyzed reactions with two or more substrates or products. I. Nomenclature and rate equations. *Biochim. Biophys. Acta* **67,** 104–137 (1963).
117. Dimitrijevic, M., Grujic-injac, B. & Lajsic, S. The synthesis of a new phospholipid from the koilin glandular layer of chicken gizzard. *Hoppe-Seyler's Z. Physiol. Chem* 477–480 (1979).
118. Wanty, C. *et al.* The structure of the neisserial lipooligosaccharide phosphoethanolamine transferase A (LptA) required for resistance to polymyxin. *J. Mol. Biol.* **425,** 3389–3402 (2013).
119. Gao, R. *et al.* Dissemination and mechanism for the MCR-1 colistin resistance. *PLoS Pathog.* 1–19 (2016). doi:10.1371/journal.ppat.1005957
120. Luirink, J., Heijne, G. Von, Houben, E. & Gier, J. De. Biogenesis of inner membrane proteins in *Escherichia coli*. *Annu. Rev. Microbiol.* **59,** 329–355 (2005).
121. McCall, K. A., Huang, C. & Fierke, C. A. Function and mechanism of zinc metalloenzymes. *J. Nutr.* **130,** 14375–14465 (2000).
122. Gottlieb, H. E., Kotlyar, V. & Nudelman, A. NMR chemical shifts of common laboratory solvents as trace impurities. *J. Org. Chem.* **62,** 7512–7515 (1997).

Appendices

Appendix 1: Media and master mixes

***Streptomyces* Antibiotic Activity Media (SAM)**	**Bennett's**	**Czapek Mineral Mix**
15 g glucose 15 g soytone (soya peptone) 5 g NaCl 1 g yeast extract 1 g $CaCO_3$ 2.5 mL glycerol ddH_2O to 1 L 15 g agar (optional) pH to 6.80 Autoclave	10 g potato starch 2 g casamino acids 1.8 g yeast extract 2 mL Czapek mineral mix ddH_2O to 1 L 15 g agar (optional) pH to 6.8 Autoclave	10 g KCl 10 g $MgSO_4 \cdot 7H_2O$ 12 g $NaNO_3$ 0.2 g $FeSO_4 \cdot 7H_2O$ 200 µL conc. HCl ddH_2O to 100 mL Filter sterilize

2ZYM-2X Lac media	**Trace elements**	**20X NPSC**
93 mL 2ZY medium 200 µL 1M $MgSO_4$ 4 mL 50X Lac 5 mL 20X NPSC 100 µL trace elements x µL antibiotic	1 g $FeSO_4 \cdot 7H_2O$ 8.8 g $ZnSO_4 \cdot 7H_2O$ 0.4 g $CuSO_4 \cdot 7H_2O$ 0.15 g $MnSO_4 \cdot 4H_2O$ 0.1 g $Na_2B_4O_7 \cdot 10H_2O$ 0.05 g $(NH_4)_6MO_7O_{24} \cdot 4H_2O$ Add salts to 250 mL ddH_2O, add 0.2 mL conc. HCl. Add ddH_2O to 1 L.	53.5 g NH_4Cl 32.23 g Na_2SO_4 68 g KH_2PO_4 71 g Na_2HPO_4 ddH_2O to 1 L pH to 6.7 Autoclave

2ZY medium	**50X Lac**
10 g yeast extract 20 g tryptone ddH_2O to 1 L Autoclave	25 g glycerol 2.5 g glucose 10 g α-lactose ddH_2O to 100 mL Filter sterilize

2X Gibson Master Mix
320 µL 5X ISO buffer 6.4 µL 1U/µL T5 exonuclease (M0363S; NEB) 20 µL 2U/µL Phusion polymerase (non hot start) (F-530L; ThermoFisher) 40 µL 40U/µL Taq ligase (L6060L; D-Mark Bio) 413.6 µL ddH_2O Dilute T5 exonuclease stock 10-fold in 1X ISO to get 1 U/µL

5X ISO buffer
3 mL 1M Tris-HCl pH 7.5 300 µL 1M $MgCl_2$ 1.5 g PEG-8000 300 µL 1M DTT 0.0199 g NAD 60 µL 100 mM dGTP 60 µL 100 mM dATP 60 µL 100 mM dCTP 60 µL 100 mM dTTP 2.16 mL ddH_2O

Appendix 2: Primers

Chapter 3

Primer Name	Sequence
MCR-1_CTD_Fwd	5'-TAAGCATATGGAGTATAAAAAAGCCAGTGCGCC-3'
MCR-1_CTD_Rev	5'-GGCCTCGAGTCAGCGGATGAATGCGGTGC-3'

Chapter 4

Primer Name	Sequence
MCR-1_E246A	Fwd: 5'-GTGTTCGTCGTCGGTGCGACGGCACGCGCCGATC-3' Rev: 5'-GATCGGCGCGTGCCGTCGCACCGACGACGAACAC-3'
MCR-1_H395A	Fwd: 5'-CACCAAATGGGCAATGCCGGGCCTGCGTATTTTAAG-3' Rev: 5'-CTTAAAATACGCAGGCCCGGCATTGCCCATTTGGTG-3'
MCR-1_D465A	Fwd: 5'-CAATGCTGTATGTCAGCGCTCATGGCGAAAGTCTG-3' Rev: 5'-CAGACTTTCGCCATGAGCGCTGACATACAGCATTG-3'
MCR-1_H478A	Fwd: 5'-GAACGGTGTCTATCTAGCTGGTATGCCAAATGC-3' Rev: 5'-GCATTTGGCATACCAGCTAGATAGACACCGTTC-3'
MCR-1_E468A	Fwd: 5'-GTCAGCGATCATGGCGCAAGTCTGGGTGAGAAC-3' Rev: 5'-GTTCTCACCCAGACTTGCGCCATGATCGCTGAC-3'
MCR-1_T285A	Fwd: 5'-CATCGTGCGGCACATCGGCGGCGTATTCTGTGC-3' Rev: 5'-GCACAGAATACGCCGCCGATGTGCCGCACGATG-3'
MCR-1_R402A	Fwd: 5'-CCTGCGTATTTTAAGGCATATGATGAAAAGTTTG-3' Rev: 5'-CAAACTTTTCATCATATGCCTTAAAATACGCAGG-3'
MCR-1_E363A	Fwd: 5'-CCAATCCTTATAACGCATGCCGCGATGTCGG-3' Rev: 5'-CCGACATCGCGGCATGCGTTATAAGGATTGG-3'
MCR-1_C281A	Fwd: 5'-CAATTTTAGCAATGTCACATCGGCCGGCACATCGACGGC-3' Rev: 5'-GCCGTCGATGTGCCGGCCGATGTGACATTGCTAAAATTG-3'
MCR-1_C364A	Fwd: 5'-CAATCCTTATAACGAAGCCCGCGATGTCGGTATG-3' Rev: 5'-CATACCGACATCGCGGGCTTCGTTATAAGGATTG-3'
MCR-1_C414A	Fwd: 5'-CAAATTCACGCCAGTGGCTGAAGGTAATGAGCTTG-3' Rev: 5'-CAAGCTCATTACCTTCAGCCACTGGCGTGAATTTG-3'
MCR-1_N328A	Fwd: 5'-GTATCTTGTGGCGTGATGCTAATTCGGACTCAAAAG-3' Rev: 5'-CTTTTGAGTCCGAATTAGCATCACGCCACAAGATAC-3'
MCR-1_N329A	Fwd: 5'-CTTGTGGCGTGATAATGCTTCGGACTCAAAAGG-3' Rev: 5'-CCTTTTGAGTCCGAAGCATTATCACGCCACAAG-3'
MCR-1_S330A	Fwd: 5'-GTGGCGTGATAATAATGCGGACTCAAAAGGCG-3' Rev: 5'-CGCCTTTTGAGTCCGCATTATTATCACGCCAC-3'

Primer Name	Sequence
MCR-1_K348A	Fwd: 5'-CAATTTGCCGATTATGCATCCGCGACCAACAAC -3' Rev: 5'-GTTGTTGGTCGCGGATGCATAATCGGCAAATTG -3'
MCR-1_H390A	Fwd: 5'-GATATGCTGATCATGCTGGCCCAAATGGGCAATCAC-3' Rev: 5'-GTGATTGCCCATTTGGGCCAGCATGATCAGCATATC-3'
MCR-1_M392A	Fwd: 5'-GATCATGCTGCACCAAGCGGGCAATCACGGGCC-3' Rev: 5'-GGCCCGTGATTGCCCGCTTGGTGCAGCATGATC-3'
MCR-1_H466A	Fwd: 5'-CTGTATGTCAGCGATGCTGGCGAAAGTCTGGG-3' Rev: 5'-CCCAGACTTTCGCCAGCATCGCTGACATACAG-3'
MCR-1_T112A	Fwd: 5'-CAAAATGCCCTACAGGCCGACCAAGCCGAGAC-3' Rev: 5'-GTCTCGGCTTGGTCGGCCTGTAGGGCATTTTG-3'
MCR-1_N108A	Fwd: 5'-GATACGACCATGCTCCAAGCTGCCCTACAGACCGAC-3' Rev: 5'-GTCGGTCTGTAGGGCAGCTTGGAGCATGGTCGTATC-3'
MCR-1_Q107A	Fwd: 5'-GATACGACCATGCTCGCAAATGCCCTACAGAC-3' Rev: 5'-GTCTGTAGGGCATTTGCGAGCATGGTCGTATC-3'
MCR-1_E116A	Fwd: 5'-CAGACCGACCAAGCCGCGACCAAGGATCTATTAAAC-3' Rev: 5'-GTTTAATAGATCCTTGGTCGCGGCTTGGTCGGTCTG-3'
MCR-1_P195D	Fwd: 5'-CGTAGCTATGTCAATGATATCATGCCAATCTAC-3' Rev: 5'-GTAGATTGGCATGATATCATTGACATAGCTACG-3'
MCR-1_Fwd	5'-GTTGCTACATATGATGCAGCATACTTCTGTGTGG-3'
MCR-1_Rev	5'-TAGATGGCTCGAGGCGGATGAATGCGGTGCG-3'
MCR-1_TM1_Fwd	5'- GTTGCTACATATGATGCAGCATACTTCTGTGTGG-3'
MCR-1_TM1_Rev	5'- GTTGCTAAAGCTTCGCGATGGGATAGGTTTGG-3'
GA_MCR-1_46	5'- CCTATCCCATCGCGAAGCTTGACAATCTCGGCTTTGTGC-3'
GA_MCR-1_73	5'-CCTATCCCATCGCGAAGCTTCGCTATGTGCTAAAGCCTGTG-3'
GA_MCR-1_99	5'- CCTATCCCATCGCGAAGCTTACGGTCTATGATACGACCATGC-3'
GA_MCR-1_123	5'- CCTATCCCATCGCGAAGCTTGCAGCGTTTATCATGCGTATC-3'
GA_MCR-1_147	5'- CCTATCCCATCGCGAAGCTTTATCCGACTTGGGGCAAGG-3'
GA_MCR-1_175	5'- CCTATCCCATCGCGAAGCTTTTCAGCAGTCATTATGCCAGTTTC-3'
GA_MCR-1_194	5'- CCTATCCCATCGCGAAGCTTAATCCGATCATGCCAATCTACTC-3'
GA_MCR-1_215	5'-CCTATCCCATCGCGAAGCTTGCGCCAAAAGATACCATTTATCAC-3'
GA_MCR-1_Rev	5'-GTGGTGGTGGTGGTGCTCGAGGCGGATGAATGCGGTGCG-3'

Primer Name	Sequence
MCR-1_73	5’- GTTGCTAAAGCTTCGCTATGTGCTAAAGCCTGTG-3’
MCR-1_99	5’- GTTGCTAAAGCTTACGGTCTATGATACGACCATGC-3’
MCR-1_123	5’- GTTGCTAAAGCTTGCAGCGTTTATCATGCGTATC-3’
MCR-1_147	5’-GTTGCTAAAGCTTTATCCGACTTGGGGCAAGG-3’
MCR-1_175	5’- GTTGCTAAAGCTTTTCAGCAGTCATTATGCCAGTTTC-3’
MCR-1_194	5’- GTTGCTAAAGCTTAATCCGATCATGCCAATCTACTC-3’
MCR-1_215	5’- GTTGCTAAAGCTTGCGCCAAAAGATACCATTTATCAC-3’

Appendix 3: ^{1}H and ^{13}C NMR spectra of *O*-(*p*-nitrophenylphosphoryl)ethanolamine TFA salt (3)

Chemical shifts in ^{1}H NMR and ^{13}C NMR spectra are reported in parts per million (ppm) relative to tetramethylsilane (TMS), with calibration of the residual solvent peaks according to values reported by Gottlieb *et al.* (chloroform: δ_H 7.26, δ_C 77.16; acetone: δ_H 2.05, δ_C 29.84, 206.26; methanol: δ_H 3.31, δ_C 49.00; DMSO: δ_H 2.50, δ_C 39.52; acetonitrile: δ_H 1.94, δ_C 1.32, 118.26)[122]. When peak multiplicities are given, the following abbreviations are used: s, singlet; d, doublet; t, triplet; q, quartet; sept., septet; dd, doublet of doublets; m, multiplet; br, broad; app., apparent; *gem*, geminal. ^{1}H NMR spectra were acquired at 700 MHz with a digital resolution (Brüker parameter: FIDRES) of 0.299 Hz/point and coupling constants reported herein therefore have uncertainties of ±0.6 Hz. All assignments of protons and carbons relied on data from 2-dimensional NMR experiments including COSY, HMQC, and HMBC. Melting points (mp) are uncorrected.

O-(*p*-Nitrophenylphosphoryl)ethanolamine TFA salt **3** (^{1}H NMR; 700 MHz; DMSO-d_6)

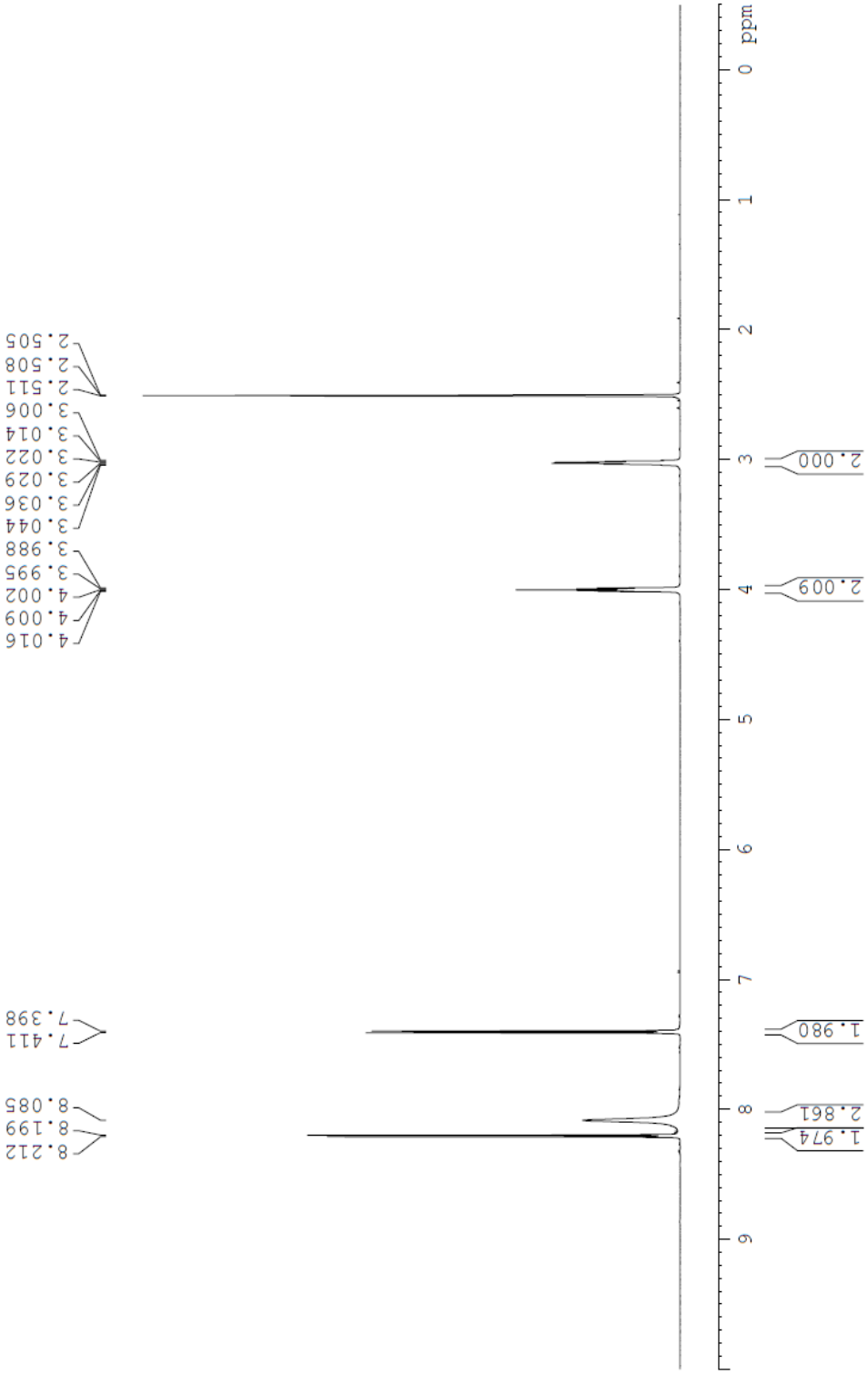

^{1}H NMR (700 MHz, DMSO-d_6): δ 3.02 (m, 2H, CH_2NH_3^+), 4.00 (m, 2H, CH_2O), 7.40 (d, J = 9.2 Hz, 2H, ArH), 8.00–8.18 (brs, 3H, NH_3^+), 8.20 (d, J = 9.2 Hz, 2H, ArH).

^{1}H NMR assignments:

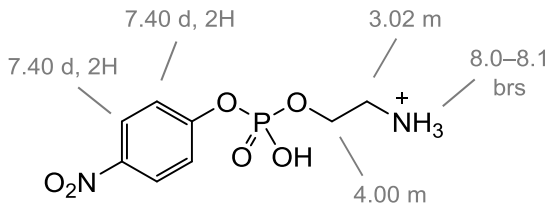

3

O-(*p*-Nitrophenylphosphoryl)ethanolamine TFA salt **3** (^{13}C NMR; 175 MHz; DMSO-d_6)

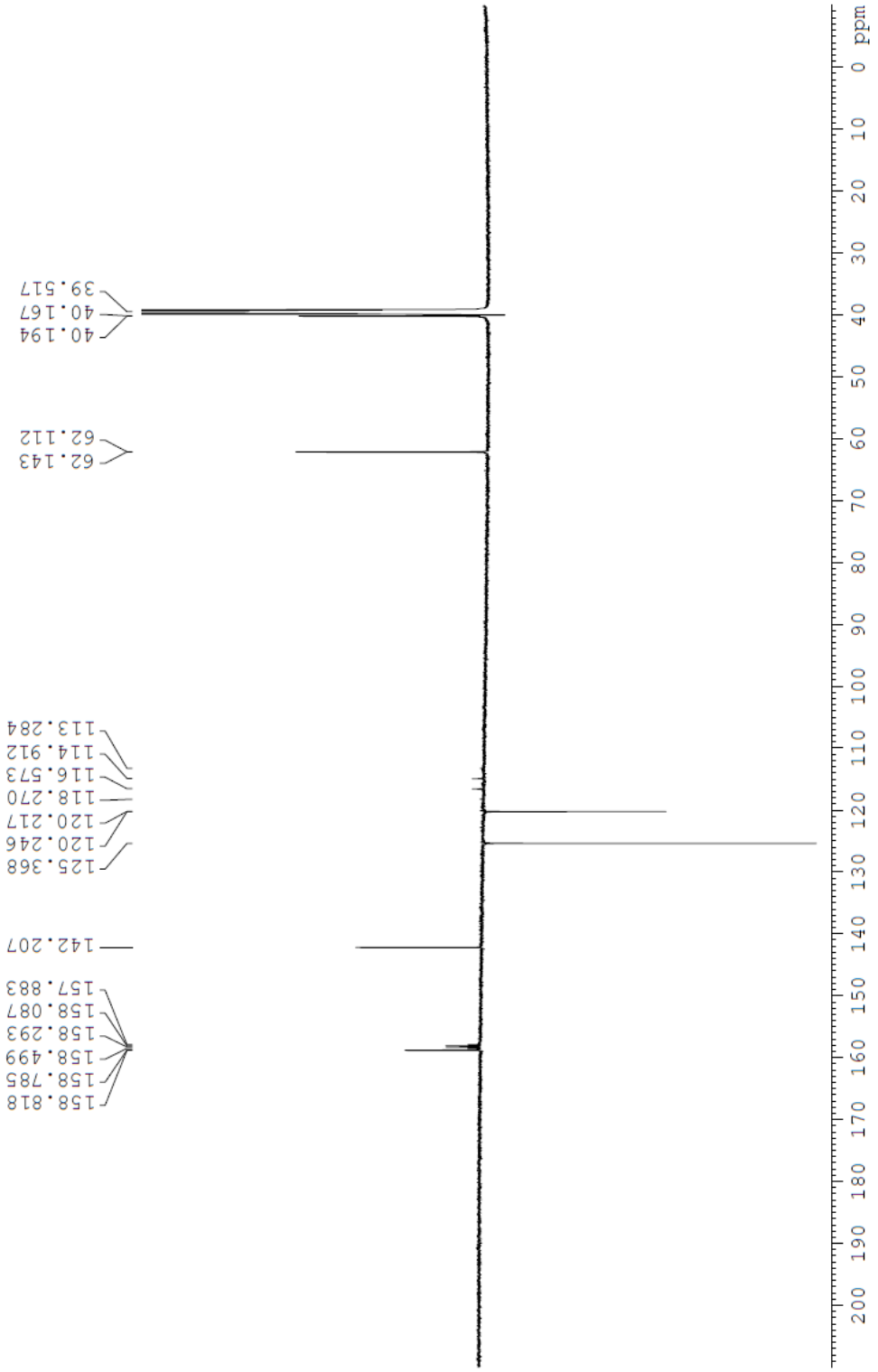

^{13}C NMR (175 MHz, DMSO-d_6): δ 40.18 (d, $^{3}J_{C,P}$ = 4.7 Hz, $CH_2NH_3^+$), 62.13 (d, $^{2}J_{C,P}$ = 5.5 Hz, CH_2O), 115.74 (q, $^{1}J_{C,F}$ = 292.5 Hz, $CF_3CO_2^-$), 120.22 (d, $^{3}J_{C,P}$ = 5.2 Hz, 2C, *o*-Ar*C*H), 125.36 (2C, *m*-Ar*C*H), 142.20 (Ar*C*NO_2), 158.19 (q, $^{2}J_{C,F}$ = 36.2 Hz, $CF_3CO_2^-$), 158.82 (d, $^{2}J_{C,P}$ = 5.7 Hz, Ar*C*OP).

^{13}C NMR assignments:

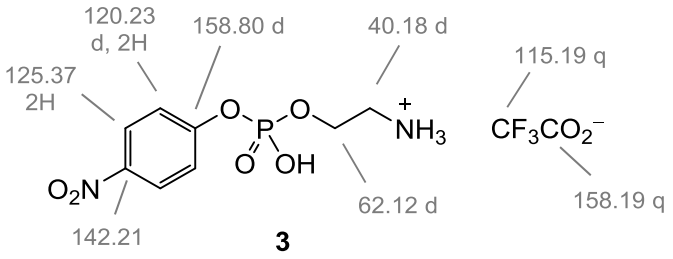

3

Appendix 4: Sequence alignment of several phosphoethanolamine transferases.

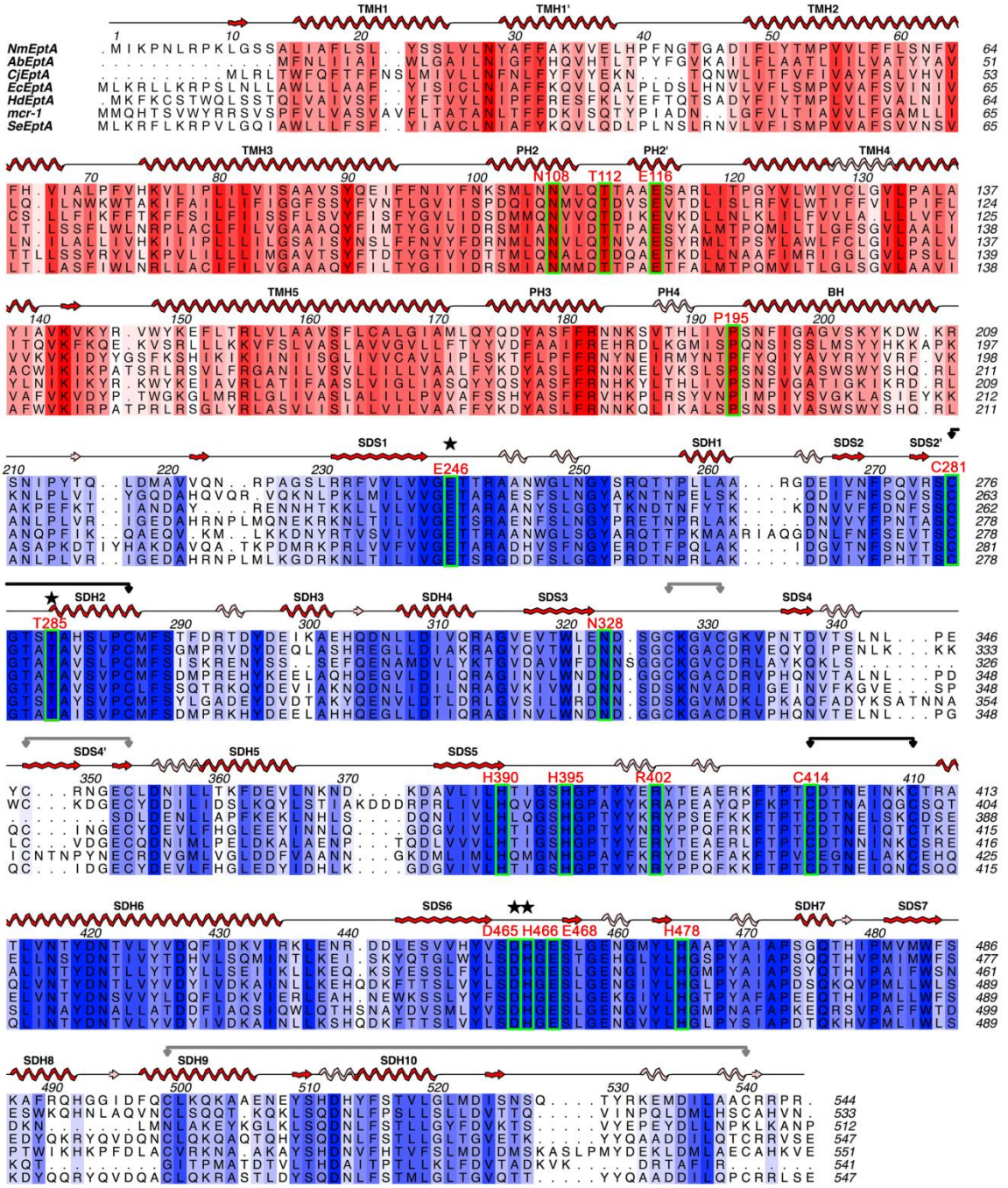

Alignment of seven different phosphoethanolamine transferases: EptA in *Neisseria meningitidis* (*Nm*) and *Acinetobacter baumannii* (*Ab*), PmrC in *Salmonella enterica* (*Se*) and HD0852 in *Haemophilus ducreyi* (*Hd*), EptA in *E. coli* (*Ec*) and EptC in

Campylobacter jejuni (*Cj*), and MCR-1 in *E. coli*. The secondary structure of *Nm*EptA (full length, PDB 5FGN) is above the sequences with α-helices and β-sheets in red and π-helices, 3_{10}-helices, and β-bridges in pink. The sequence is shaded for physico-chemical similarity, where red represents the transmembrane domain and blue represents the soluble domain. Disulfide bonds are shown with black arrows for conserved cysetines and gray arrows for semi-conserved cysteines. The residues involved in coordinating the *Nm*EptA zinc ion are marked with a star. The residues outlined in green represent 100% residue conservation among the PEtN transferases and the red numbers above the alignment indicate the amino acid position in MCR-1. Adapted from Anandan *et al.*[74]